Basement fault influence on the Bicorb-Quesa Salt Wall kinematics, insights from Magnetotelluric and Paleomagnetic techniques on Salt Tectonics

Marc Rubinat Cabanas

Institut de Recerca Geomodels
Grup de Recerca Consolidat de Geodinàmica i Anàlisi de Conques
Departament de Geodinàmica i Geofísica
Universitat de Barcelona

Basement fault influence on the Bicorb-Quesa Salt Wall kinematics, insights from Magnetotelluric and Paleomagnetic techniques on Salt Tectonics

Thesis submitted by Marc Rubinat Cabanas for the degree of Doctor in Geology.

This thesis has been done within the framework of the Exploration, Analysis of Basin and Orogenic Systems Doctorate Program of the University of Barcelona (2004-2006 Biennium) under the supervision of Dr. Eduard Roca i Abella.

Marc Rubinat Cabanas

Barcelona, April 2012

Dr. Eduard Roca i Abella

This thesis has been completed whitin the Geodynamics and Basin analysis Group of the University of Barcelona (Grup de Recerca Consolidat reconegut per la Generalitat de Catalunya; referències 2005SGR-000397 i 2009SGR-1198) and the Geomodels Research Group (financed by the Generalitat of Catalunya, Instituto Geológico y Minero de España (IGME) and some private national and international companies). In addition this thesis has been first developed by a Repsol-UB research grant. The research programes are within the framework of the Spanish govermental projects: CONSTRUCCIÓN DE MODELOS ESTRUCTURALES 3D (CGL2004-05816-C02-01), MODELIZACIÓN ESTRUCTURAL 4D (CGL2007-66431-C02-01) y INTECTOSAL: CGL2010-21968-C02-01. We also want to thank Midland Valley Exploration and Paradigm for the software licences kindly provided for the realization of the thesis.

Dedicat al Pol

Que està arribant

Agraïments:

Després de tots aquest anys arriba el moment de seure i veure amb satisfacció que una part del teu camí arriba a la fi en i veure que han estats molts els que t'han acompanyat per poder assolir aquesta fita.

Primer de tot agrair al meu director de tesis l'Eduard Roca tot el temps que li ha dedicat a la tesis especialment durant aquests darrers temps de frenesís, les teves exhaustives correccions ajuden a millorar.

Al grup de Magnetotellurica, en especial el Juanjo Ledo, la Pilar Queralt, l'Oriol Rosell, la Lena Escalas, l'Anna Martí, la Xenia Ogaya, La Perla Piña i l'Eloi Vilamajo per la seva infinita paciència i els bons moments al camp.

Al grup de Paleomagnetisme especialment a la Bet Beamud i la Ruth Soto que tant hem estat discutint per portar a bon port el que al començament semblava una tasca tan complicada.

A tots els amics i companys de la facultat amb els que hem compartit dinars, sopars, calçotades, paelles, riures, discussions,..., Oskar Vidal, Jordi Bausa, Oriol Ferrer, la Patricia Cabello, la Ximena Moreno, l'Oscar Gratacós, el Angel Rodes, el Daniel Bello, L'Alex Amilibia, el Miqui Marin, la Ylenia Aimar, l'Anna Carmona, Anna Quintà, Jorge Belenger, Mireia Butillé, Diego Iaffa, Bahman Soleimany, Cristina Biete, Marco Snidero, Manoel Vacarcel, David Garcia, Berta López, Pablo Martínez, Joana Mencos, Teresa Beamud, Nuria Carrerra, Marta Guinau, Oriol Falivene, l'Oscar Fernández, a molts que ja he citat abans i a d'altres que segur m'oblido que sou molts els que meu acompanyat durant aquest temps.

Al Hostal lar Gallego on l'Antonio, l'Angeles, el Ramon, la Isabel i el Salvador m'han tractat com un mes de la família durant les meves llargues estades al camp

Als meus amics d'espele que tant m'ajuden a desconnectar, el Dani, el Javi, Roger, Jeni, el Junior i els Ferros.

Als meus amics de sempre, aquells que portant tants anys acompanyant-me, animant-me, fent-me passar bones estones, disfrutant de cada moment que estic ells, l'Uri el Miqui, el Tismi, el Jordi, La Duna, el Xavi i el Joan.

A la meva família, els meus avis la Mercedes, L'Arcadio i l'Ana que t'han m'han cuidat, al meu germà, la Maria i L'Unai que són un gran recolzament als meus

cosins, l'Ivan i el David, als meus oncles, la Berta, el Manel, l'Alfredo i l'Anna i tants d'altres que m'encoratgen a continuar lluitant.

Evidentment als meus pares, el Francesc i l'Arcàdia, gràcies als valors que m'han inculcat durant tots aquests anys ara he arribat fins aquí.

I finalment a la Gemma que m'ha acompanyat tots aquests anys recolzant-me, estimant-me, i intentant entendrem, el teu suport ha estat imprescindible.

Índex

Resum Extens

La presència de materials evaporítics condiciona l'estructura que es desenvoluparà en un àrea ja que les propietats reològiques de les evaporites són molt diferents a les d'altres materials. Especialment la sal, que es deforma plàsticament, és menys densa i més dèbil que la majoria dels materials (Jackson i Talbot, 1986; Jackson i Vendeville, 1994). Aquestes propietats permetran la formació de coixins salins, diapirs salins, parets salines, llengües salines, etc. La generació d'aquestes estructures i el fet de que la sal sigui impermeable propicia la formació de trampes per hidrocarburs i la possibilitat d'emmagatzemar CO_2 o altres residus. Aquest fet els hi dóna a les estructures salines interès econòmic i facilita l'avenç científic en la matèria, com mostra la publicació d'articles que han millorat el coneixement d'aquestes estructures a partir dels anys '90 (ex. Vendeville i Jackson 1992; Jackson 1995; Letouzey et al. 1995; Ge et al. 1997; Rowan et al. 2003; Stewart 2006; Hudec i Jackson 2007, etc.)

L'efecte causat a una cobertora fràgil, pel moviment de una falla normal de basament sobre la qual tenim un nivell de desenganxament dúctil ha estat ampliament estudiat (Koyi et al. 1993; Nalpas i Brun 1993; Jackson i Vendeville 1994; Vendeville et al. 1995; Stewart i Clark 1999; Withjack i Callaway 2000; Dooley et al. 2003; 2005). També, amb la mateixa disposició de materials fràgils-dúctils, ha estat investigada la inversió de les falles normals de basament durant una etapa compressiva (Letouzey et al. 1995; Stewart i Clark 1999; Krzywiec 2004; Ferrer et al. 2012). Per altra banda, la deformació de pell prima provocada per una època compressiva a sobre de un nivell de desenganxament també ha estat estudiada (ex. Chapple 1978; Davis i Engelder 1985; Coward i Stewart 1995; Sans i Koyi 2001), i amb la mateixa geometria les conseqüències de una compressió

en un diapir previ (Vendeville i Nilsen 1995; Canerot et al 2005; Roca et al 2006; Callot et al. 2007; Dooley et al. 2009). Tanmateix, no hi ha cap estudi previ publicat en revistes científiques internacionals que descrigui la deformació per compressió de la pell prima prèviament afectada per una falla de basament. Per tal d'omplir aquest buit, s'ha estudiat la paret salina de Bicorb-Quesa, molt adequada ja que està localitzada a sobre d'una falla de basament, en una zona afectada per compressió amb deformació de pell prima (Roca et al 1996, 2006).

Actualment, per l'estudi de la tectònica salina les dades més utilitzades són la sísmica (ex. Netzeband et al 2006, Fiduk i Rowan 2012) i els estudis de camp (ex. Jackson et al 1990; Roca et al 1996; Sans 2003). A més a més, mitjançant tècniques com la restitució estructural (ex. Worrall i Snelson, 1989; Hossack, 1995; Rowan i Ratlift, 2012) i els models tant numèrics com analògics (ex. Jackson i Talbot 1989; Zaleski i Julien 1992; Podladchikov et al 1993; Chemia et al 2008) s'aprofundeix en el coneixement de la tectònica salina i les diverses àrees d'estudi. En aquesta tesi, els magnífics afloraments del Segment de Paret Salina (SPS, anomenat SWS en anglès) de Bicorb-Quesa, (tant de la cobertora com de la pròpia paret diapírica) ens permeten aprofundir en el coneixement de la tectònica salina ja que no és habitual que aflorin tant bé i tant extensament els materials diapírics. A més a més, aquesta tesi vol mostrar la possibilitat d'utilitzar altres dades que estan àmpliament esteses en altres camps de la geologia però molt poc en l'estudi de tectònica salina: les dades magnetotel·lúriques (Hoversten et al. 2000; Newman et al. 2002; Key et al. 2006) i les paleomagnètiques (Weinberger et al. 1995; 1997; Henry et al. 2000). L' utilització d'aquestes dades ens permetrà aplicar la tècnica de restitució amb més informació i per tant millorant aquesta.

Marc Geològic

El Bicorb-Quesa SPS, anteriorment anomenat Bicorb-Quesa Diapir, es troba situat al Domini Valencià. El Domini Valencià és una plataforma

sub-horitzontal de 40 km^2 de materials d'edat Mesozoica-Cenozoica, majoritàriament carbonats, desenganxats del basament als materials evaporítics del Keuper. Aquesta plataforma carbonatada es troba tallada per un sistema de foses amb direccions ENE-WSW i NNW-SSE al centre de les quals s'hi poden trobar segments de parets diapíriques com les del Bicorb-Quesa SPS.

El Domini Valencià es troba situat al límit de dos cadenes muntanyoses, al Nord trobem la Cadena Ibèrica i al Sud la Cadena Bètica. Tradicionalment aquest domini ha estat inclòs en la Cadena Bètica i definit com la part més externa de la Zona Prebètica. La Zona Prebètica, al seu torn, constitueix la part més externa del cinturó de plecs i encavalcaments de la Cadena Bètica (García-Rodrigo 1960; Azéma et al. 1979; García-Hernández et al. 1980; De Ruig 1992).

La Cadena Ibèrica és una cadena muntanyosa amb direcció NW-SW que està formada per la inversió de conques de rift intracontinentals que es formen entre el Permià Superior i el Cretaci Superior i invertides durant l'Oligocè a Eocè (ex. Alvaro et al., 1979; Guimerà et al 1990).

La Zona Prebètica es tracta d'una zona on la cobertora para-autòctona carbonatada (Mesozoica-Cenozoica) està afectada per plecs i encavalcaments desenganxats del basament Varisc en el Triàsic (Vera, 1983). Les discordances associades amb els plecs i encavalcaments han permès identificar estadis compressius entre l'Oligocè i el Tortonià (ex. Calvo et al., 1978; De Ruig et al., 1987; Beets i De Ruig, 1992; Montenat et al.; 1996; Roca et al 1996). El sostre del basament Varisc localitzat sota la Zona Prebètica cabussa pocs graus cap al sud-est i es troba afectat per una sèrie de falles normals molt verticals (Carbó 1982; Castaño i Carbó 1995; ter Borgh et al. 2011). A sobre del nivell de desenganxament, la cobertora està deformada amb plecs caixa, falles inverses, falles normals i diapirs formats per evaporites triàsiques. Les direccions d'aquestes estructures són ENE-WSW tot i que també podem trobar altres orientacions (De Ruig 1992; Roca et al. 2006; ter Borght et al. 2011). En aquest context de cobertora deformada contractivament, al sud predominen les

estructures que absorbeixen més deformació (encavalcaments i plecs) i aquestes decreixen significativament cap al NNE. D'acord amb aquest decreixement de la deformació es distingeixen tres dominis estructurals: El Prebètic Intern, el Prebètic Extern i el Domini Valencià (García-Rodrigo 1960; Azéma et al. 1979; García-Hernández et al. 1980; De Ruig 1992).

La Zona Prebètica ha estat afectada per diverses etapes en les quals s'han generat o deformat diapirs. Durant el Juràssic el desplaçament per gravetat de la sal cap a les parts internes de la conca generà diapirisme a les parts internes de la zona Prebètica (Martinez del Olmo 1999). Després, durant el Miocè Inferior-Mig, una fase extensional relacionada amb l'obertura del Mediterrani genera un nou creixement de diapirs al llarg de la zona Prebètica (De Ruig 1992; Santisteban et al. 1994; Roca et al. 1996; Martínez del Olmo 1999; Roca et al. 2006). Els diapirs generats són escanyats durant la formació de la Cadena Bètica (Moseley 1981; De Ruig 1992,1995; Roca et al. 1996,2006;). Després d'aquesta deformació compressiva tota l'àrea d'estudi es troba afectada per una etapa extensiva durant el Miocè tardà, que genera la reactivació d'algunes falles i diapirs preexistents a la cobertora (Ott d'Estevou et al. 1988; De Ruig 1995; Roca et al. 1996).

Dades Magnetotel·lúriques

El mètode magnetotel·lúric és una tècnica electromagnètica de font natural que permet caracteritzar la conductivitat elèctrica del subsòl mitjançant la mesura simultània de les variacions de camp elèctric i magnètic a la superfície de la Terra. La penetració del camp electromagnètic depèn de la conductivitat i de la freqüència de la senyal. Els fonaments del mètode estan extensament explicats a Vozoff (1991) i Simpson i Bahr (2005).

En la zona d'estudi s'han realitzat un total de 60 punts de mesura dividits en tres perfils: un que travessa perpendicularment el diapir i dos localitzats a fora d'aquest tallant perpendicularment falles principals de

l'àrea d'estudi. Aquests perfils mostren un canvis de resistivitat que són fàcilment correlacionables amb les diferents litologies. Les resistivitats altes corresponen a les evaporites seques (sal i anhidrita), les roques metamòrfiques del basament, les roques volcàniques i les dolomies. Les resistivitats mitjanes corresponen a les calcàries i finalment les resistivitats baixes corresponen a les argiles, sorres i evaporites humides (guix i sal humida). Gràcies a aquestes imatges s'ha pogut caracteritzar el basament i veure els gruixos dels diferents materials en profunditat.

Entre la informació més valuosa que ens ha proporcionat aquest mètode cal destacar la presència d'una falla de basament amb un salt de 1000 metres cabussant cap al N localitzada sota del Bicorb-Quesa SPS i que va ser activa entre el Pèrmic i el Triàsic, i entre el Juràssic Superior i el Cretaci. En canvi a la resta dels perfils el basament és pràcticament pla, només un petita falla de 100m ha estat localitzada sota la falla que relleva el Bicorb-Quesa SPS, la falla de Carroig. També hi destaca l'acumulació de sal seca en el centre del Bicorb-Quesa SPS i al bloc inferior de les falles principals de la zona que provoquen l' inclinació dels blocs en direcció oposada a les falles.

Estructura de Bicorb-Quesa

El Bicorb-Quesa SPS es troba situat a la part central del Domini Valencià, es tracta d'una estructura allargada de 12 km de llarg i que es va eixamplant progressivament cap a l'est fins a assolir els dos quilòmetres d'amplada a la seva culminació est. En aquest punt s'intersecta amb el segment de paret salina de Navarrès, que s'estén 15 quilòmetres seguint una direcció sud-sud-est. La terminació oest del Bicorb-Quesa SPS coincideix amb la intersecció de dues semifosses: la semifossa de Sácaras amb direcció NW-SE i la de Juanera amb direcció ENE-WSW. Flanquejant la paret diapírica i en certa continuïtat amb aquestes fosses trobem les semifosses de Bicorb i Quesa situades al Nord i Sud de la paret, respectivament.

L'estructura de Bicorb-Quesa SPS es troba fortament condicionada per la presència del nivell dúctil i diapíric del Triàsic Mig-Superior. Aquest nivell desenganxa la deformació dels materials localitzats a sobre i a sota, donant estructures molt diferents a sota de la sal (deformació de pell gruixuda) i a sobre (deformació de pell prima) (Nalpas i Brun 1993; Vendeville et al 1995; Withjack i Callaway 2000; Dooley et al. 2005). Així doncs podem diferenciar tres estils estructurals a la zona: el del basament, el del nivell de desenganxament i el de la cobertora.

L'estructura de basament

Els perfils magnetotel·lúrics, així com les dades gravimètriques de la regió (Carbó 1980) i l'alçada relativa dels diferents materials ens han mostrat la situació de un basament pràcticament pla, tallat per la falla de basament de Bicorb-Quesa, sota el Bicorb-Quesa SPS. També ens ha permés localitzar la petita falla de basament localitzades sota la falla de Carroig, ja anomenades abans. Però aquestes dades també ens han indicat la presència d'una falla de basament cabussant cap a l'est sota del Navarrès SPS.

L'estructura del Triàsic Mig-Superior

Gràcies a poder diferenciar sis unitats dins de la paret salina, cinc del Keuper (K1 a K5) i una del Muschelkak superior, ha estat possible cartografiar les parets salines, fet que ens ha aportat molta informació sobre l'evolució del diapir. Entre aquests materials el K1 és el que té el major contingut de sal en tota la seqüència evaporítica. Aquest fet fa que aquesta unitat sigui la que inicií el diapirisme i nucleji els diapirs.

El Bicorb-Quesa SPS és lleugerament asimètric, té el flanc nord vertical i el flanc sud cabussa uns 50 graus cap al sud. L'estructura interna de la paret diapírica és molt complexa, amb un gran nombre de plecs, zones de cisalla i falles. Entre aquestes estructures destaquen

dos anticlinals d'escala quilomètrica, un localitzat a l'est i l'altre a l'oest amb el nuclis formats de K1, i separats entre ells per un sinclinal format majoritàriament per K2-K5. Les estructures d'aquests dos anticlinals són molt similars, tenen direcció NNE-SSW i estan limitades per una sèrie de zones de cisalla i falles que els separa de la successió K2-K5 localitzada a les vores del diapir. Aquests anticlinals es generen com a bulbs nucleats en sal com mostra la estructura interna d'aquest, on destaquen grans plecs amb direcció NNE-SSW, paral·lels a la paret però on sovint trobem zones caòtiques amb la presencia de zones bretxificades degut a la extrusió de sal. L'anàlisi de quasi 300 eixos de plecs menors també corrobora dos funcionaments diferenciats entre aquests bulbs de K1 i les vores de K2-K5. Els eixos de K1 mostren una clara tendència vertical, formats degut a un creixement del diapir mitjançant plecs tipus cortina (Talbot i Jackson 1987, Jackson i talbot 1989) , mentre que en la successió K2-K5 els que predominen són els eixos subhoritzontals amb direcció NNW-SSE a WNW-ENE. Aquests van ser generats prèviament als tipus cortina ja que son tallats per aquests. Així doncs foren formats anteriorment al creixement del diapir durant una època compressiva ja que tenen una direcció que coincideix amb la direcció de màxim escurçament de les Cadenes Bètica i Ibèrica.

En un d'aquests anticlinals trobem localitzats materials del Muschelkalk majoritàriament sobre K1 i localment sobre K2-K3. Els materials del Muschelkalk es troben afectats pels plecs principals de direcció NNE-SSW. Així doncs aquests materials del Mushchelkalk constitueixen una klippe tectònica que mostra el bloc superior d'un encavalcament que afecta a la seqüència del Keuper. Aquest es troba afectat pels plecs de creixement del diapir i, per tant, l'emplaçament d'aquesta unitat es dóna anteriorment a l'emplaçament del diapir actual. La formació d'aquests dúplex intrasalins ha de produir-se en una època compressiva. Així doncs, aquesta estructura pot haver-se emplaçat contemporàniament a la compressió produïda per les Serralades Ibèrica o Bètica.

Aquests estadis de creixement del diapir no són els únics que

queden enregistrats en l'actual paret salina. Al flanc nord del diapir es poden observar materials del K4 limitats per falles i zones de cisalla, es podria tractar de les restes del coll d'un diapir que va ser escanyat. Una paret salina al escanyar-se genera soldadures secundàries i estructures tipus Q-tip (Rowan i Vendeville 2006; Dooley et al. 2009) com la descrita anteriorment. Aquest primera paret salina, segons les restes de materials del Keuper que es troben en el Miocè i que reomple les semifoses que flanquejen la paret salina, va ser emplaçat durant el Miocè Inferior-Mig (Roca et al., 1996; Anadón et al., 1998).

L'Estructura de la cobertora

Al Nord destaca la presència de la semifossa de Sácaras. Aquesta es desenvolupa com a resposta a la formació de la falla de la Solana que cabussa cap al SW. El bloc inferior, en les parts més properes a la falla, es troba flexionat, cabussant cap el NE. Aquesta flexió que aixeca la plataforma també es dona a la resta de falles principals que tallen la cobertora indicant la formació de diapirs reactius sota d'aquestes falles. El bloc superior de la falla de Solana el trobem inclinat 10-35º cap al NE. A prop de la falla el bloc superior el trobem deformat, formant un sinclinal, tal i com també passa en d'altres falles principals. La geometria d'aquests plecs ens indica que són plecs de propagació de falla extensiva i que la formació de la falla va ser precedida per aquests.

Al Oest destaca la semifossa de la Juanera, la qual està limitada al nord per la falla extensiva del Carroig, que cabussa cap al sud. Aquesta falla connecta amb la terminació oest del diapir i té un salt de falla que arriba als 1000 metres. Els dipòsits sedimentats, d'edat Miocè Inferior-Mig, d'aquesta fosa es troben afectats tant per la falla com per falles antitètiques relacionades amb aquesta, mostrant-nos moviments de la falla posteriors a la sedimentació del Miocè Inferior-Mig. També hi destaca una estructura anterior a la formació de la falla i la sedimentació dels materials. Es tracta d'un anticlinal que està localitzat a la prolongació del diapir sobre el que

es disposen de manera discordant els materials del Miocè Inferior-Mig.

Al sud-oest està localitzada la semifossa de Quesa, que es pot considerar la prolongació de la semifossa de la Juanera tot i que té una polaritat inversa ja que la falla principal que la genera (Falla de Los Charcos) cabussa cap al NW. Aquesta falla arriba a tenir un salt de 900 metres i com en les anteriors trobem el bloc inferior inclinat a causa del moviments de la sal. El bloc superior el trobem compartimentalitzat per falles, moltes de les quals cabussen cap al NW. En aquesta semifossa trobem materials que van des del Miocè Inferior al Superior (Ruiz-Sanchez i Santisteban 2004).

En el NE de l'àrea d'estudi trobem situada la semifossa de Bicorb-Quesa. Aquesta es troba relacionada a la formació de la falla de Cazuma, que cabussa cap al SE i arriba a tenir un salt de falla de 1300 metres. És la de més salt en l'àrea d'estudi i com en les altres falles principals trobem un diapir reactiu a sota del bloc inferior, que plega el pla de falla i flexiona la cobertora. En el bloc inferior trobem falles menors menys plegades i desplaçades que l'anterior. La disposició discordant del Miocè d'aquestes últimes falles ens ajuda a datar-les com a coetànies al Miocè Superior. Pel que fa referència al bloc superior, el trobem inclinat cap al NNW i presenta alguna falla menor extensional. D'acord amb la sedimentació de la semifossa aquestes últimes falles i la de Cazuma són coetànies al Miocè Inferior (Roca et al 1996).

Al voltant de la paret salina trobem que el Miocè Inferior-Mig està flexionat, flexió que provoca l'aixecament dels materials cabussant en direcció oposada a la paret salina. Aquesta flexió es més important a la paret nord. Les geometries d'estrats de creixement daten aquesta flexió com a Miocè Mig, i seria coetània a l'emplaçament de l›encavalcament de baix angle dirigit cap al NW del Pico de la Olla que talla els materials flexionats del Miocè. Aquest encavalcament afecta als materials Miocens inferiors però no als més joves, podent datar-lo com a Miocè Mig i relacionar-lo amb l'emplaçament de les Bètiques.

A la part més occidental del diapir, així com a altres zones, aflora un anticlinal discordant amb els materials Miocens dels que hem parlat anteriorment, que té la sèrie Juràssica-Cretàcica aprimada. Al flanc posterior d'aquest anticlinal, localitzat a la semifossa de Quesa, trobem falles inverses d'alt angle, formades posteriorment o durant la formació de l'anticlinal. Al flanc anterior, localitzat a la semifossa de Bicorb, trobem falles aparentment inverses però que al restituir-les en realitat són falles normals que cabussen cap al NW. Aquestes falles presenten diferències estratigràfiques en el Cretaci però probablement puguin presentar-les en materials anteriors d'acord amb els models d'extensió de una cobertora desenganxada a un nivell dúctil sobre una falla de basament (Nalpas i Brun 1993, Vendeville et al. 1995, Withjack i Callaway 2001, Dooley et al. 2003). Aquestes diferencies estratigràfiques ens permet datar la formació d›un diapir reactiu durant el Júrassic-Cretàcic. Aquest diapir reactiu es rejoveneix formant un anticlinal diapiric amb relleu positiu abans del Miocè Inferior-Mig, havent de interpretar doncs la formació d'aquest anticlinal durant la deformació compressiva paleocena causada per la Cadena Ibèrica.

Dades paleomagnètiques

El paleomagnetisme ens permet determinar la intensitat i direcció del camp magnètic terrestre en el moment de la sedimentació de la roca o bé en el moment de la remagnetització d'aquests materials mitjançant l'estudi del magnetisme terrestre romanent als diferents materials magnètics o paramagnètics. Aquest fet ens permet conèixer les rotacions que han patit els sediments.

Per tal de conèixer les possibles rotacions a l'àrea d'estudi s'han mostrejat 41 localitzacions dividides entre les diferents litologies. Del total de les localitzacions, setze 16 s'han mostrejat en els llims vermells del K3, 9 a les calcàries del Juràssic-Cretàcic i 16 més als materials detrítics del Miocè, dels quals 12 en el Miocè Inferior-Mig i 4 en el Miocè Superior.

Les mostres del Keuper presenten tres temperatures, una component viscosa de baixa temperatura que desapareix cap als 250ºC, una component de temperatura mitjana (entre 250-520ºC) i una altre component d'alta temperatura (entre 550-690ºC). Després d'aplicar la correcció tectònica s'observa que les diferents estacions s'agrupen. La component d'alta temperatura (HTC), mostra inclinacions entre 5º i 37º, i declinacions que van de 292º a 352º. Hem de tenir en compte que les direccions de referència a la Península Ibèrica són de 358.4/15.6 (α95=7) pel Triàsic superior (Osete et al 1997 i Osete i Palencia 2006) i 003.1/41.6 (α95=5.2) per el Miocè (Krijgsman et al., 1996, Pérez-Rivarés et al., 2004 i Larrasoaña et al., 2006). Tenint en compte l'error, la majoria de les mostres s'agrupen amb una inclinació corresponent al Triàsic superior i una rotació antihorària de 15-30º. Això mostra que aquesta magnetització es primària i que no ha sofert rotacions d'eix horitzontal, nomes una d'eix vertical. Pel que fa referència a la component de temperatura mitjana (ITC) mostra una declinació 286-344º amb inclinacions que van de 23-64º. Tenint en compte que la magnetització més antiga (HTC) no ha estat involucrada amb rotacions d'eix horitzontal, la ITC tampoc ho pot haver estat. Les inclinacions de la ITC són més altes que les de referència Triàsiques i més baixes que les Miocenes i per tant s'han hagut que remagnetitzar entre aquestes dues edats. Hem de tenir també en compte que entre el Juràssic i el Cretaci Inferior les declinacions varien de 18 a 34º amb relació a les del Triàsic, mentre que les mostres presentades en aquest treball suggereixen la mateixa rotació antihorària que la HTC. Així doncs la remagnetització ha de tenir lloc entre el Cretàcic Superior i el Miocè Inferior.

Les mostres d'edat Juràssica-Cretàcica tenen una desmagnetització erràtica atesa la seva baixa intensitat. Així que no s'han pogut utilitzar per extreure'n paleopols.

Les mostres miocenes tenen totes dues components, la primera viscosa de baixa temperatura i una segona component que va fins als 570ºC o 690ºC depenent de la litologia de les mostres. Les mostres localitzades al Nord de la paret salina tenen una direcció que correspon al

Miocè (003.1/41.6) mentre que les localitzades al Sud si observen rotacions. A la semifossa de Quesa les mostres es troben rotades horàriament entre 15-26º. Les situades a les semifosses de Juanera i Playamonte es troben rotades antihoràriament de 10-19º. El fet de no observar diferències de rotacions entre les mostres del Miocè Inferior i Superior de les diferents fosses ens indica que la rotació d'aquestes mostres es dóna posteriorment a la deposició dels materials del Miocè Superior.

Evolució de la Paret Salina de Bicorb-Quesa

L'estudi de l'actual estructura de la paret salina i els seus voltants junt amb la informació que hem obtingut de la geometria en profunditat mitjançant la magnetotel·lúrica i les rotacions de l'interior del diapir i els seus voltants que ens proporciona el paleomagnetisme, ens permet comprendre la història evolutiva de l'àrea d'estudi. Aquesta informació, unida als estudis tectosedimentaris previs realitzats a l'àrea d'estudi (Roca et al 1996; Anadón et al 1998), ens ha dut a diferenciar un total de set etapes de deformació. Els tres primers estadis estan relacionats amb etapes extensionals i els altres quatre corresponen al desenvolupament dels cinturons de plecs i encavalcaments Ibèric i Bètic.

Estadi de Rift Permic-Triàsic inferior

Les dades de Paleomagnetisme ens mostren variacions molt importants de gruix en la successió prejuràssica localitzada sota el Bicorb-Quesa SPS i en canvi no ens mostren cap variació sota les semifosses de Juanera i Sacarás. Aquest canvi de gruixos enregistra la primera fase deformacional de l'àrea d'estudi. Es tracta de l'estadi inicial de rifting intracontinental relacionat amb el trencament de Pangea i la divergència d'Euràsia i Àfrica (Dewey et al 1989; Malod i Mauffret 1990; Hanne et al 2003). Aquesta etapa extensional genera la formació de la falla de basament de Bicorb-Quesa, amb canvis de sedimentació al bloc inferior i superior de 1100 i

600m, respectivament. Probablement en aquest estadi també es generen altres falles de basament de la zona com les falles localitzades sota les parets salines de Xúquer i Navarrès.

Estadi de rift Juràssic-Cretàcic inferior

Aquest segon estadi deformatiu de l'àrea el trobem relacionat amb l'obertura del Oceà Atlàntic, (García-Hernández et al. 1980, Klitgorg i Schouten 1986, Ziegler 1989, Arias Abéllan et al., 1996). A l'àrea d'estudi aquest moviment el trobem enregistrat un altre cop en els materials situats al damunt de la falla de basament de Bicorb-Quesa, on la successió juràssica-cretàcica inferior té 1000m al bloc superior i 700m al bloc inferior. Aquest moviment de la falla de basament i la presencia de sal sobre aquesta generen la formació d'un plec forçat en els materials de la cobertora localitzats a sobre de la falla. Així doncs la sal acomoda la diferència de geometria entre la falla d'alt angle del basament i el plec frontissa que es genera a la cobertora (Nalpas i Brun 1993, Jackson i Vendeville 1994, Vendeville et al. 1995, Withjack et al. 2000). A sobre del bloc inferior de la falla a la zona de la xarnera superior del monoclinal del plec frontissa, es forma un diapir reactiu incipient (Nalpas i Brun 1993, Withjack et al. 2000) amb sal provinent del bloc inferior i superior (Burliga et al 2012). La formació d'aquest diapir reactiu explica l'aprimament dels materials Juràssics-Cretàcics a la xarnera superior del plec frontissa on aquest materials nomes tenen 500m de gruix. Aquest aprimament el trobem al llarg de l'anticlinal que segueix la traça del Bicorb-Quesa SPS, i que es especialment visible al sud d'aquest. Al nord del anticlinal trobem una sèrie de falles inverses però que en realitat són falles normals sobrerotades que també són coetànies a aquesta fase de rift ja que presenten gruixos diferents de materials Juràssics-Cretàcics al bloc superior i inferior.

Etapa de Post-Rift Cretàcic-Oligocè

El gruix constant dels materials del Cenomanià-Turonià ens indica que el moviment de la falla de basament en aquesta època ja ha parat. El que

no ha parat es el moviment del diapir reactiu ja que a la xarnera superior del monoclinal del plec frontissa, on s'havia generat el diapir reactiu, el gruix de la successió cenomaniana-turoniana és de 80m. Així doncs la migració de sal continua en funcionament a causa de les diferències de càrrega litostàtica que es donen a la cobertora degut a la variació de gruix estratigràfic (Ge et al. 1997; Hudec i Jackson 2007). La formació d'aquest tipus d'estructura també s'observa al bloc superior de la falla de Carroig, on la successió cenomaniana-turoniana té un gruix de 120m. Probablement té una gènesi similar relacionada amb la petita falla de basament localitzada sota la falla. Aquestes estructures es generen mentre la àrea d'estudi està immersa en un estadi de postrift (Salas i Casas 1993; Salas et al. 2001).

Estadi compressiu Paleocè

Entre el Senonià i el Miocè Inferior l'antiga zona aprimada (diapir reactiu) es rejoveneix, donant lloc a la formació d'un anticlinal amb vergència cap al sud amb flancs bastant verticals i relleu positiu. Aquest anticlinal té el seu flanc sud tallat per una falla inversa. La localització de la falla inversa i la presència de relleu positiu descarta el fet que es pugui haver produït per extensió, així que s'ha d'haver format durant una fase compressiva. La presència de la Cadena Ibèrica prop de la zona d'estudi, generant plecs i falles inverses desenganxades en el Keuper i dirigides cap al Sud durant el Paleocè i el Miocè Inferior ens suggereix que la deformació pot haver-se propagat cap al Sud fins l'àrea d'estudi. Aquesta deformació es propaga a través del nivell de desenganxament però les falles de basament que cabussen cap al nord li dificulten la propagació més cap al sud ja que actuen com a contrafort. Les dades paleomagnètiques també indiquen una mobilització de la sal, que pateix un moviment de rotació antihorària de 15-30º entre el Cretaci Superior i el Miocè, ja que es dóna després de la remagnetització de la IMT però abans de la formació dels plecs de direcció NW. Així doncs, inferim que molt probablement la rotació es produeix durant aquesta fase compressiva.

Estadi Diapiric del Miocè Inferior-Mig

La composició dels sediments (Roca et al. 1996; Anadón et al. 1998) mostra que la paret salina de Bicorb-Quesa esdevé activa i comença a créixer a la cresta de l'anticlinal prèviament format i parcialment erosionat, just abans o al temps que comença la sedimentació dels materials del Miocè Inferior-Mig a les semifosses. L'origen de la paret salina s'explica atès l'erosió de la xarnera de l'anticlinal que es generà pel rejoveniment del diapir reactiu durant el Paleocè. Però també i juga un paper important en l'activació de la paret salina la deformació extensiva causada per l'obriment del Mediterrani occidental (Roca et al. 1996; 2006). En aquest estadi es generen les fosses de Bicorb, Quesa i Juanera: el creixement del Bicorb-Quesa SPS causa evacuació de sal, especialment al bloc superior de la falla de basament que causa l'enfonsament de la cobertora, formant falles i generant semifosses, que seran omplertes per materials del Miocè inferior-Mig.

Estadi compressiu del Miocè Mig

Durant el Miocè Mig el desenvolupament de la serralada Prebètica produeix l'escurçament de la paret salina preexistent (Roca et al. 1996; 2006) produint l'escanyament del diapir i una sortida massiva de materials diapírics com indiquen els registres sedimentaris (Roca et al. 1996; Anadón et al. 1998). Un cop la paret salina s›ha tancat, la propagació cap al NNW de la deformació es centra a la zona de la paret salina degut a la seva major debilitat, i a la dificultat de la compressió a desplaçar-se pel nivell de desenganxament que es trobarà més baix degut a la falla de basament. Així doncs les parets del SPS es pleguen i posteriorment es genera un encavalcament dirigit cap al NNW, el encavalcament de Picos de la Olla, que afecta als materials del Miocè Inferior-Mig plegats per la compressió.

Altres estructures compressives a l'àrea d'estudi són els dúplex

intrasalins que afecten materials del Muschelkalk que es disposen a sobre de la sèrie del Keuper i que es troben plegats pels plecs de direcció ENE-WSW. També dintre de les roques del diapir, les formacions K2-K5 localitzades a les bores de les parets es deformen formant plecs amb direcció paral·lela a la direcció de propagació (WNW-NNW), probablement generant plecs tipus baina. Aquests plecs són clarament anteriors a la formació del diapir, a que estan tallats per les estructures de creixement de la paret salina, però posteriors a la rotació del ITC i HTC, ja que els plecs no estan rotats. Així doncs aquestes dues estructures no podem datar-les del cert i podrien ser causades per la Cadena Ibèrica o per la Bètica.

Reactivació del diapir en el Miocè Superior

Aquest és l'últim estadi de deformació present a la zona d'estudi. La paret salina creix formant dos bulbs reblerts de K1 on predominen plecs amb eixos verticals tipus cortina i zones caòtiques (probablement zones per on ha circulat més sal o bé cap-rocks). Els bulbs es troben limitats per zones de cisalla i falles. Situada entre aquests i la paret del diapir es troben materials K2-K5 afectats per plecs longitudinals (ENE-WSW) probablement formats al començament del creixement de la paret salina, ja que també afecten als plecs de direcció WNW-NNW però estan tallats pels bulbs.

Les dades paleomagnètiques miocenes ens mostren que hi ha hagut una rotació horària de la cobertora situada al sud del diapir, durant o posteriorment a la sedimentació dels materials Miocens superiors. Aquestes dades ens permeten dir que el creixement de l'actual paret salina és causada per un desplaçament cap al sud de la cobertora situada al sud del Bicorb-Quesa SPS. Aquest desplaçament de la cobertora deixaria lloc pel creixement del diapir. Aquest moviment de la cobertora també queda enregistrat per la formació de falles normals de direcció ENE-WSW que compartimentalitzen la cobertora al sud de la paret diapírica però que no

es trobem al nord de la paret diapírica. Aquesta diferenciació es deguda a la localització de les falles de basament que separen dos dominis limitats per les parets salines de Navarrès i Bicorb-Quesa i la semifossa de Sácaras. El domini situat a l'est no es desplaça mentre que el situat a l'oest es desplaça cap al SSW. Aquest desplaçament generarà una rotació horària a la zona de màxima obertura situada al sud de Bicorb-Quesa SPS i una rotació anti-horària a les zones de transferència situades a les semifosses de Playamonte i Juanera.

Influència de les falles de basament preexistents en la iniciació i reactivació de diapirs.

L'evolució de la paret salina de Bicorb-Quesa ens ha permès veure les relacions que succeeixen en un diapir format sobre una falla de basament que ha sofert una llarga etapa evolutiva on un diapir reactiu s'ha rejovenit, ha crescut, ha estat tancat i ha crescut novament. Hem pogut observar que l'evolució està molt condicionada per la presència de la falla de basament i pel nivell de desenganxament, tot i que dintre d'aquesta geometria prèvia és molt important la direcció de propagació de la deformació. En el nostre cas, durant el Paleocè la deformació es propaga en direcció a la falla de basament per sobre del bloc superior, i durant el Miocè Mig es propaga sobre el bloc inferior també en direcció a la falla de basament. A partir d'aquesta informació hem creat un model general sobre la iniciació i desenvolupament dels diapirs per compressió de pell prima generats a sobre de una falla de basament preexistent. Cal destacar que l'estructura que es generarà depèn de múltiples factors com la velocitat de deformació, el gruix de les diferents capes, la proporció de sal en el material evaporític, etc, tal i com mostren Withjack i Callaway (2000) en el seus models extensius. Nosaltres hem analitzat dos escenaris amb un nivell de sal que desacobla la deformació del basament i la cobertora. En el primer cas el nivell de sal està desconnectat entre el bloc inferior i superior de la falla de basament i en el segon, el nivell de sal està connectat.

Iniciació dels diapirs per contracció

En el cas de tenir una deformació causada per una compressió que es propaga per el bloc superior en direcció a la falla de basament, en el model desacoblat amb la sal desconnectada, la falla de basament actuarà com a contrafort. Aquest fet portarà a la formació de plecs de desenganxament i retroencavalcaments en el bloc superior o bé algun encavalcament drecera que afecti la falla de basament. Qualsevol d'aquestes estructures no propiciaran la formació de diapirs degut a l'elevat gruix de sediments situats al bloc superior de la falla.

En el cas de una deformació compressiva com l'anterior però amb un model amb la sal connectada la deformació es pot propagar per el nivell de desenganxament adaptant-se la geometria de repla-rampa-repla. Aquesta compressió portaria a la formació de un plec de desenganxament al eix superior del plec frontissa, així com a l'escanyament de la sal localitzada a la superfície de la falla de basament. Aquest escanyament provocaria la injecció de sal cap al plec de desenganxament, augmentant el plegament. Aquest plec es formaria a sobre del bloc inferior de la falla de basament on la cobertora es més prima, podent erosionar-se i formar un diapir. Aquest es el cas de la contracció paleocena-miocena inferior del Bicorb-Quesa SPS.

En el cas de tenir una deformació causada per una compressió que es propaga per el bloc inferior en direcció a la falla de basament, la deformació serà bloquejada al capdamunt de la falla de basament. Aquesta pot ser interrompuda per la falla en el cas de que la sal estigui desconnectada i per el plec forçat en el cas que la sal estigui connectada. Això ens porta a la formació de un encavalcament o un plec desenganxat proper a la xarnera del monoclinal, podent esser incrementat per la injecció de sal i per tant a la generació de un diapir.

Reactivació o escanyament per contracció

En el cas que la deformació causada per una compressió es produeixi per sobre del bloc superior en direcció a la falla de basament forçarem el tancament dels diapirs, si es troben al bloc superior. El diapir quedarà o inferior de la falla, escanyant i es produirà una gran extrusió de sal seguida per la formació de una soldadura secundària i/o una estructura "Q-tip" (Rowan i Vendeville 2006; Dooley et al. 2009). Un cop generades aquestes estructures, seran difícils de reactivar posteriorment ja que té molt de gruix sedimentari per sobre. En el cas de que el diapir es localitzes a sobre del bloc inferior si el nivell salí estigues connectat provocaria el tancament del diapir. Aquest diapir seria difícil de reactivar ja que el nivell salí es podria desconnectar degut a la compressió.

En el cas de que la propagació de la deformació es produeixi per sobre del bloc inferior de la falla, en direcció a la falla de basament, els diapirs preexistents tant en el bloc superior com inferior seran escanyats. Com en el cas anterior, formant soldadures secundàries i/o una estructura "Q-tip". Aquestes, però, només afectaran a la part superior dels diapirs, quedant els peus del diapir intactes però desplaçats i podent esser reactivats posteriorment. Aquest és el cas de la contracció i posterior reactivació del diapir de Bicorb-Quesa en el miocè Mig i Superior respectivament.

Conclusions

Tant les dades de magnetotel·lúrica com de paleomagnetisme s'han mostrat molt útils per l'estudi de diapirs. Concretament, les dades magnetotel·lúriques ens han proporcionat una imatge de la forma del basament i de les diferents resistivitats del subsòl (és a dir, dels gruixos de les diferents unitats). Les dades paleomagnètiques, per la seva banda, ens han aportat informació molt valuosa sobre les rotacions tant de la cobertora com del diapir. Gràcies a aquesta informació, junt amb la cartografia detallada del diapir i la cobertora, i la informació disponible

sobre els materials sindiapírics, ens han permès realitzar una restitució detallada i un model evolutiu de l'àrea.

Les dades de paleomagnetisme ens mostren que la paret salina es forma sobre una falla de basament que cabussa cap al NNW. Aquesta paret salina té una història de deformació complexa. La falla de basament té la màxima extensió durant l'etapa Pèrmic-Triàsic Inferior tot i que continua activa dins el Cretaci Inferior. L'activitat de la falla de basament produeix la formació d'un plec forçat dels materials Juràssics-Cretàcics sobre els materials evaporítics del Triàsic Superior-Mig. A la xarnera superior d'aquest plec, sobre la falla de basament, es genera un diapir reactiu. Durant el Paleogen l'emplaçament de la Cadena Ibèrica produeix un rejoveniment d'aquest diapir reactiu formant un plec del que s'erosiona la seva xarnera. Durant el Miocè Inferior una etapa extensiva genera la paret salina que és escanyada durant el Miocè Mig i posteriorment torna a créixer durant el Miocè Superior. Aquest darrer creixement es genera per l'extensió cap al sud de la cobertora, que genera la rotació horària d'aquesta plataforma i la compartimentalització d'aquesta.

L'anàlisi de la historia evolutiva del diapir ens ha permès comprendre la influència que juga la falla de basament en la deformació de una cobertora desenganxada sobre un nivell evaporític. Però també la importància que té la direcció de propagació de la deformació compressiva de pell fina en aquesta cobertora prèviament afectada per una falla de basament. A partir d'aquí s'han realitzat diferents models evolutius destacant la relació de la direcció de propagació de la compressió respecte la falla de basament. Els models ens mostren que en cas que la propagació sigui de bloc inferior donarà una estructura propícia per al creixement de diapirs. En canvi, si la propagació es produeix pel bloc superior, aquest només generarà diapirs en el cas que la sal estigui connectada. En relació a la reactivació de diapirs prèviament escanyats, els models indiquen una major facilitat de reactivació en els diapirs escanyats per una compressió del bloc inferior que no pas del bloc superior, ja que els que han estat escanyats pel bloc inferior conserven el peu intacte, indret per on els diapirs podran ser

reactivats.

Chapter 1

Introduction

1.1. Motivation

Salt tectonics is economically and scientifically important because some of the major oil fields are linked with geological structures generated from evaporitic materials and because of the recent interest on understanding the role of evaporitic materials in the formation of geological structures resulting from stresses. It was on the 90's when was extended the scope of salt tectonics. In this regard and from that date many published works have contributed in the knowledge of materials behavior under different settings of salt tectonics (eg. Vendeville and Jackson 1992; Jackson 1995; Letouzey et al. 1995; Ge et al 1997; Rowan et al 2004; Stewart 2006; Hudec and Jackson 2007).

The role played by a basement fault located above an evaporitic level in a detached overburden is well known (eg.; Koyi et al. 1993; Nalpas and Brun 1993; Jackson and Vendeville 1994; Vendeville et al. 1995; Stewart and Clark 1999; Withjack and Callaway 2000; Dooley et al. 2003; 2005), as the inversion of a basement fault (e.g. Letouzey et al. 1995; Stewart and Clark 1999; Krzywiec 2004; Ferrer et al. 2012). Similarly, the effect of compression on a thin-skinned overburden (Coward and Stewart 1995; Sans and Koyi 2001; Costa and Vendeville 2002) and the effect of a thin-skinned contraction on a previously existing diapir (Vendeville and Nilsen 1995; Canerot et al 2005; Roca et al 2006; Callot et al. 2007; Dooley et al. 2009). However, no studies have yet dealt with the structure generated from a contractive thin-skinned deformation above a pre-existing basement fault. Addressing this gap is precisely one of the goals of this study and the Bicorb-Quesa Diapir has proved an excellent structure for this purpose because it is located above a N-dipping basement fault and between two thin-skinned foldbelts.

The techniques applied in the study of diapirs are always very similar and comprise seismic with increasing resolution, 3D reconstruction and restitution of the structure and models both numerical and analogue. On the other hand, studies of diapirs located on the ground are made mostly from the field study of the cover, syndiapiric materials and also from the internal structure. This thesis expands the

possibilities in the study of diapirs located on the ground making use of techniques that have been rarely used in this field such as the use of magnetotelluric and Paleomagnetism. The use of these techniques is widely used in other fields of geology, but not on salt tectonics. This techniques has proven useful contributing in a new vision in this topic.

The study of the diapir Bicorb-Quesa has resulted an excellent structure for this study as it is located on the edge of two tectonic zones (Iberic Chain and Betic Chain) and has been affected by several compressions and extensions phases but preserving their traces.

1.2. Goals

The goals of this thesis can be classified in two groups: i) the aplication of different techniques barely applied in the branch of salt tectonics and ii) the effect of basement faults on the evolution of salt tectonics.

Next are expound the concrete aims of the thesis:

1.- Decipher the geometry, fault evolution and the possible irregularities of the basement located in the study area.

2.- Elaborate a geological detail mapping of the study area.

3.- Study the internal structure of the Bicorb-Quesa diapir.

4.- Study the rotations that have been occured both inside and outside the diapir.

5.-Reconstruct the diapir evolution

6.- Study the influence of a previous basement fault on thin-skinned structures.

1.3. Structure of the thesis

This thesis is presented as a compendium of papers. Its structure is next explained:

Chapter 2: Because of the limitations on the extend of the geological setting of each paper we find convenient to include in this chapter an extended introduction of the geology of the area. Nevertheless, this chapter does no present

a complete geological history of the area but contains the most important tectonic phases involved in the evolution of the diapir.

Chapter 3: Contains the scientific paper: M. Rubinat, J. Ledo, E. Roca, O. Rosell and P. Queralt. Magnetotelluric characterization of a salt diapir: a case study on Bicorb-Quesa Diapir (Prebetic Zone, SE Spain) Journal of the Geological Society January 2010 v. 167 no. 1 p. 145-153

This paper investigates about the possibility of using magnetoteluric (MT) techniques with diapir studies. To test the technique a profile that cuts perpendicularly the diapir structure was made. The profile allows us to observe the geometry of the diapir, the presence of a basement fault and the different thickness of the strata in the difernet blocks of the fault.

Chapter 4: Contains the scientific paper: M. Rubinat, E. Roca, M. Escalas, P. Queralt, O. Ferrer, J.J. Ledo Basement fault influence in the Bicorb-Quesa Diapir evolution (eastern Betics, Iberian Peninsula): contractional thin-skinned salt diapir initiation and reactivation above a pre-existing extensional basement fault. Accepted in the International Journal of Earth Science

This article details the diapir structure through a detailed overburden mapping of the Bicorb-Quesa diapir. There are also presented 8 cross-sections, 3 of which with the support of MT profiles for a better understanding of the basement and overburden structure. Analysis of MT data enables us to distinguish between the different tectonic events occurred in the area and facilitates the accomplishment of a working model for a basement fault which has underwent compression on different directions.

Chapter 5: Contains the scientific paper: M. Rubinat, E.Beamud R. , Soto and E.Roca Paleomagnetism applied to analyse the kinematics of salt diapirs: the Bicorb-Quesa diapir (Prebetic Zone, SE Spain) submitted in the Journal of Structural Geology.

This paper makes a thorough study the internal structure of the diapir. This information and the rotations of both the diapir and Miocene materials tell us the evolution of the area, especially the last evolutionary stages of the diapir rise and overburden faulting.

Chapter 6: This chapter contains a general discussion and the main conclusions obtained in this thesis.

Chapter 7: This chapter contains the Bibliography of this thesis.

Chapter 2

Geological Setting

Resum del Capítol (Summary in Catalan)

Tot i existir un apartat d'ambient geològic en cadascun dels capítols que corresponen a articles científics, les limitacions d'espai en les revistes trobem necessària una explicació mes amplia de l'àrea d'estudi i el seu context geològic ja que part de la feina realitzada es basa en la millora del coneixement de l'àrea d'estudi. A mes a més la lectura d'aquest capítol estalviarà al lector haver de llegir els geological settings que es troben situats al començament de cada article, ja que sovint parts d'aquests son comuns entre ells.

L'àrea d'estudi es troba situada al mig del domini Valencia també conegut com a Massís del Carroig, es tracta de una zona localitzada entre dos grans unitats tectòniques, la Cadena Bètica al Sud i la Cadena Ibèrica al Nord. Tot i que generalment el Domini Valencià habitualment es considerat com la zona més externa de la Zona Prebètica que es la zona més externa de la Cadena Bètica.

La serralada Ibérica es tracta d'una serralada amb doble vergència formada per la inversió de conques Mesozoiques durant l'Oligocè amb una direcció d'estructures predominants NW-SW. La Zona Prebètica es una zona de plecs i encavalcaments desenganxades del basament als materials evaporitics Triàsics.

Summary

Although the presence of a geological setting in each of the chapter that corresponds to scientific articles, the constrains of space in the journals made necessary a further explanation of the geological setting, more because of part of the work done is based on improve the knowledge of the study area. Besides reading this chapter will allow omitting read the geological settings located at the beginning of each article, because sometimes these parts are common between them.

The study area is located in the middle of the Valencian Domain, this is an area located between two major tectonic units, Betic Chain in the South and the Iberian Chain on the North. Generally the Valencian Domain is thoughtful as the most external part of the Prebetic Zone that it is the outer zone of the Betic Chain.

The Iberian Chain is a NW-SW trending mountain belt which was formed by the inversion of an intracontinental rift basin during the Oligocene. Meanwhile the Prebètics Zone is formed by a thrust-and-fold detached from the basement to Triassic evaporitic materials.

Geological Setting

The study area (Fig.2.1) highlighted by a rugged geography with shows a difference of almost 1000m of height difference between highest mountain of the area, Pico del Carroig, with 1126masl and the the village of Quesa with 220masl. It is located on the Prebetic Zone which constitutes the most external part of the foreland fold and thrust belt of the Betic Chain. The Betic Chain is located at the southern of Iberian Peninsula and joins with the African Rif form and arc-shaped orogen. The Betic Chain has been divided tradicionaly in two parts the Internal Betics and the External Betics Fig 2.2. The Internals Betics it is constituted by an allochtonous stack of thrust sheets mainly composed by Triassic and older Methamorphic rocks (e.g. Egeler and Simon 1969; Torres-Roldán 1979; García Dueñas et al 1992; Vissers et al 1995). Meanwhile the external Zone is formed by the trusting and folding of the Mesozoic-Cenozoic cover detaching on Triassic evaporite and mudstone layers from the Variscan basement in front of the migrating Internal Zone (e.g. Vera, 1983). For interested readers in the complex Betic range is possible to find more complete information in several publications (e.g. Azañon et al 2002; Platt et al 2003; Vera 2004)

The External Betic is made up of NE to ENE trending folds, NW directed thrusts and SE directed back-thrusts (fig. 2.3. and 2.4.) (e.g., De Ruig et al. 1987; Ott d'Estevou et al. 1988; Banks and Warburton 1991; Van der Straaten 1993; Lonergan et al., 1994; Platt et al., 2003). On the External Prebetics unconformities in the stratigraphy levels has been localized and associated with stages of folding and thrusting, identifying compresionals stages dated as Oligocene-Aquitanian, Aquitanian-Burdigalian, Burdigalian-Langhian and Serravallian-Early Tortonian (e.g., Calvo et al. 1978; De Ruig et al. 1987; Beets and De Ruig 1992; Montenat et al. 1996; Roca et al. 1996)

The External Prebetic is divided in Subbetic close to the Inner zone where domain the pelagic facies and the thrust stacks and the Prebetic, located in the outers parts of the Betic Range, where domain the shallow and Marine facies. On the Prebetics the defromation decreases significantly towards the north-northwest (Figs. 2.3 and 2.4). Based on such decrease of compressive deformation, three structural domains can be distinguished in the eastern Prebetics the Internal Prebetic, the External Prebetic and the Valencian Domain (e.g. Azéma et al. 1979; García-Hernández et al. 1980; De Ruig 1992).

The strongly deformed Internal Prebetic, located southwards (Fig. 2.3 and 2.4),

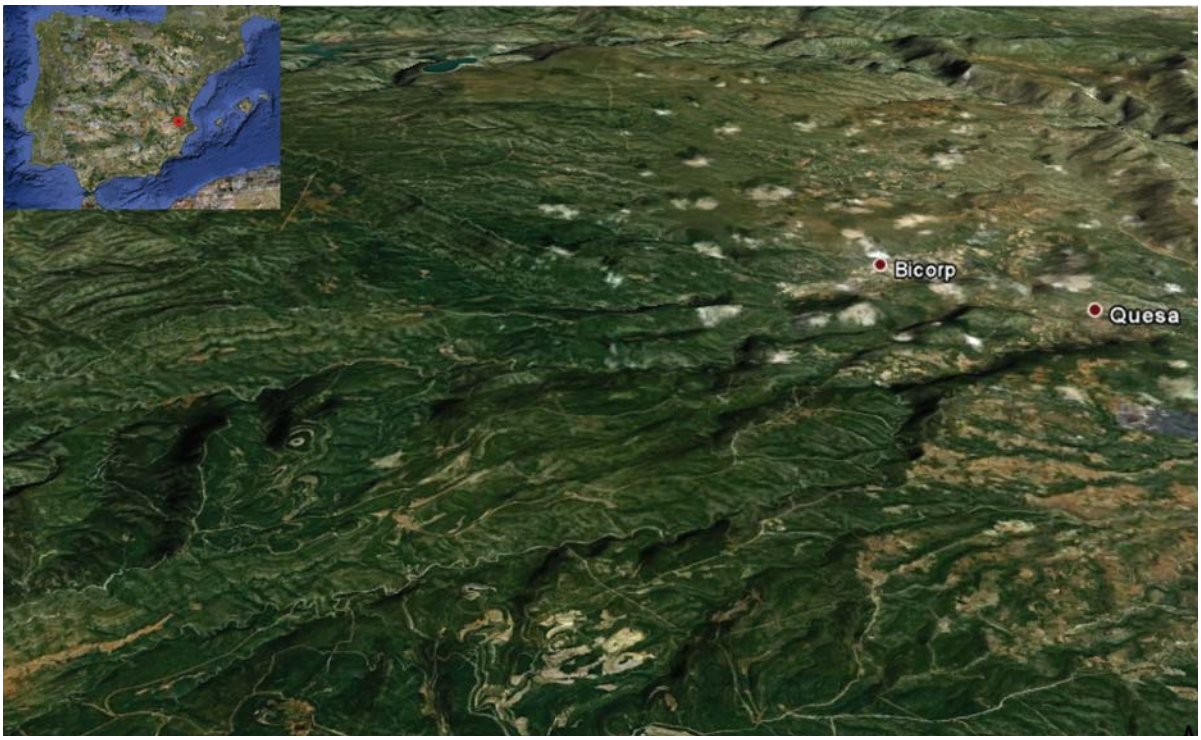

Figure 2.1. Geographic location and morphological appearance of the studied area. (satellite images from Google Earth).

which shows a complex structure with a large variety of orientations of fold and faults that can be agruped in three main trends: 1) the Betic trend with a trends of folds and faults that varies from -ENE to -NE where the folds verge predominantly northwards and have associated thrusts 2) A -NW to -WNW trending folds that are related with a dextral strike slip system (Moseley 1968; De Ruig 1992) 3) Structures trending to -N, -NNE which are located on the east and are composed by faults west vergent,

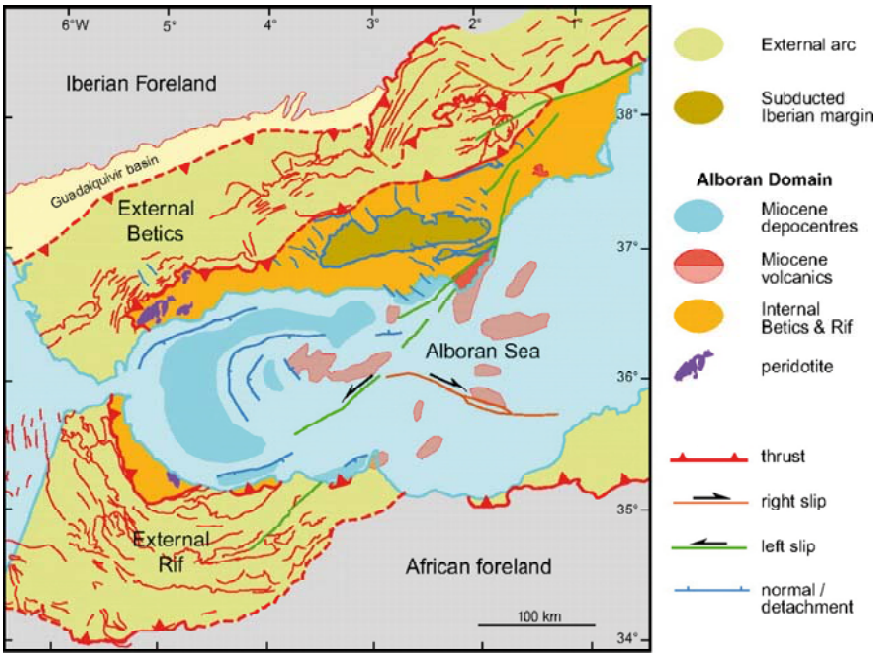

Figure 2.2. General map of the Betic Chain, showing the different tectonic units and a general distribution of the materials. Modified from Platt 2007

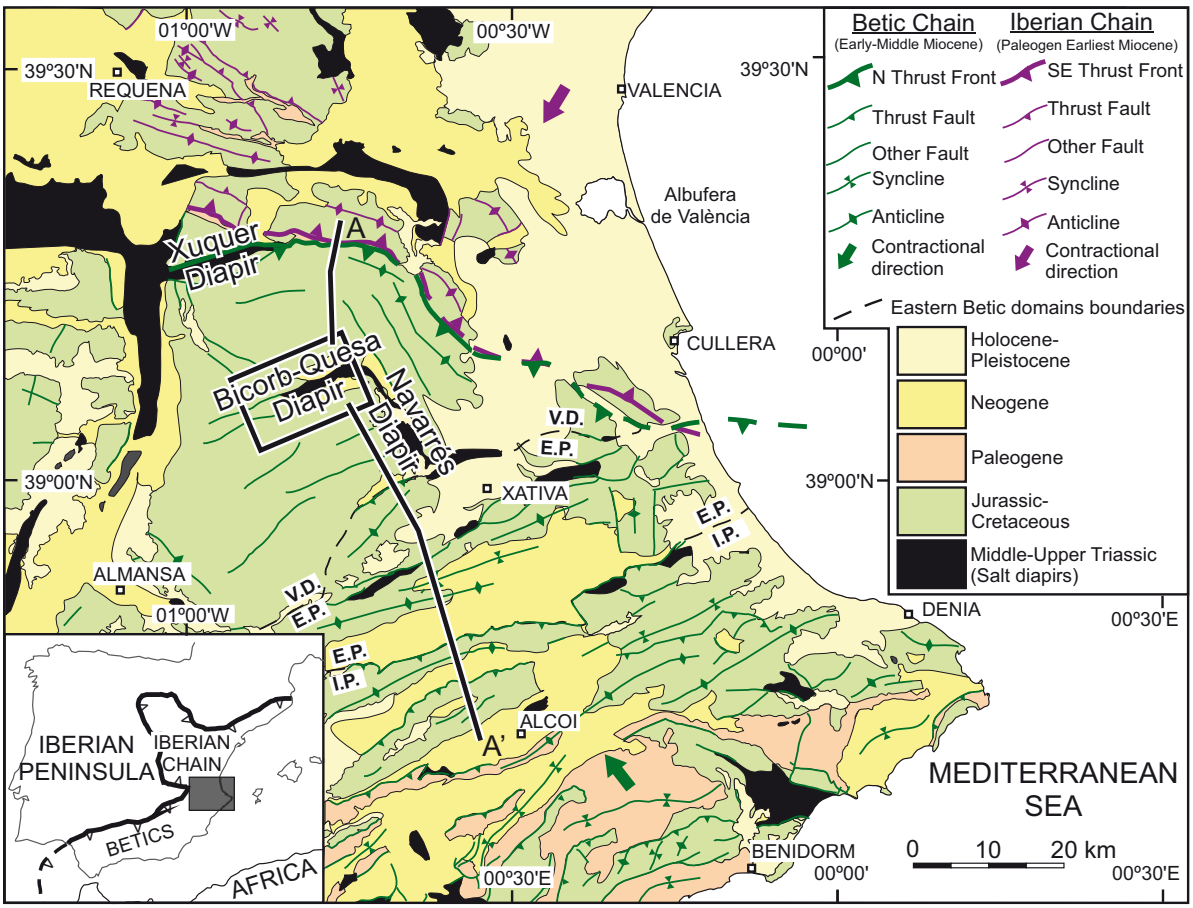

Figure 2.3. Geological map of the eastern Prebetic Zone and adjoining south-eastern part of the Iberian Chain (SE Spain). Note the different age and opposite sense of the deformation propagation in the Iberian and Betic chains. I.P. means Internal Prebetic, E.P. External Prebetic and V.D. Valencian Domain. A-A': location of the cross-section shown in Fig. 2.4. Black box: location of study area (Fig. 2.11).

minor trust and drextal strike slip faults (De Ruig et al. 1987; De Ruig 1990). Further there are also present, specially on the western area, complex diapiric fault zones which elongate and narrow diapirs that divide the overburden in rectangular segments. These diapirs assume part of the compression stating that are previous to the betic compression (De Ruig et al 1992).

The External Prebetic is characterized by ENE-trending box anticlines separated by broad synclines and cut by oblique to transverse normal faults (Figs. 2.3. and 2.4.). The anticlines are cored by Middle-Upper Triassic evaporites and mudstones, locally showing the northern limbs overturned and thrusted over the adjacent synclines (García-Rodrigo 1960; De Ruig 1992). Most of these anticlines also include squeezed diapirs in their crests. The development of these External Prebetic contractional structures is related to the moderate positive inversion of a pre-existing horst-and-graben system pierced by salt diapirs (De Ruig 1992; Martínez del Olmo 1999; Roca

et al. 2006). On the northeast of External domain the structure change showing a large dome and basin reflecting the interference between the Betic trend and the Iberian trend (De Ruig 1992).

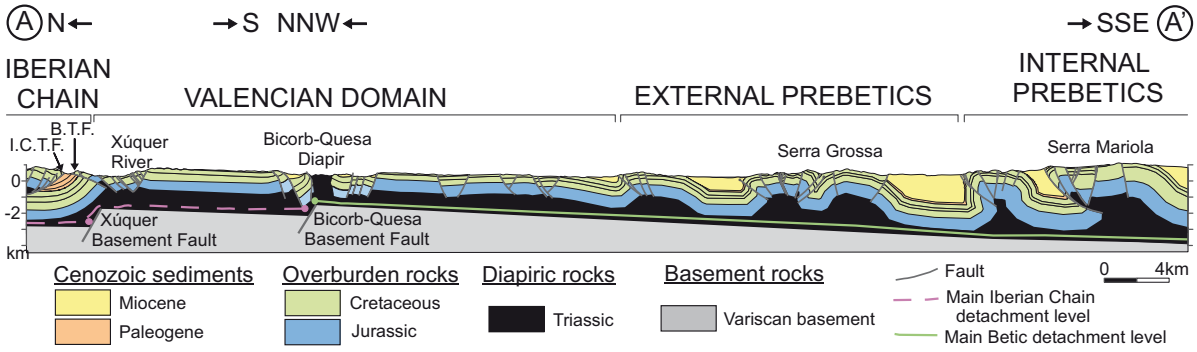

Figure 2.4. Regional cross-section depicting the main structural features of the Prebetic and Iberian Chain foreland fold-and-thrust belts (see location in Fig. 2.3). Note that N-dipping extensional fault basement faults control the location both of salt diapirs and thrust fronts (modified from Roca et al. 2006).

The Valencian Domain or Carroig Massif is characterized by a 40 km wide thrust sheet located between the Iberian Chain and the External Prebetic (Fig. 2.3), and exhibiting less than 2 km of displacement to the North (Roca et al. 2006). This thrust sheet consists of a central subhorizontal platform of 1000-1500 m thick Jurassic-Cretaceous carbonates (mainly dolostone and limestone) bounded by NNW and ENE-trending folds and thrusts at its eastern and northern boundaries respectively (Fig. 2.2). Either the platform and these folds and thrusts are cut by two nearly orthogonal sets of normal faults that strike ENE-WSW and NNW-SSE. These normal faults bound a complex system of narrow grabens that were pierced by elongated diapirs of Triassic evaporite and mudstone during the Miocene (Moissenet 1985; 1989) (Figs. 2.3 and 2.4). The grabens are usually filled by Miocene continental and lacustrine sediments that depict growth strata geometries thinning towards the diapir walls (Santisteban et al. 1989; Roca et al. 1996; Anadón et al. 1998). One of the salt diapirs raising along the axis of these grabens is the Bicorb-Quesa SWS, and the Navarres SWS which are the main target of this study.

At north of the Valencian Domain, is located the southern end of the Iberian Chain. The Iberian Chain is a NW-SW trending mountain belt whitch was formed by the inversion of an intracontinental rift basin. The Iberian Basin are dated between Late Permian to Late Cretaceous with a variable thickness and inverted during the Paleogene (e.g. Álvaro et al. 1979;Guimerà and Àlvaro 1990)

2.1.Stratigraphy

2.1.1.Basement

On this thesis the Variscan Basement has been considered as the metamorphic Paleozoic materials and the Lower Triassic Bundsandstain materials, due to as the tectonically as the geophysically have the same answer. Both materials are characterized by the Prebetics outcrop lack so the information comes from nearest areas as the Subetics and Iberian massif and exploratory oil well drilled during the 70' and 80'. The Paleozoic is composed by sandstones, shales and quarzites that were

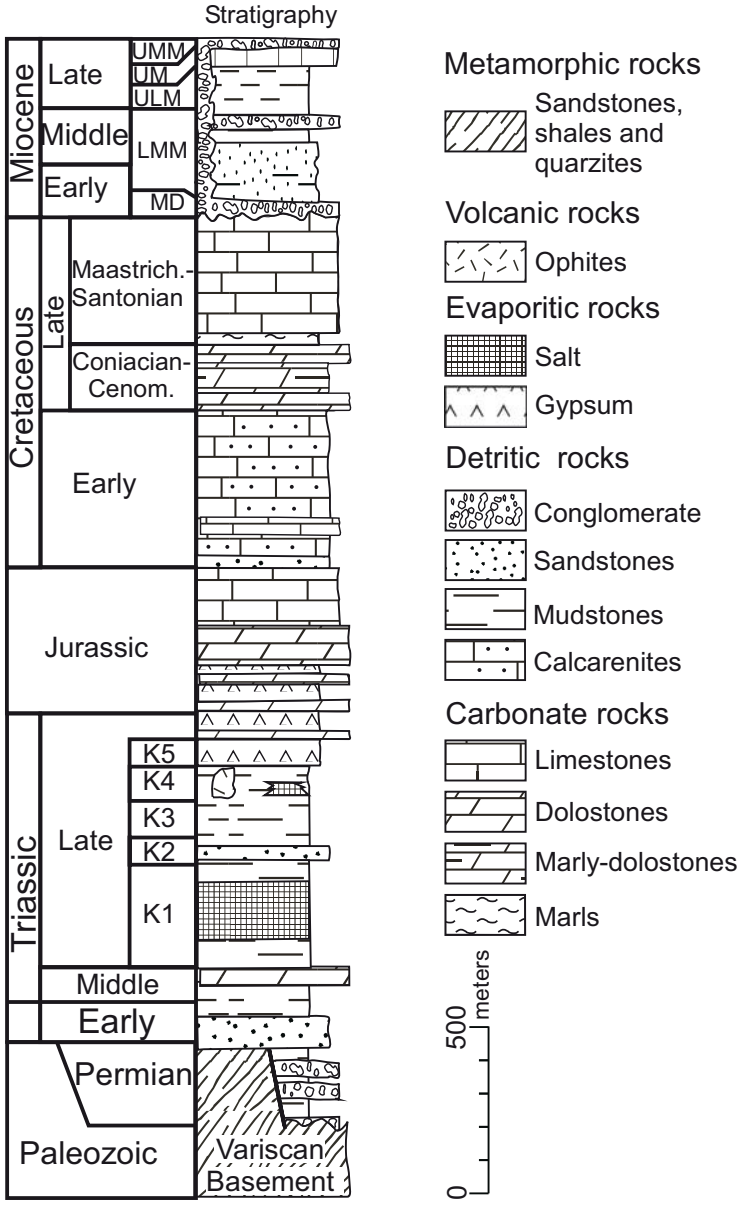

Figure 2.5. Stratigraphic sequence of all the area. MD:Marine Deposits; UMM: Upper Middle Miocene; ULM: Upperless Miocene; UL: Upper Miocene; UMM: Upper most Miocene.

metamorphised and deformed during the Late Devonian to Late Carboniferous Variscan orogeny (Bartrina et al. 1990; Martínez-Poyatos et al. 2004). The Bundsandtein is made a ca. 50-150m. of red or white sandstones with a less proportion of intercalated conglomerates and shales (Fig 2.5; Suarez Alba 2007), syn-rift continental siliciclastic rocks that were deposited during the first stages of the extensional opening of the Tethys (Arche and López-Gómez 1996; Sopeña and Sánchez-Moya 2004).

2.1.2.Diapir materials

The older materials outcropping in the study area are dolostones equivalent to Muschelkalk facies M3, corresponding to a shallow marine carbonate platform with a mean thickness of ca. 50 m (Suaréz Alba 2007), this formation is Ladinian in age (Pérez-Lopez and Pérez-Valera 2007). According with the well data the M3 is located above a ca. 30m of shale, sandstones and anhydrite, corresponding to the M2 formation (Suaréz Alba 2007). This unit is the oldest detachment level and according with the Sedimentary data (Suaréz Alba 2007) and the seismic data (Bartrina et al 1990).

The Keuper is mainly composed by continental deposits. Traditionally, it has been divided in five units (e.g. Ortí 1974; De Torres and Sánchez 1990; Ortí and Pérez-Lopez 1994) (Fig. 2.5): Jarafuel Fm. (K1) formed by grey mudstones, laminated gypsum and in less proportion carbonates and sandstones with a thickness of ca. 100-200m (Fig 2.5 and 2.6). On this unit the well data show the presence of salt, usually, that can achieve over the 200m (Ortí and Pérez-Lopez 1994); Manuel Fm. (K2) composed by red sandstones (Figs. 2.6 and 2.7), with climbing ripples his thickness is ca. 50-200m; Cofrentes Fm. (K3) made up of red and green shales that have a very consistent thickness of ca. 50m. (Figs. 2.5 and 2.7; Suaréz Alba 2007); Quesa Fm. (K4) formed by red gypsiferous mudstones and evaporates where anhydrite is more abundant than salt, the thickness ranges from ca 40m to 550m (Fig 2.8). Are very frequent the presence of bipyramidal quartz crystal “jacintos de composterla”; Ayora Fm. (K5) formed by laminated gypsum with minor levels of dolomites that have ca. 30 to 60m. (Fig. 2.5.); above the Triassic there is the Imón/Zamorano Fm. also called K6, that is a 30 m. thick Rhaetian-Hettangiensian dolostone level (e.g. Pérez-Lopez et al. 1992; Pérez-Lopez et al. 1996, Suarez-Alba et al 2007) that is possible to located inside the diapirs (Ortí 1973).

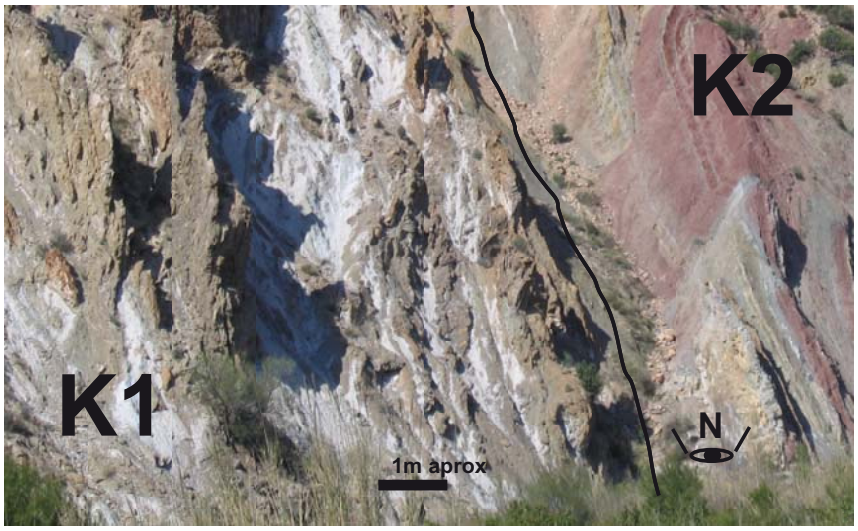

Figure 2.6.
Oblique photograph of the K1-K2 materials.

Figure 2.7.
Oblique photograph of the K2-K3 materials

Figure 2.8.
Oblique photograph of K4 materials

2.1.3.The Mesozoic overburden

The overburden rounded the diapir is formed by a sub-horizontal platform of Mesozoic carbonates. The stratigraphic sequence described in these platforms is composed by sedimentary units deposited during two different episodes: a rift event that is more localized during Jurassic and more extensive during Early Cretaceous (Hanne et al. 2003; Castro et al 2008); a post-rift event (De Ruig 1992; Hanne et al 2003). The Jurassic is composed by ca. 200m of anhidrites and ca. 500 m of Jurassic

limestone (Fig. 2.5) (Aurell et al. 2002). The Lower Cretaceous (Albian-Aptian) is made up of ca. 400 m of sediments composed by tidal and marine platforms with intercalation of fluvial and coastal sandstones (Figs. 2.5 and 2.9; Meléndez 1979; García-Hernández et al. 1980). The post-rift sequence is composed by a shallow marine sequence with a very homogeneous Turonian to Cenomanian dolostones and Senonian limestones (Martín-Chivelet et al. 2002). The dolostones have a very homogenous 200m of thickness, where is possible to distinguish a marly layer between two homogeneous dolostones layers (Figs. 2.5 and 2.9; Rios et al 1980). The Senonian limestones are partially eroded, being difficult to ascertain the real thickness. However, they exhibit a maximum thickness of 500 m in the study zone, although a thicknesses of 800 m has been described in nearby areas (García 1981).

Figure 2.9. Oblique photograph of the Lower Cretaceous to Senonian materials

2.1.4.Syndiapiric materials

Five of the half-grabens present in the study zone are characterized by the presence of syntectonic sediments. The Miocene basin-fill is similar in all of them, although the Bicorb Basin shows the most complete record for this reason we descrive it. The Bicorb basin comprises a 650 m thick sequence where is possible to distinghish:

-Marine deposits with quarsitic sandstones and conglomerates corresponding to upper Oligocene to lowermost Miocene deposits (Fig. 2.5; Anadón et al. 1994)

-The Lower-Middle Miocene unit mainly formed in alluvial environments (Santisteban et al. 1989; Anadón et al. 1994). This unit is upper Aragonian (Langhian, early Mid-Miocene) in age (Santisteban et al. 1994) is ca. 450 m thick. It is formed by a complex interlayering of red mudstones, conglomerates, and sandstones of alluvial origin, and minor lacustrine limestones (Lower-Middle Miocene (Fig2.5). The presence of resedimented keuper material "jacintos de Compostela" on different layers and rates denote different stages of the diapir evolution recording the rise and clousure of the diapir (Roca et al. 1996, 2006).

-The Upperless Miocene, comprises a transitional fluvial-lacustrine interval formed by grey and red mudstones and sandstones which is overlain by a sequence of mudstones, limestones and dolostones (Figs 2.5 and 2.10). This unit is early Tortonian or even younger (Anadón et al. 1994). Within this subunit there is an unconformity in which the sediments change their dip from 35-25º to 10-5º. On the thin sandstone beds 'jacintos de Compostela' are also described (Roca et al 1996). This unit according with the isotopic and sedimentation record was sedimented during the reactive and active stage of the diapir (Utrilla et al. 1998.)

Figure 2.10.
Oblique photograph of the Uperless Miocene materials.

-The Upper Miocene characterized by lacustrine deposits, which mainly consist of thin bedded limestones with abundant gastropods. These limestones, up to are present across the basin and close to its margins corresponding with the passive diapir according with isotopic data and sediments (Utrilla et al. 1998).

-The Upper most Miocene, a 50 m. thick alluvial sequence of conglomerates overlaid these sediments during the last stages of deformation (Fig. 2.5).

-The Quesa Basin shows a lower unit as developed as in the Bicorb basin. However, in the upper unit only the subunit A is described. In the Quesa half-graben the upper unit is present in the western termination of the basin. Regarding on the Juanera, Escalona and Bolbaite basins only the lower unit has been described.

2.2.Structure

The main target of the study is the Bicorb-Quesa SWS and its surrounding Fig. 2.11., athougth we also take in count the Navarres SWS because is perpendicular to the Bicrorb-Quesa SWS and provides interesting information on the area evolution. The Bicorb-Quesa SWS is located along the Bicorb-Quesa graben system which crosses the central part of the subhorizontal platform of the Valencian Domain following an ENE-WSW direction. It is an ENE- elongated diapir 12 km long, widens progressively from 100 m. at its western termination to nearly 2 km width to the east. (Fig. 2.11). It is composed by Middle and Upper Triassic deposits. It is surrounding by two syndiapiric half-graben the Bicorb half-graben on the North and Quesa half-Graben southwards (Fig. 2.11). The Bicorb-Quesa SWS and its basins have been studied in detail, both its stratigraphy (Ortí 1974, Santisteban et al., 1989, Utrilla et al., 1998, Anadón et al., 1998, and 2000, Peñalver and Gaudant 2010) and external geometry and evolution (De Ruig, 1992, Roca et al. 1996, 2006), just the internal diapir structure had not been studies in detail.

2.2.1.Basement

The basement on the study area was study by Carbó 1982, detecting anomalies below the Bicorb-Quesa and Navarres SWSs, however was not possible to distinghish between the salt wall anomalies and the fault anomalies. However Roca et al. 1996 detect differences of attitude between the northwest and southwest platforms assuming that this difference is caused by a basement normal fault. As happen on Bicorb-Quesa SWS the Navarres SWS seems to have a Basement fault according with the difference on the topography, with the platform located eastwards more elevated than the one located westwards. Both indicates a fault basement located below the Navarres SWS dipping towards east and raising the throw southwards. The magnetotelluric data (Fig 2.12) effectively show the presence of a 1000m vertical throw north dipping basement fault located below the Bicorb-Quesa SWS and a nearly basement flat below the Juanera half-graben and Sácaras half-graben where just can be notice the presence of a 100m vertical throw and south dipping fault below the Carroig Fault (Fig 2.12).

Above the Variscan Basement top, the thickness and structure of the overlying Permian-Lower Triassic successions cannot be directly deciphered from the available

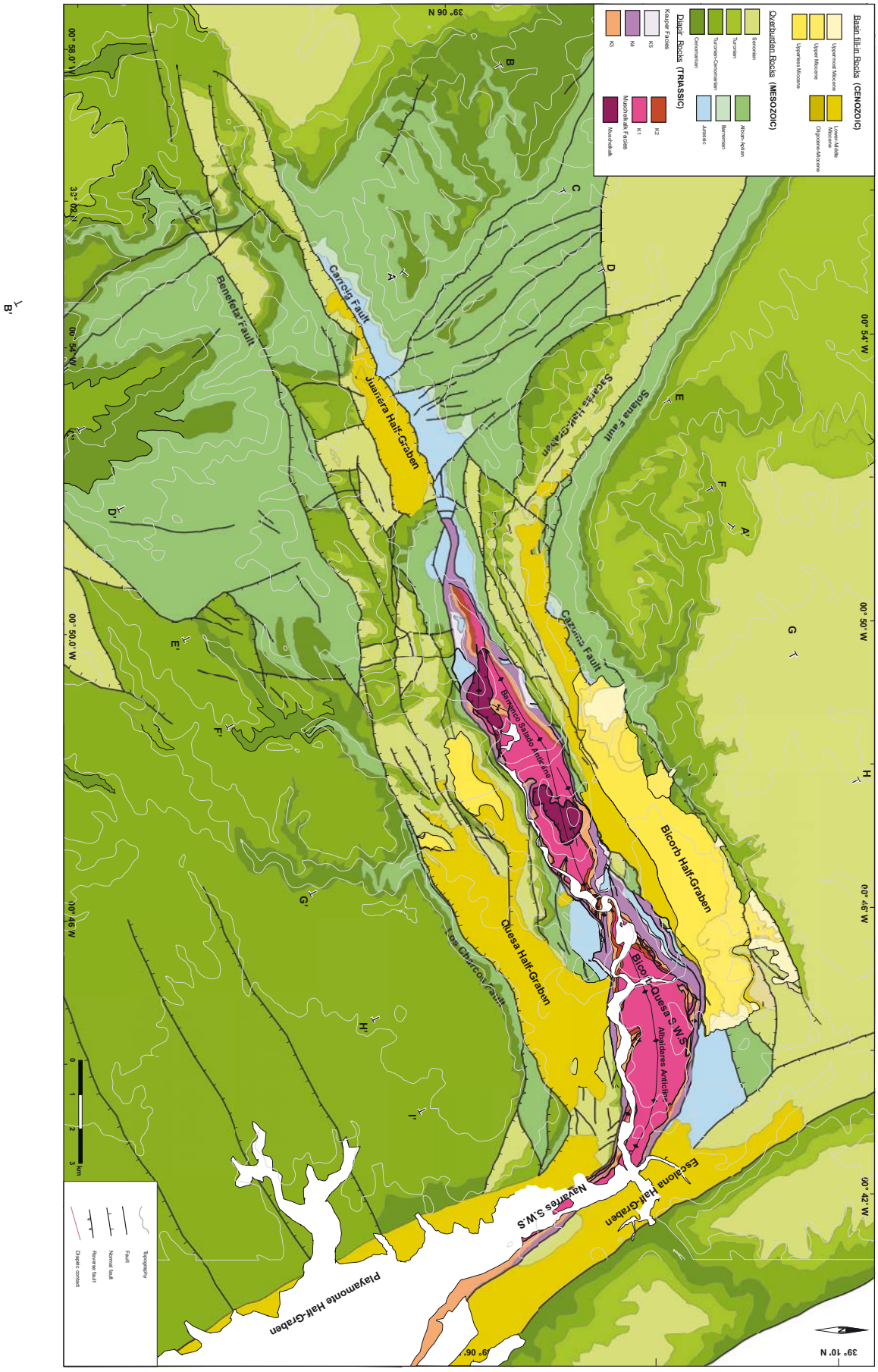

Figure 2.11. Detailed geological map of the study area. (there is in a bigger format adjoined to the thesis).

data. Both magnetotelluric and gravimetric data do not have enough resolution to distinguish these successions from the overlying Middle-Upper Triassic diapiric level. However, comparing the thickness of the "Triassic" conductor with the regional Middle-Upper Triassic thickness (about 600-800m; Lanaja 1987; Bartrina et al. 1990), we can infer that it is relatively thick (400-500m) in the hanging-wall of the Bicorb-Quesa Fault and very thin (<200m) in the remaining areas. Such changes in thickness suggest a contemporaneous extensional motion of the Bicorb-Quesa basement fault, similar to the motion described in other N- and E-trending basement faults of the Iberian Chain (Arche and Lopez-Gomez 1996; Arche et al. 2007).

2.2.2.Overburden structure

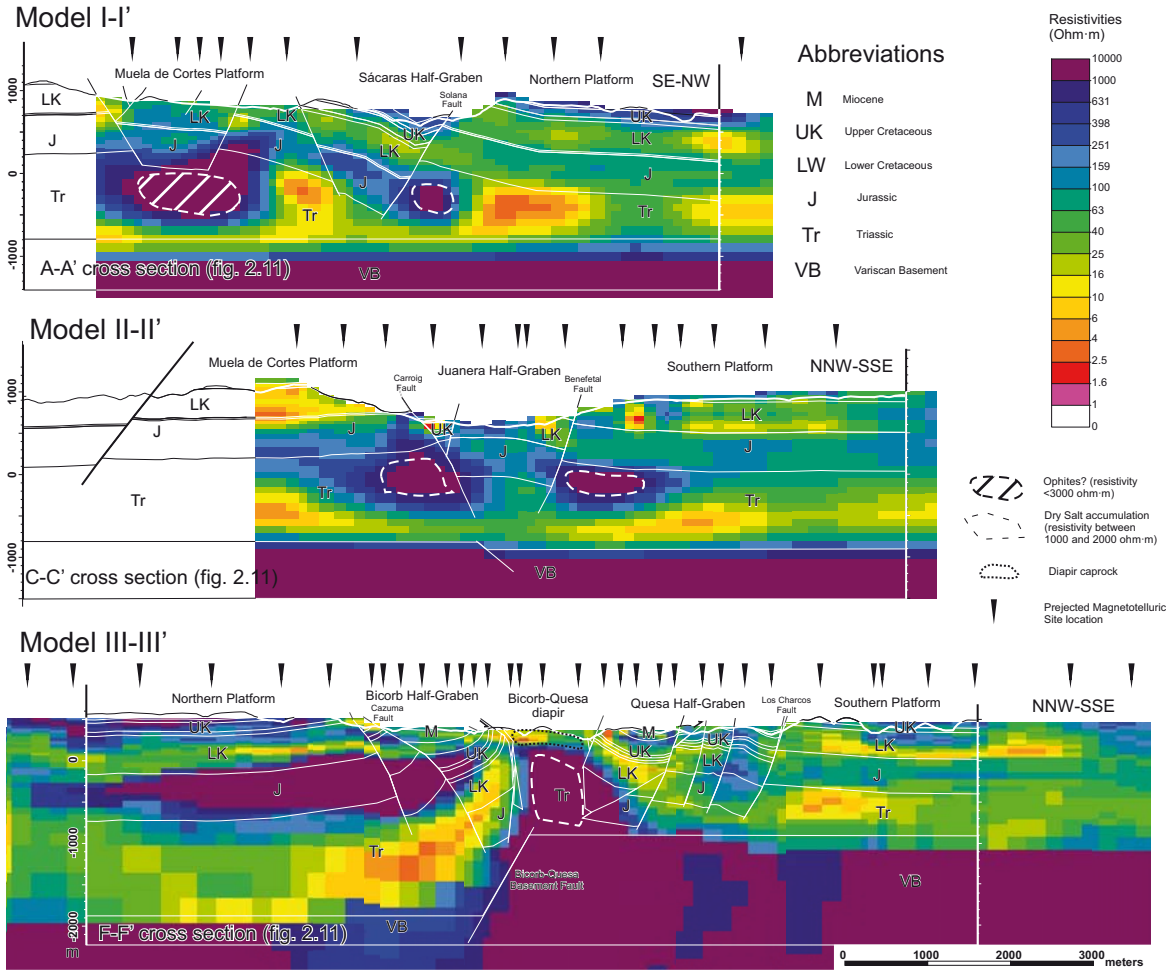

Figure. 2.12. 2D Magnetotelluric models of the study area and Bicorb-Quesa Diapir (see Fig. 2.11 for location) with the Fig. 2.13 corresponding cross-section. I-I and II-II': new models through the Sácaras and Juanera half-grabens. II published model across the Bicorb-Quesa Diapir and adjoining Bicorb and Quesa half-grabens. The vertical elongated triangles represent the projected MT recorded stations.

2.2.2.1 Northern segment (Sácaras Half-graben)

The Sácaras Half-graben system is located northwest of the western end of the Bicorb-Quesa SWS (Fig. 2.11). It is a half-graben that developed from the extensional motion of the SW-dipping Solana Fault and tilts 10-35º toward the NE of its hanging-wall overburden block (cross-section AA' in Fig. 2.13). As in the other major extensional faults cutting the overburden (the Cazuma and Carroig Faults), this hanging-wall block is deformed close to the fault by a syncline whose geometry indicates that the overburden faulting was preceded by the growth of extensional fault propagation folds. On the other side of the fault, which is the footwall block, the overburden is flexed up with a tilting that increases with the fault displacement (Fig. 2.13 cross-section AA'). This flexure, also present in all major overburden-cutting faults, is related to the inflation of Middle-Upper Triassic salt in the reactive diapirs that developed in the fault footwalls and it also produces the bending of the overlying fault surface.

2.2.2.2.Western segment (JuaneraHalf-graben)

The Juanera Half-graben (Fig. 2.11) is bounded on the northwest by a SE-dipping extensional fault. This fault, the Carroig Fault, connects with the western end of the Bicorb-Quesa SWS and depicts a dip slip which increases eastwards to up to 900-1000m close to this connection (cross-sections CC' and DD' in Fig. 2.13). The horizontal arrangement of the Variscan basement top in the magnetotelluric I-I' profile (Fig. 2.12) shows that the Carroig fault is also rooted in the ductile Middle-Upper Triassic layer. However, the higher elevation of the subhorizontal overburden in the Muelas de Cortes platform in relation to the overburden located south of the Juanera Half-graben (cross-sections CC' and DD' in Fig. 2.13) and the profile II-II' in figure 2.12 suggests that its location is controlled by the motion of an underlying buried basement fault.

The age of the Carroig Fault motion and therefore of the Juanera Half-graben has to be placed between the early-middle Miocene and the post early-middle Miocene period. This is constrained by the presence of early to middle Miocene continental deposits in the hanging-wall fault block adjacent to the fault. These deposits are cut by the Carroig Fault and the related antithetic faults meanwhile the underlying overburden is folded by the precursor extensional fault-propagation fold (syncline) (cross-sections BB' to DD' in Fig. 2.13).

Earlier than this extensional deformation, no other Alpine deformations have

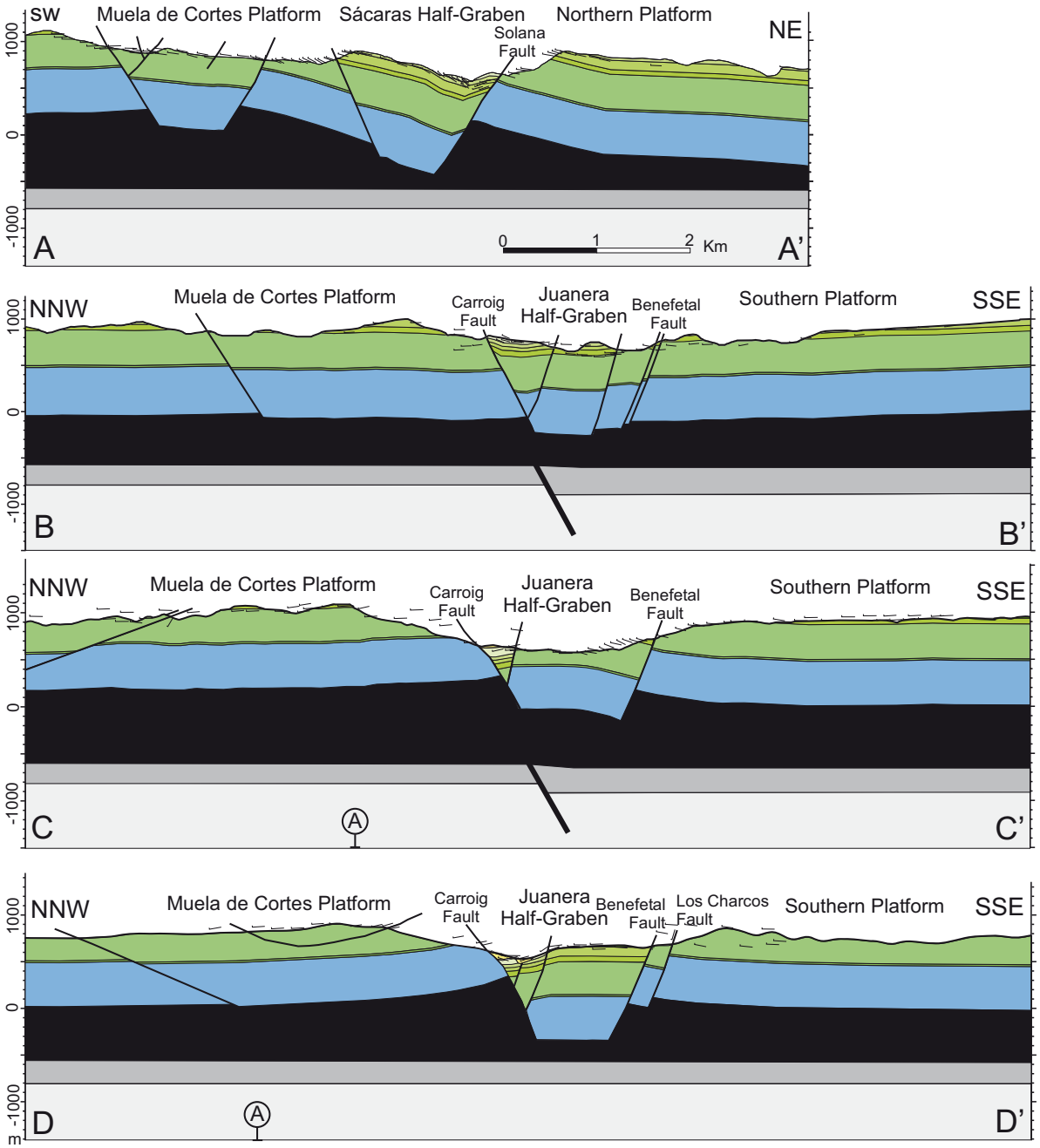

Figure 2.13. Continued on next page.

been observed in the area, except close to the Bicorb-Quesa SWS, where the unconformable arrangement of the lower-middle Miocene deposits over different Upper Cretaceous units (Fig. 2.11) points to the development of an ENE-trending Paleogene to earliest Miocene anticline. This anticline, located in the western prolongation of the Bicorb-Quesa SWS, plunges westwards and disappears beneath the Juanera Half-graben infill (Fig. 2.11).

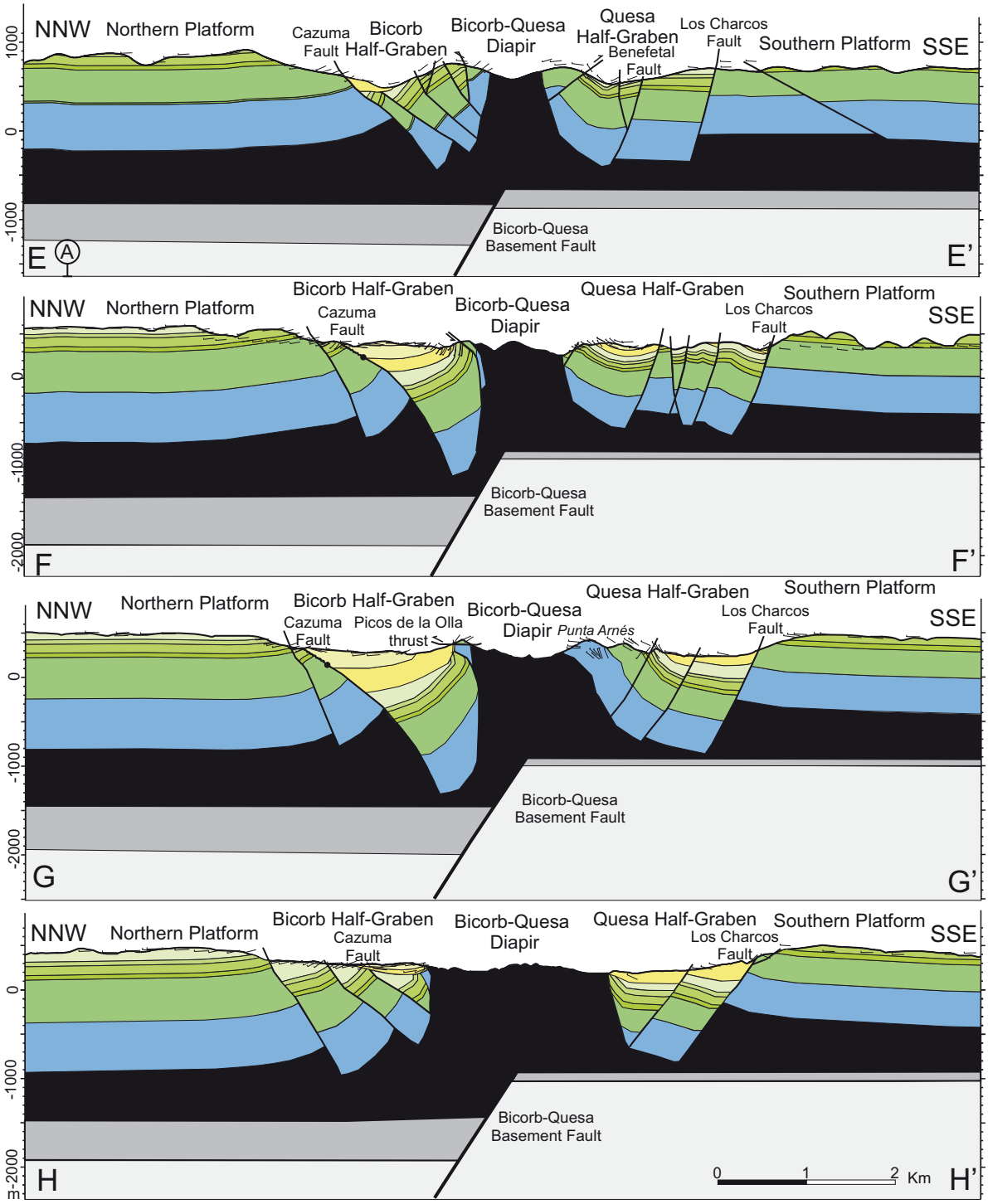

Figure 2.13. West to East serial geological cross-sections through the study area (see Fig. 2.11 for location) showing the decoupling of the deformation above and below the Middle-Upper Triassic evaporites. Note the Bicorb-Quesa Diapir development on top of an N-dipping extensional basement fault and the overburden complex structure with both contractional and extensional faults on the diapir walls.

2.2.2.3. Eastern segment (Bicorb and Quesa Half-grabens)

The geological map (Fig. 2.11) and the cross-sections EE' to HH' in Figure 2.13 clearly show that the overburden structure in this rift segment is much more complex.

In outline, it corresponds to two opposite-verging half-grabens (the Bicorb and Quesa Half-grabens) fringing a central anticline pierced by the Bicorb-Quesa SWS.

The southeastern half-graben (the Quesa Half-graben) could be considered as the eastern extension of the Juanera Half-graben (Figures 2.11). The structural polarity of faulting and tilting nevertheless is different in the two half-grabens. Unlike the Juanera Half-graben, the overburden here is mainly tilted to the southeast and the main bounding extensional fault in not located in the northwestern margin but in the southeastern one. This main extensional fault (Los Charcos Fault) dips northwestwards and connects westwards with the main antithetic fault of the Carroig Fault (the Benefetal Fault). Los Charcos Fault increases his vertical throw to the east from 350m to 900m (cross-sections DD' to HH' in Fig. 2.13) at same time that the footwall southeast tilting increases. Meanwhile in the hanging-wall, the overburden is tilted to the southeast and compartmentalized by many NW-dipping extensional faults, among which is the eastern prolongation of the Benefetal Fault. This overburden, as in the Juanera Half-graben, is also unconformably overlain by Miocene successions. On the Quesa Half-graben, it is possible to distinguish two extensional events. The last one involves all the Miocene materials, while the other only involves the Lower-Middle Miocene (dated by Ruiz-Sanchez and Santisteban 2004) (Fig. 2.11 and cross-section FF' in Fig. 2.13).

On the northern side of the Bicorb-Quesa SWS, the Bicorb Half-graben consists of a NW-tilted block bounded northwards by SE-dipping extensional faults (cross-sections DD' to HH' in Fig. 2.13). The main fault is the ENE-trending Cazuma Fault which shows a dip slip of about 1000-1300m, and it is the highest of the half-graben main faults in the study area. Its large dip slip produces salt unloading below the fault and the rise of a reactive diapir, which folds the materials located above (Vendeville and Jackson 1992). On the footwall, north of the Cazuma Fault, there are minor faults parallel to the main one. These minor faults are less folded and present less displacement (Fig. 2.13 cross-sections FF' and GG'). The Cazuma hanging-wall is NW-tilted and presents some minor extensional faults. On top of the Mesozoic materials, the Miocene sediments are disposed discordantly (Fig. 2.11 and 2.13 cross-sections EE' to HH'). The lower-middle Miocene sediments are coeval both with the extension of Cazuma Fault and with the hanging-wall faults, while the footwall faults are coeval with the upper Miocene sediments (Roca et al. 1996).

The serial cross-sections in Figure 2.13 clearly show that both the Mesozoic and the early-middle Miocene successions of the Bicorb and Quesa Half-grabens are bent up, close to the Bicorb-Quesa SWS. This bending-up is not equal at both diapir edges but much more accentuated at the northern diapir edge where the lower-

middle Miocene appears vertical or even overturned. In this last edge, growth-strata geometries date the bending-up as middle Miocene, which is more or less coeval with the emplacement of the Picos de la Olla low-angle thrust (Roca et al. 1996). This NW-directed thrust, cut by the diapir, affects the lower-middle Miocene deposits but not the younger ones (Fig. 2.11 and Fig. 2.13 cross-section GG').

Before the development of these early-middle Miocene structures, the subcrop map in Figure 8 clearly shows the presence of pre-early middle Miocene ENE-trending anticline in the present-day location of the Bicorb-Quesa SWS that had been partially or totally eroded prior to the sedimentation of the Miocene deposits. This anticline, pierced by the Bicorb-Quesa SWS, depicts a south-verging fold and has its hinge locally preserved at the southeastern flank of the diapir (Punta Arnés and Barranco Salado Alt; Fig. 2.11). The Jurassic-Cretaceous successions folded by this anticline are thinner than in the rest of the study area and are cut by pre-Miocene faults (Fig. 2.13 cross-sections EE' to HH'). These faults, in the forelimb (=northwestern part of the Quesa Half-graben), are high-angle SE-directed reverse faults formed during or after the anticline development. In contrast, in the backlimb (=southeastern part of the Bicorb Half-graben), they are, apparently, NW-directed reverse faults that are over-rotated faults and that, after unfolding the bent-up lower-middle Miocene deposits, became NW-dipping extensional faults. The age of the formation of these last faults is probably put in the Mesozoic, according to the models of Nalpas and Brun (1993), Vendeville et al. (1995), Withjack and Callaway (2001), Dooley et al. (2003). These models have the same configuration as our study area (basement, salt layer and overburden) and they show the formation of normal faults above the basement fault as well as the thinning of the overburden.

2.2.2.4. The Navarrés SWS and surroundings

The Navarrés SWS opens on the east limit of the Bicorb-Quesa SWS it is a elongated diapir with NNW- trend that spreads 15 km southwards with a constant width of 1 km (Fig 2.3). This diapir has not been as study as the Bicorb-Quesa only Ortí (1974) works on the diapir stratigraphy and structure and Rios et al (1980) and de Ruig (1992) on the surrounding structures. This is caused because the Quaternary materials overlie part of the diapir structure (fig 2.3). The Navarres SWS is surrounded by Bolbaite Half-graben at west and Escalona half-Graben at east (Fig. 2.11) these half graven are filled by lower Miocene materials.

2.3.Bicorb-Quesa Salt Wall structure

The characterization of the internal structure of the Bicorb-Quesa SWS has been possible thanks to the variable and distinguishable stratigraphy depicted by

the Middle to Upper Triassic rocks that constitute the diapirs and salt walls of the study area (Fig. 2.11). Thus, in the Bicorb-Quesa SWS, surface mapping (Fig. 2.11) and magnetotelluric data (2.12) clearly shows that the dry salt coring the salt wall correlates at surface with the intensely folded and sheared sequences of the Keuper K1 unit.

The geological mapping of this unit as well as of the other easily distinguishable diapir-integrating units evidences that the internal structure of the Bicorb-Quesa and northern Navarrés SWSs is rather complex with variably oriented folds, shear zones and faults cut by the sheared salt wall edges (Fig. 2.11). More precisely, the mapping shows that these salt wall segments are constituted by two folded and sheared anticlines cored by Muschelkalk and/or diapiric K1 units: the Barranco Salado and Albaidares anticlines (Fig. 2.11). These two anticlines are arranged along the salt wall axis and are separated by an ESE-trending syncline in which extensionally faulted upper Keuper (K2 to K5) and lowermost Jurassic successions crop out (Fig. 2.11).

The structure of the Barranco Salado and Albaidares anticlines is very similar (fig.2.11). They are double-plunging folds fringed by outward verging synclines that disappear towards the periclinal anticline ends. Also, both anticlines are affected by the same kind of faults and shear zones. Ones developed inside the diapiric K1 unit that, trending NNE-SSW, are located along the western boundary of the outward verging synclines; and, others, parallel to the salt wall axis that get in contact the inner parts of the anticline (mainly K1 and Mushelkalk) with the folded “non-diapiric” upper successions of the Keuper (K2 to K5). These last longitudinal faults and shear bands, located close the salt wall edges, disappear at the anticline ends and show the geometry of reverse faults in the anticline areas fringed by outward verging synclines and the geometry of normal faults in the areas where the syncline are absent (this is close to the anticline periclinal ends).

The double-verging geometry of the central parts of the Barranco Salado and Albaidares anticlines as well as the presence of these two kind of bounding shear bands denotes that the development, in these anticline parts, of salt diapirs with incipient bulbs. The development of these salt diapirs is evidenced by the existence of salt springs in these areas as well as by the presence of chaotic brecciated bodies inside the K1 unit that, affected by dissolution collapse landforms, can be interpreted as cap rocks. Also it is corroborated by the analysis of 293 minor-scale fold (Fig. 2.14) and shear band data collected mainly in the diapiric K1 unit. This dataset shows that fold axes and planes dip few degrees in the periclinal anticline ends but not in the central anticline parts where they are mainly vertical or highly dipping (Fig. 2.13). This fold pattern denotes a sharp change in the salt flow along the anticlines from

horizontal in the periclinal anticline ends to vertical in the anticline parts fringed by outward verging synclines. It should be noted that the transition between these two anticline portions with a different salt flow coincides with the described NNW-trending shear zones which can be consequently interpreted as boundaries of the anticline diapiric areas.

Besides of these curtain folds derived from the vertical salt flow, the Keuper successions of both Barranco Salado and Albaidares anticlines are also deformed by other fold sets with low-dipping axes. Among them outlines the set of NNW- to WNW-trending folds that, affecting the upper Keuper (K2 to K4) successions of the anticline limbs, appears clearly depicted in the map of Fig. 2.11. These folds mainly plunge northwestwards and are cut both by the Bicorb-Quesa salt wall edges and the longitudinal faults and shear bands formed along the anticline limbs. Consequently, they must to be interpreted as folds that probably formed before or during the earlier stages of the Bicorb-Quesa salt wall development.

The Barranco Salado and Albaidares anticlines, however, are not exactly alike. The Barranco Salado Anticline includes in its outcropping inner part Muschelkalk rocks that have been not observed in the Albaidares Anticline; and this last anticline, instead, appears flanked by a set parallel narrow upright tight to isoclinal folds that are absent in the Barranco Salado Anticline (Fig. 2.11). These last folds also deform the oblique WNW to NW-trending folds and, affecting the entire Keuper succession, have sometimes overturned limbs cut by thrusts or shear zones.

As far is concerned to the Muschelkalk carbonates cropping out in the Barranco Salado Anticline, they constitute two isolated sheets that rest upon the K1 and, locally, K2 and K3 Keuper units (Fig. 2.11). Consequently, they belong to the remains (klippes) of the hanging wall of a major thrust that placed the Muschelkalk over folded Keuper units. The emplacement age of this thrust is well constrained by the geometry of the Muschelkalk klippes that are both folded by the Barranco Salado and related longitudinal folds and cut by the longitudinal faults and shears zone developed along the southern anticline limb (Fig. 2.11). These geometric relationships indicate that emplacement of this thrust took place before the development of the present-day diapir salt wall but after an older folding of the Keuper units. Taking into account this relative chronological age, the regional deformational history and the adjoining overburden structure, Roca et al (1996; 2006) suggested that this thrust emplacement occurred during the middle Miocene development of the Prebetic fold-and-thust belt just after the closure of an older diapir.

The existence of this older diapir is proved by: a) the stratigraphical and

structural features of the sediments filling the Bicorb Half-graben (Roca et al. 1996; Anadón et al. 1998); and b) the presence of a squeezed diapiric stem (locally

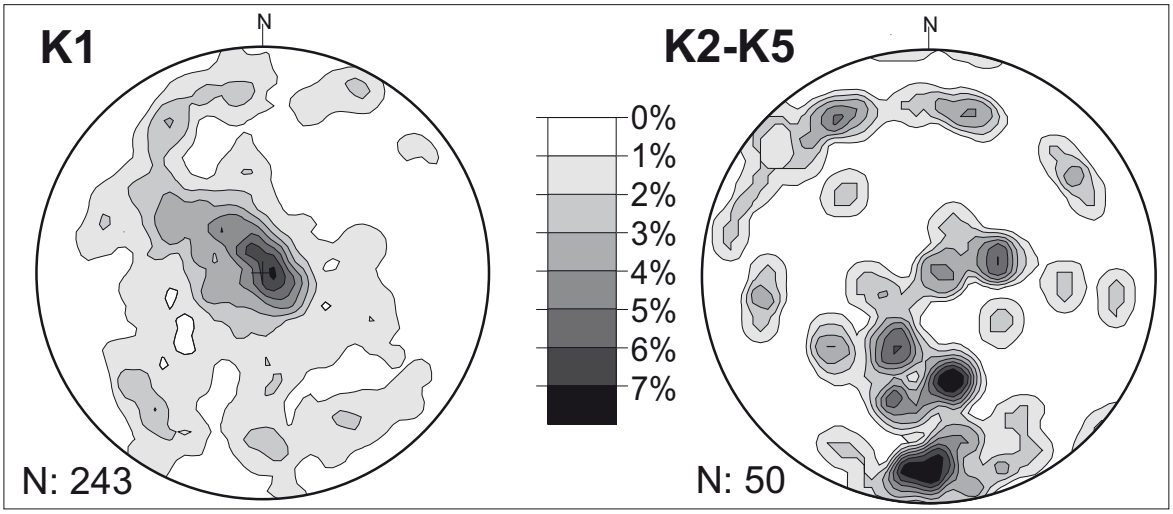

Figure 2.14. Left: fold axes measured in the K1 unit coring the Barranco Salado and Albaidares anticline culminations; Right: fold axes measured in the K2 to K5 units as well in the K1 unit outcrops located at the periclinal ends.

represented by a secondary weld) on the northern flank of the Bicorb-Quesa salt wall segment. This squeezed stem is represented by the anastomosed body of Upper Triassic rocks that crops out northwestwards of a narrow stripe of Jurassic and K5 at the northwest limb of the Albaidares Anticline (Fig. 2.11). Bounded by two ENE-trending shear zones, this strongly deformed body is constituted by a mélange of the Keuper units that is thrusted by the Cretaceous successions of the Picos de la Olla Thrust. This thrust also affects the lower Miocene fill of the Bicorb Half-graben (Anadón et al. 1998) and is cut by the ENE-trending shear zone that constitutes de northwestern edge of the late Miocene Bicorb-Quesa salt wall segment. Accordingly the formation of the underlying mélange of Keuper units must be placed during the early-middle Miocene when the sedimentary record of the Bicorb Half-graben denotes an increase of salt extrusion (Anadón et al. 1998) that has been associated with a contractional diapir reactivation.

AVÍS IMPORTANT

El text del Capítol 3 ha estat retirat seguint instruccions de l'autor de la tesi, en existir participació d'empreses, existir conveni de confidencialitat o existeix la possibilitat de generar patents

AVISO IMPORTANTE

El texto del Capítulo 3 ha sido retirado siguiendo instrucciones del autor, al existir participación de empresas, convenio de confidencialidad o la posibilidad de generar patentes.

IMPORTANT NOTICE

The text of Chapter 3 has been withdrawn on the instructions of the author, as there is participation of undertakings, confidentiality agreement or the ability to generate patent

Chapter 4

The influence of basement structure on the evolution of the Bicorb-Quesa Diapir (eastern Betics, Iberian Peninsula): contractive thin-skinned deformation above a pre-existing extensional basement fault

Resum del Capítol (Summary in Catalan)

Aquest capítol conté el segon article del compendi que forma la tesis. En aquest capítol presentem dos nous perfils magnetotel.lúrics i l'estructura de la cobertora de Bicorb-Quesa. L'anàlisi de l'estructura de la cobertora i les dades de magnetotel. lúrica ens permeten realitzar una restitució de l'àrea d'estudi diferenciant set etapes tectòniques.

La primera fase tectònica es dóna entre el Pèrmic i el Triàssic Inferior, es tracta d' una etapa extensiva en la què es forma la falla de basament. La segona fase, també extensiva, es dóna entre el Juràssic Superior i el Cretàcic Inferior en què la falla de basament pateix una reactivació causada per l'obertura del Oceà Atlàntic. La localització de materials evaporítics entre el basament i els materials carbonàtics porten a la generació d'un plec d'acomodament en els materials carbonàtics. Durant aquesta fase es comença a formar un diapir reactiu a sobre de la falla de basament. Posteriorment, entre el Cretaci i l'Oligocè, durant una etapa de Post-Rift, el diapir reactiu continua evolucionant mostrant canvis de gruixos en aquests materials. Durant el Paleocè tenim el primer estadi contractiu que afecta l'àrea d'estudi, aquest estadi està causat per la compressió que produeix l'emplaçament de la Cadena Ibèrica i com a conseqüència es rejoveneix el diapir reactiu i es formen falles inverses al flanc nord del diapir reactiu. Després, entre el Miocè Inferior i Mig es produeix el creixement de la paret salina degut a l'erosió de l'anticlinal que forma el diapir reactiu i una etapa extensiva causada per l'obertura del Mediterrani. Aquesta durant el Miocè Mig és escanyada per l'emplaçament de la Cadena Bètica. Posteriorment durant el Miocè Superior la paret salina es reactiva.

Aquesta restitució de l'evolució de la zona ens permet veure que la falla de

basament i els materials evaporítics que funcionen com a desenganxament condicionen tota l'evolució posterior de l'àrea d'estudi. En aquest context té molta importància la direcció de la compressió en relació de la falla de basament. Aquestes observacions ens porten a realitzar un model sobre l'evolució de les estructures en un règim compressiu de pell prima prèviament afectat per una extensió de pell gruixuda. Aquest model posa de relleu que quan la propagació es produeix al llarg del bloc inferior hi han més possibilitats tant de formar una estructura favorable a la generació d'un diapir com a la reactivació posterior d'un diapir escanyat.

Summary

This chapter contains the second article of the thesis compendium. In this chapter we present two new magnetotelluric profiles and the Bicorp-Quesa overburden structure. The analysis of the structure and the magnetotelluric data allow us to make a restoration of the study area that leads to conclude that the study area is affected by seven tectonic stages.

The first tectonic phase consists of an extensive stage produced between the Permian and the Lower Triassic, during this phase the basement fault was formed. The second phase, also extensional, occurs between the Jurassic and Lower Cretaceous and the basement fault becomes active again because of the Atlantic Ocean opening. The evaporitic material located between the Jurassic-Cretaceous carbonaceous materials and the basement leads to the generation of a hinge fold in the carbonaceous materials. During this phase it begins the formation of a reactive diapir above the basement fault. Subsequently, between the Cretaceous and Oligocene, during a Post-Rift stage, the reactive diapir continues rising showing changes in thickness of these materials. A contractive event during the Paleocene caused by the emplacement of the Iberian Chain rejuvenates the reactive diapir and generates reverse faults on the reactive diapir northern flank. Later, between the Lower-Middle Miocene, an extensional period because of the formation of the Mediterranean opening the salt wall rise. This salt wall was squeezed during the Middle Miocene because of the emplacement of the Betic Chain. Finally, during the Upper Miocene this diapir was reactivated.

This reconstruction of the area evolution allows us to understand the importance of the basement fault, the presence of evaporitic materials and the direction of compression in the area. These observations brought to the realization of an evolution model of the structures in a thin-skinned compressive deformation affected by a previous basement fault. This model emphasizes that when the contractive deformation

occurs along the footwall there are more possibilities to develop a diapir and to reactivate a previously squeezed one.

The influence of basement structure on the evolution of the Bicorb-Quesa Diapir (eastern Betics, Iberian Peninsula): contractive thin-skinned deformation above a pre-existing extensional basement fault

M. Rubinat, E. Roca, M. Escalas, P. Queralt, O. Ferrer, J.J. Ledo

Institut GEOMODELS - Group of Geodynamics and Basin Analysis, Departament de Geodinàmica i Geofísica, Facultat de Geologia, Universitat de Barcelona, 08028-Barcelona, Spain.

Email: mrubinat@ub.edu Tel:+34 934035957 Fax: 934 021 340

Abstract: *On the basis of an analysis of structural surface data in addition to previously available and new magnetotelluric data it was possible to reconstruct the evolution of the Bicorb-Quesa Diapir. This was initiated as a reactive diapir in relation to a basement fault. The reactive diapir was rejuvenated by a thin-skinned compression during the Paleogene, and rose during an extensional early-middle Miocene phase. Later, in the middle Miocene, the diapir was squeezed and then, in the late Miocene, was extensionally reactivated. The current reconstruction allows us to analyse a diapir affected by a thin-skinned contractional deformation located on top of a pre-existing basement fault. Our study highlights the role played by the geometric relationship between the propagation direction of the cover deformation and the basement fault.*

Keywords Salt diapir, rejuvenation, contraction, extension, basement fault, Betics.

4.1.Introduction

The influence of basement extension on an overburden detached above an evaporitic layer is well known (Nalpas and Brun 1993; Jackson and Vendeville 1994; Vendeville et al. 1995; Withjack and Callaway 2000; Dooley et al. 2003; 2005), as is the inversion of a basement fault with the same configuration (Letouzey et al. 1995; Krzywiec 2004; Ferrer et al. 2012). Similarly, the effect of compression on a thin-skinned overburden (Coward and Stewart 1995; Sans and Koyi 2001) and the effect of a thin-skinned contraction on a previously existing diapir (Vendeville and Nilsen 1995; Roca et al 2006; Callot et al. 2007; Dooley et al. 2009) have been documented. However, no studies have yet dealt with the structure produced by a contractive thin-skinned deformation above a pre-existing basement fault. Addressing this gap is one of the goals of this study, and the Bicorb-Quesa Diapir has proved an excellent structure for this purpose because it is located above a N-dipping basement fault (Rubinat et al. 2010) and between two thin-skinned foldbelts.

The Bicorb-Quesa Diapir is a well-studied diapir with a long deformation history. It was initiated with the formation of a drape fold and a subsequent reactive diapir above the basement fault. Thereafter, during the latest stages of the south Iberian Chain contractional deformation, the reactive diapir was rejuvenated (in the present paper). Later, the rejuvenated diapir rose during an early-middle Miocene extensional phase and was squeezed during the north propagation of the Betic contractional deformation (Roca et al 1996; 2006). Finally, it was reactivated by means of a Late Miocene extension (Roca et al. 1996; 2006). As a result of this evolution, it constitutes an example of a salt diapir formed over a basement fault that was: 1) rejuvenated when a contractional thin-skinned deformation propagated toward the hanging-wall block of the basement fault; and 2) reactivated by cover deformations propagating in the opposite direction on the footwall block of the basement fault.

This polyphase deformation of the Bicorb-Quesa Diapir and of one of the other salt diapirs present in the eastern Prebetics foldbelt has been recognized for a long time and has been used to propose different models of diapir reactivation during later extension, shortening and strike-slip deformations (De Ruig 1992; 1995; Roca et al. 1996; 2006). However, these earlier studies did not take into account the pre-Cenozoic structure of the area and the underlying basement structure. Thus, although geophysical data indicate the presence of basement faults beneath several salt diapirs (Carbó 1982; Castaño and Carbó 1995; Rubinat et al. 2010), basement faulting was not taken into consideration. Only a purely thin-skinned extensional model was used to analyse the kinematic evolution of the diapirs.

In the present paper, we seek to improve our understanding of the relationships between the basement, salt diapir and overburden structures in the Bicorb-Quesa diapir area in an effort to shed light on the role played by a pre-existing basement fault in diapir evolution. On the basis of this analysis, a new kinematic scenario is proposed, highlighting the role played by previous basement faults in the initiation and reactivation of salt diapirs driven by a thin-skinned contractional deformation.

4.2.Geological setting and a summary of the structural evolution

The Bicorb-Quesa Diapir is located in the northeastern zone of the Prebetics (Fig. 4.1), which belongs to the most external part of the NNW-oriented foreland fold-and-thrust belt of the Betic Chain (Blumenthal 1927; Vera 1983). The Prebetics crop out widely at the eastern end of the chain where it consists of a para-autochthonous Jurassic to Miocene carbonate cover detached from an Iberian basement made up of Lower Triassic detrital rock and Variscan-deformed rock of the Paleozoic (Vera, 1983). This autochthonous Iberian basement dips a few degrees to the southeast and is cut by high-angle extensional faults in the basement (Carbó 1982; Castaño and Carbó 1995; Rubinat et al. 2010; ter Borght et al. 2011). In contrast, above the detachment level (Middle-to-Upper Triassic evaporites), the Jurassic to Cenozoic (Miocene) cover is much more deformed with box-fold anticlines, steep dipping faults and salt diapirs cored by Triassic evaporites (Figs. 4.1 and 4.2). The trend of these structures is predominantly ENE-WSW although other orientations are also present (De Ruig 1992; Roca et al. 2006; ter Borght et al. 2011).

In this deformed cover, contractional deformation is predominant and decreases significantly toward the north-northwest. This results in a tapered geometry in cross-section that thins north-northwestwards (Fig. 4.2). Recording the decrease of contractional deformation, three structural domains have been distinguished in the eastern Prebetics: the Internal Prebetics, the External Prebetics and the Valencian Domain (Fig.4.1). (For details, interested readers can see García-Rodrigo 1960; Azéma et al. 1979; García-Hernández et al. 1980; De Ruig 1992; Roca et al. 2006).

The overall structure of the Eastern Prebetics reveals a complex deformation history. During the Jurassic, it was characterized by the opening of the Tethys passive margin and it was affected by salt diapirism probably driven by gravitational failure in the internal area (Martínez del Olmo 1999). Later, an early to middle Miocene extensional phase, which was related to the opening of the Valencia trough, generated a graben system (De Ruig 1992; Santisteban et al. 1994; Roca et al. 1996; Martínez del Olmo 1999; Roca et al. 2006) and led to the triggering and development of diapirs

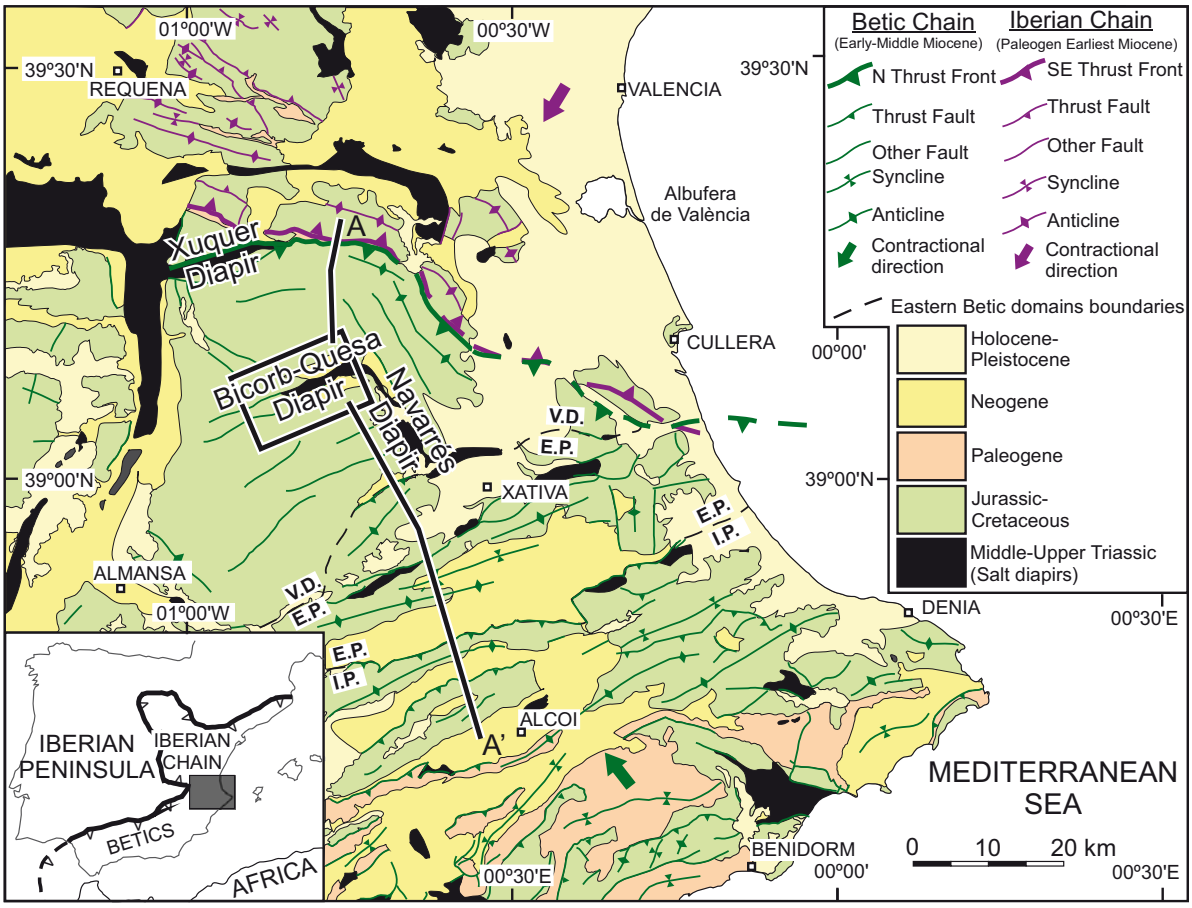

Figure 1. Geological map of the eastern Prebetic Zone and adjoining south-eastern part of the Iberian Chain (SE Spain). Note the different age and opposite sense of the deformation propagation in the Iberian and Betic chains. I.P. means Internal Prebetic, E.P. External Prebetic and V.D. Valencian Domain. A-A': location of the cross-section shown in Fig. 4.2. Black box: location of study area (Fig. 4.4).

along the graben axes (Roca et al. 2006).

Over this pre-existing structure, the building of the Betic Chain resulted in the development of a thin-skinned foldbelt detached on the Middle-to-Upper Triassic salt layer which, propagating to the northwest, led to the squeezing of the diapirs and the formation of complex contractional structures that linked them (Callot et al. 2007), the inversion of pre-existing faults, and to displacement to the north above the evaporites of the Prebetics (Roca et al. 2006). After this contractional deformation, the entire structure was affected by a younger late Miocene extension episode that generated the extensional reactivation of some pre-existing overburden faults and diapirs (Ott d'Estevou et al. 1988; De Ruig 1995; Roca et al. 1996).

To complete this geological setting of the Bicorb-Quesa Diapir emplacement, it should be noted that the northern boundary of the eastern Prebetics (the northern

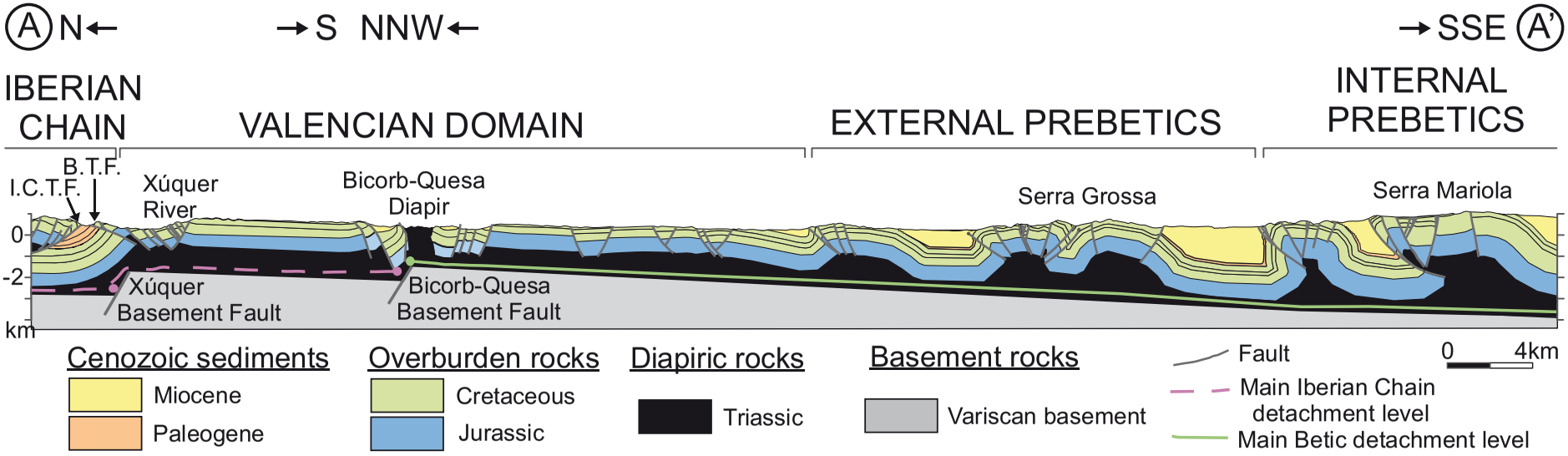

Figure 4.2. Regional cross-section depicting the main structural features of the Prebetic and Iberian Chain foreland fold-and-thrust belts (see location in Fig. 4.1). Note that N-dipping extensional fault basement faults control the location both of salt diapirs and thrust fronts (modified from Roca et al. 2006).

edge of the Valencian Domain) coincides with the southwest frontal thrust of the Iberian Chain (Fig. 4.1). The Iberian Chain is an intraplate doubly-vergent fold-and-thrust belt located in the central and eastern parts of the Iberian Peninsula (Fig. 4.1). It formed from the tectonic inversion of Late Permian-Early Cretaceous basins during the Paleogene-early Miocene times (Alvaro et al. 1979; Guimerà and Alvaro 1990) and, consequently, before the main contractional deformation of the eastern Prebetics. North of the study area, the Iberian Chain consists of a system of SW-verging thrusts and folds, which wasdetached in the Middle-Upper Triassic evaporites and also pierced by salt diapirs (Moissenet 1985; Guimerà et al. 2004). The southwest front of this system is located 15km north of the Bicorb-Quesa Diapir and consists of a SW-verging thrust detached at the Middle-Upper Triassic evaporites (Fig. 4.2).

4.3.Stratigraphy

The Variscan basement is composed of Paleozoic sandstones, shales and quartzites that were metamorphosed and deformed between the Late Devonian and the Late Carboniferous Variscan orogeny (Bartrina et al. 1990; Martínez-Poyatos et al. 2004). Above the Variscan basement, the Permian to Lower Triassic sediments are mainly made up of syn-rift continental siliciclastic rocks that were deposited during the early stages of the extensional opening of the Tethys Sea (Fig. 4.3) (Arche and López-Gómez 1996; Sopeña and Sánchez-Moya 2004).

The Middle to Upper Triassic in the eastern Iberian plate is constituted by layered evaporite sequences with platform carbonates and fine-grained detrital interbeds. In the study area, it particularly consists of a thin basal evaporite layer (Röt facies), a 50-200m thick succession of Middle Triassic carbonates (Fig. 4.3) (Muschelkalk facies; Suarez Alba 2007) and a 600-700m thick succession of continental evaporites and fine clastics that are Upper Triassic in age (Keuper facies) (Bartrina et al. 1990; De Torres and Sánchez 1990). In this upper succession, salt is abundant and, on the basis of the predominant lithology, three stratigraphic units have been distinguished (Ortí 1974; Ortí and Salvany 1990): a Lower Evaporite Unit, formed by thick salt-layered sequences with thin interbeds of grey gypsiferous marls, sandstones and carbonates; a red Mid-Detrital Unit, composed by sandstones and mudstones; and an Upper Evaporite Unit, formed by salt, gypsum and red gypsiferous mudstones (Fig. 4.3).

On top of the ductile-deformed Middle-Upper Triassic, there is a 1500-1700m thick overburden made up of a Jurassic-Cretaceous carbonate-dominated sequence

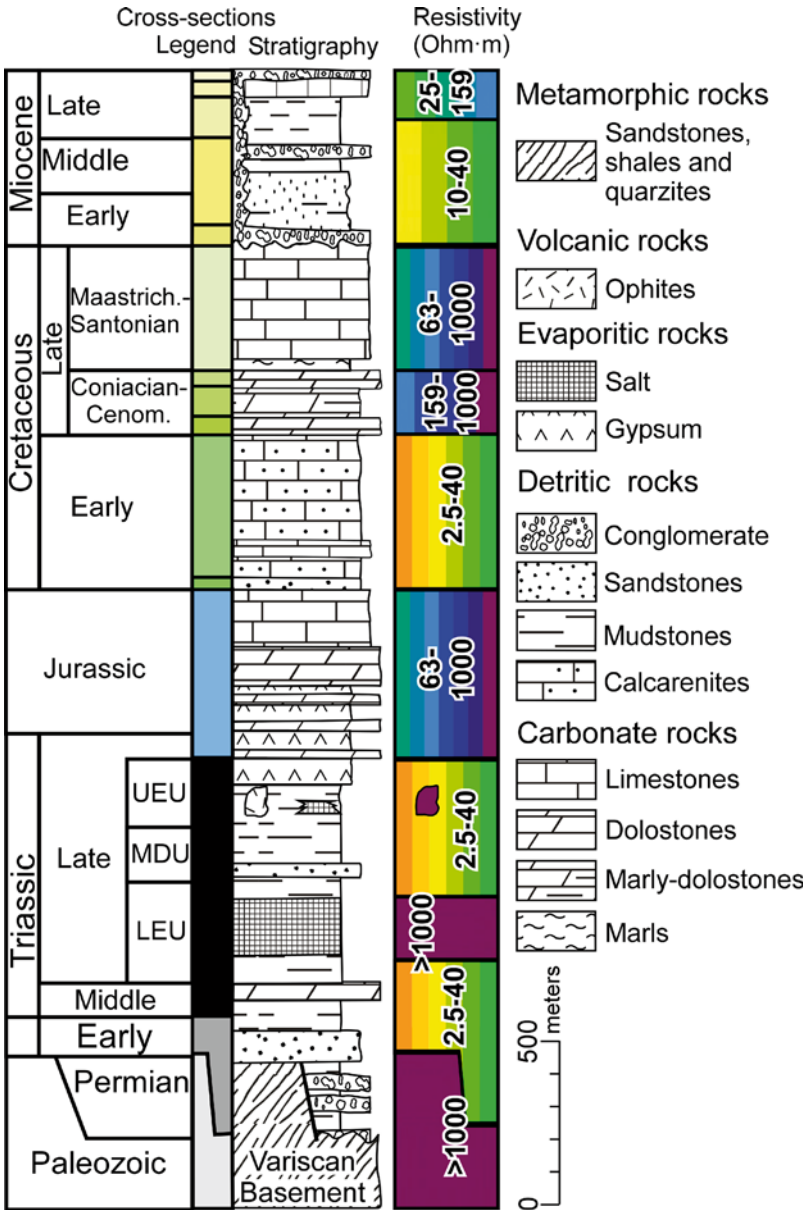

Figure 4.3. Stratigraphic chart of the study area with the map and cross-sections colour legend used for each differentiated unit, as well as the corresponding resistivity interval

(Meléndez 1979; Rios et al. 1980 Garcia et al. 1981; Lanaja 1987). This overburden is unconformably overlain by Cenozoic terrigenous successions that crop out in the half-grabens (Fig. 4.3). Although some marine upper Oligocene to lowermost Miocene deposits are present locally, most of these Cenozoic successions are early-middle to late Miocene in age and were deposited in both alluvial and lacustrine environments (Santisteban et al. 1989; Anadón et al. 1998; 2000; Fig.4.3).

4.4 The Bicorb-Quesa Diapir

The Bicorb-Quesa Diapir is an ENE-elongated salt diapir located in the central part of the Valencian Domain (Fig. 4.1). It is about 12km long and widens progressively eastwards up to nearly 2km in width at the eastern end of the diapir (Fig. 4.4). At that point, the Bicorb-Quesa Diapir joins the Navarrés Diapir, which spreads 15km southwards following a NNW trend (Fig. 4.1). To the west, the Bicorb-Quesa Diapir termination coincides with the junction of the NW-trending Sácaras Half-graben and the ENE-trending Juanera Half-graben (Fig. 4.5). These two half-grabens are in lateral continuity with the Bicorb and Quesa Half-grabens flanking the diapir and are also filled with Miocene deposits (Fig. 4.5).

The 3D structure of this diapir and the surrounding overburden and underlying basement have been analysed by means of detailed geological mapping (Figure 4.4), the construction of a series of cross-sections and the acquisition of two new magnetotelluric profiles (Fig. 4.6). Before describing this 3D structure, the main features and results of the new magnetotelluric survey are presented.

4.4.1.Bicorb-Quesa magnetotelluric data

The magnetotelluric (MT) method is a natural-source electromagnetic (EM) technique that allows us to characterize the electrical conductivity distribution of the subsurface by simultaneously measuring the time variation of the electric and magnetic fields on the Earth's surface. The penetration of the electromagnetic field is a function of the electrical conductivity of the Earth (σ) and the frequency of the signal (f). The fundamentals of the method have been extensively presented by Vozoff (1991) and Simpson and Bahr (2005).

The use of the magnetotelluric technique to determine the deep structure of the study area is not new. Rubinat et al. (2010) performed a 2D magnetotelluric model of the Bicorb-Quesa diapir that revealed its main features at depth as well as those of the adjoining overburden and underlying basement. To create a more complete image of the subsurface structure, we carried out two new magnetotelluric profiles across the western part of the study area where the Bicorb-Quesa Diapir does not crop out (Fig. 4.4). These new models (I-I and II-II' of Fig. 4.6) are based on the record of 26 new measuring stations (sites) using broadband ADU-06 MT stations from Metronix (Fig. 4.5). The sampling frequency ranged between 4096 Hz and 2 Hz. To determine the direction of the geological structures (strike) and the TE and TM modes, we applied the McNeice-Jones (McNeice and Jones 2001) multi-site, multi-frequency MT tensor decomposition based on Groom and Bailey (1989).

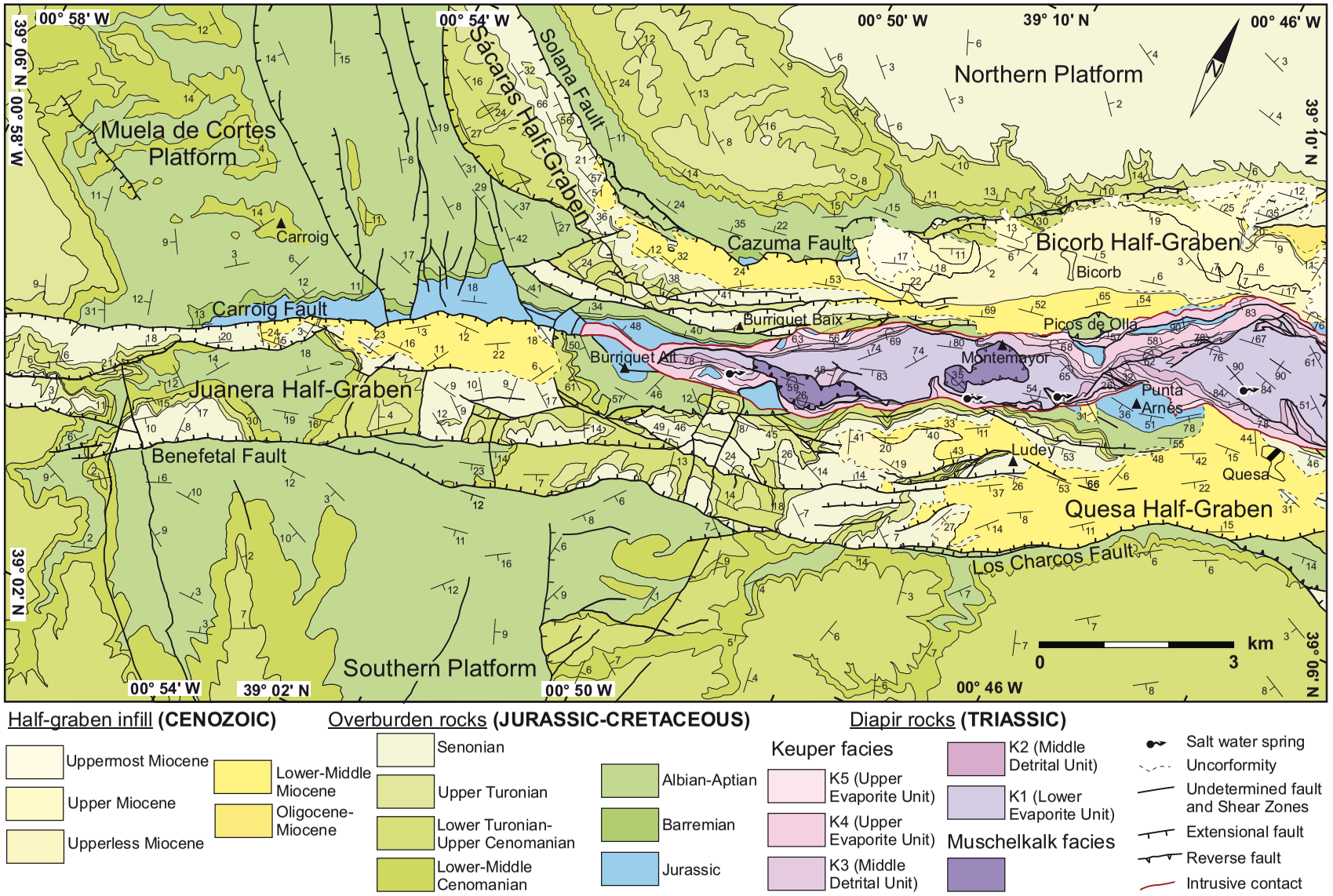

Figure 4.4. Detailed geological map of the study area.

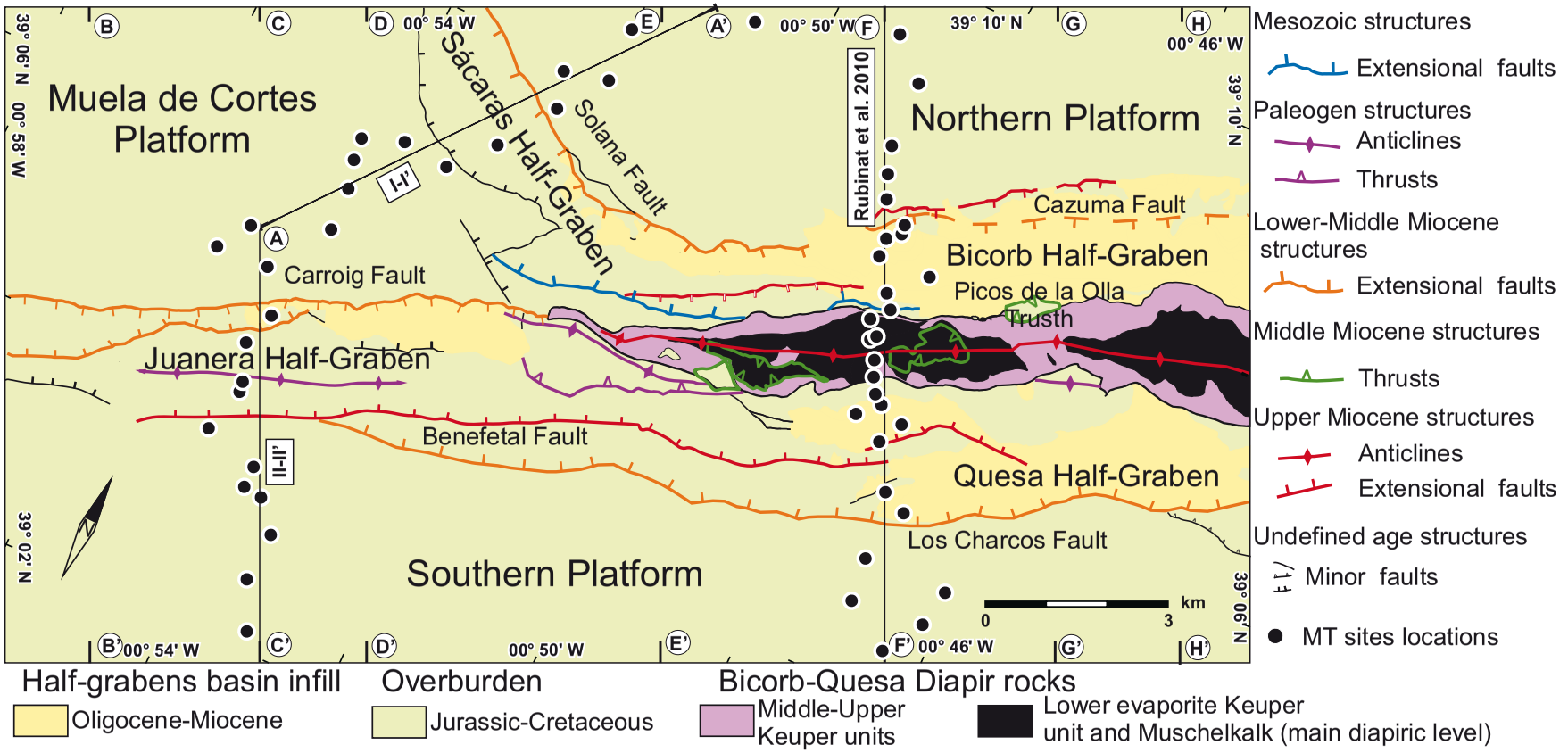

Figure 4.5. Simplified geological map of the study area with the main Bicorb-Quesa Diapir and overburden structures. Paleogene, lower-middle and upper Miocene structures are differentiated to outline the polydeformational history of the area. I-I´, II-II´ and Rubinat et al. 2010: location of the magnetotelluric models in Fig. 4.6; A-A' to H-H': location of the cross-section in Fig.4.7

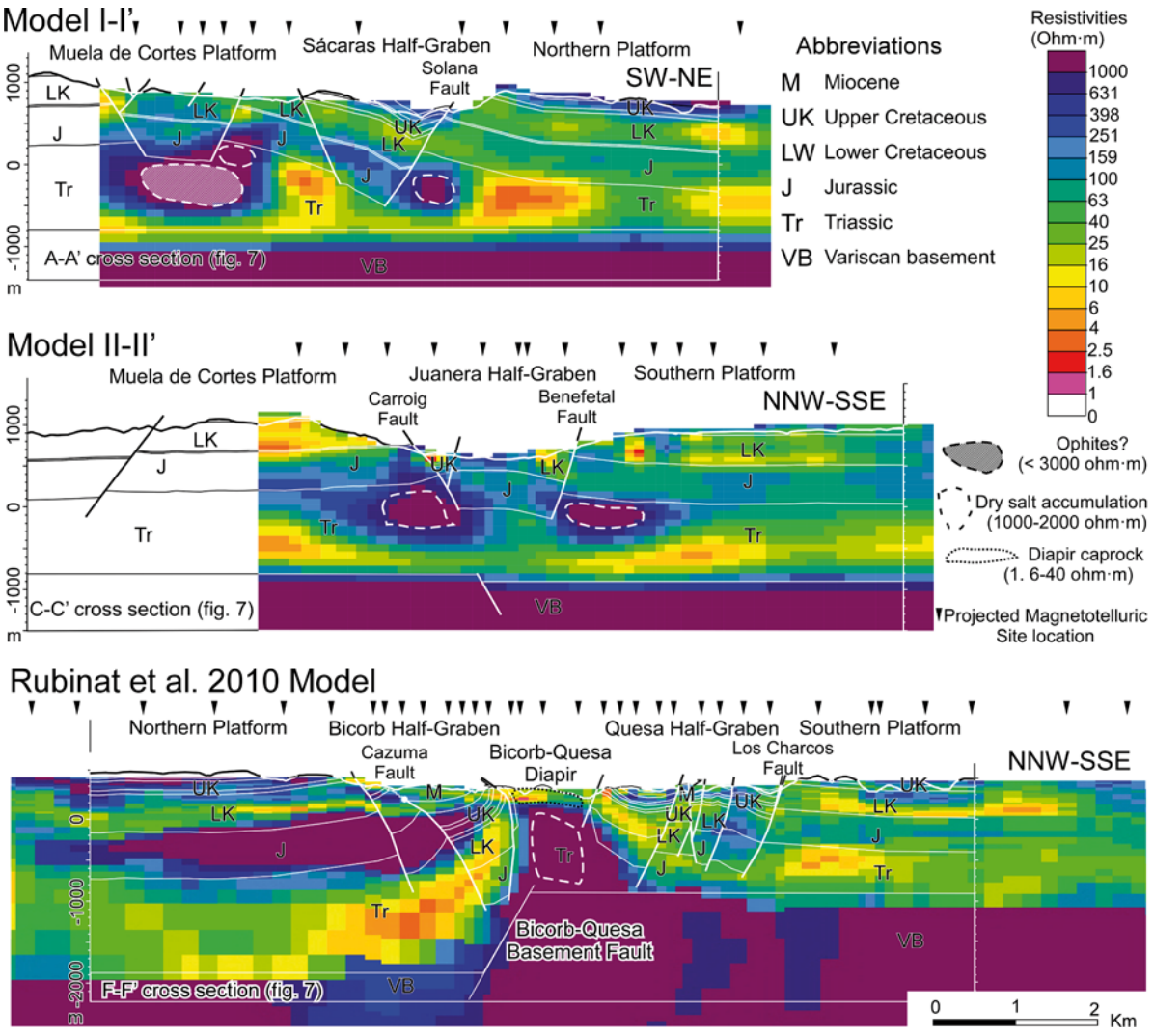

Figure 4.6. 2D Magnetotelluric models of the study area and Bicorb-Quesa Diapir (see Figure 4.4 for location) with the Fig. 4.7 corresponding cross-section. I-I and II-II': new models through the Sácaras and Juanera half-grabens. Rubinat et al. 2010: published model across the Bicorb-Quesa Diapir and adjoining Bicorb and Quesa half-grabens. The vertical elongated triangles represent the projected MT recorded stations.4

As in Rubinat et al. (2010), the analysis of the dimensionality shows a regional 2D response within the range of 0.001-1s, with some local distortion. The geoelectric strike direction of these predominant 2D structures is close to N63^0 for model I-I' and N138^0 for the model II-II', which are perpendicular to the main outcropping geological structures.

In addition, the inversion of the acquired data in these new models points to significant resistivity contrasts in the bedrock, which, when combined with the geological cross-sections obtained from field data, establishes a good correlation between resistivity and lithology (Fig. 4.3). In this correlation, the highest resistivity

values fit in with dry evaporites (salt and anhydrites), basement metamorphic rocks, volcanic rocks and dolostones, the medium resistivity values correspond to limestones, and the lowest values fit in with mudstones, sandstones and wet evaporites (gypsum and wet salt) (Fig. 4.3). As a result, the MT models provide a lithostratigraphic image that substantially helps us to better understand the structure of the Bicorb-Quesa Diapir and surrounding areas, supplying information that cannot be derived from the surface geology. The data allow us to recognize changes in Mesozoic stratigraphic thickness, determine the geometry of the basement top and decipher the motion and migration of the salt inside the diapiric rocks. In this regard, the Bicorb-Quesa MT models (Fig. 4.6) show:

The existence of an N-dipping extensional basement fault beneath the Bicorb-Quesa Diapir that was active during the sedimentation of both Permian-Lower Triassic and Upper Jurassic-Cretaceous successions (Rubinat et al 2010).

The diapiric accumulation of Upper Triassic dry salt in the core of the Bicorb-Quesa Diapir (Rubinat et al 2010) and a salt accumulation in the uplifted footwall of the main extensional faults, bounding the Juanera and Sácaras Half-grabens forming reactive diapirs (Vendeville and Jackson 1992).

The presence of an almost flat basement in the profiles that do not cross the diapir.

4.4.2.The Bicorb-Quesa structure

The structure of the Bicorb-Quesa area is strongly conditioned by the presence of a ductile and diapiric Middle-Upper Triassic level. This evaporite-detrital level decouples the deformation, resulting in a completely different structural style in the sub-salt basement (thick-skinned) and supra-salt cover (thin-skinned) deformations (Nalpas and Brun 1993; Vendeville et al 1995; Withjack and Callaway 2000; Dooley et al. 2005). The main features of these three different structural levels (sub-salt basement, Middle-Upper Triassic detachment level and Jurassic to Miocene overburden) are detailed below.

4.4.2.1.Basement structure

Their resistivity signature (Fig. 4.6) and the available gravimetrics (Carbó 1980) indicate that the Variscan basement is cut by an ENE-trending fault below the

outcropping Bicorb-Quesa Diapir. This fault, the Bicorb-Quesa Fault, sinks the NNW fault block with a vertical throw that decreases progressively westwards from about 1000 metres in the magnetotelluric profile until it disappears close to the western end of the present-day outcropping diapir (Rubinat et al. 2010). West of this location (Fig. 4.6), beneath the Juanera and Sácaras Half-grabens, the top of the Variscan basement appears nearly horizontal with a depth similar to the one observed in the SSE block of the Bicorb-Quesa Fault (900-1000m below sea level). The presence of a 100m vertical throw and south dipping fault below the Carroig Fault can be observe (Fig. 4.6 Model II-II')

Above the Variscan basement top, the thickness and structure of the overlying Permian-Lower Triassic successions cannot be directly obtained from the available data. Both magnetotelluric and gravimetric data do not have enough resolution to distinguish these successions from the overlying Middle-Upper Triassic diapiric level. However, comparing the thickness of the "Triassic" conductor with the regional Middle-Upper Triassic thickness (about 600-800m; Lanaja 1987; Bartrina et al. 1990), we can infer that it is relatively thick (400-500m) in the hanging-wall of the Bicorb-Quesa Fault and very thin (<200m) in the remaining areas. Such changes in thickness suggest a contemporaneous extensional motion of the Bicorb-Quesa basement fault similar to the motion described in other N- and E-trending basement faults of the Iberian Chain (Arche and Lopez-Gomez 1996; Arche et al. 2007).

4.4.2.2.Middle-Upper Triassic structure

The upper evaporite sequence constitutes the main décollement and source layer for diapirs in the eastern Iberian plate (Moissenet 1985; Guimerà and Álvaro 1990; De Ruig 1992; Martínez del Olmo, 1999). However, as regards diapirism, it should be noted that it seems to be triggered mainly by the salt flow of the thick salt-layered sequences of the Lower Evaporite Unit (Fig.3). In fact, although all the Middle-Upper Triassic units are present in the Bicorb-Quesa Diapir outcrop, surface mapping (Fig. 4.4) clearly shows that the dry salt coring the diapir correlates at the surface with the intensely folded and sheared sequences of the lower part of the Keuper facies (K1) as usually occurs in diapirs (Dooley et al. 2009).

The Bicorb-Quesa Diapir disappears progressively to the west and has a width of about 1km except close to the junction of the Bicorb-Quesa and Navarrés Diapirs, where it attains a width of 2km (Fig. 4.4). According to the magnetotelluric data (Rubinat et al. 2010), the cross-sectional shape of the salt wall is asymmetric, with the northern edge nearly vertical and the southern one dipping up to 50º to the south

(Fig.6). The internal structure of the salt wall is very complex with variably oriented folds, shear zones and faults that record a complex deformational history. However, the presence of a thrust with Muschelkalk materials above the diapir (Figure 4.4) leads us to deduce that this structure occurred during a compressive stage prior to the placement of the diapir.

Outside the Bicorb-Quesa Diapir, the thickness of the Middle-Upper Triassic is rather constant below the overburden horizontal platforms but not beneath the half-grabens. Here, the Middle-Upper Triassic is much thinner beneath the hanging-wall blocks of the extensional faults but thicker in the footwall of the major half-graben bounding faults. This thickening is prominent along the faults bounding the Bicorb, Juanera and Sácaras Half-grabens (the Cazuma, Carroig and Solana Faults) where the Middle-Upper Triassic is up to 700m thick (Fig. 4.7). In contrast, the thinning of the Middle-Upper Triassic beneath the half-grabens is especially conspicuous close to the Bicorb-Quesa diapir (the Bicorb, Quesa and western part of the Juanera half-grabens) where this level seems to disappear completely. The origin of these changes in thickness should be attributed to the migration of the Keuper salt, which withdrew from under the thicker overburden areas to the areas where the overburden was thinner (in the Bicorb-Quesa Diapir and beneath the extensional faults creating reactive diapirs) (Vendeville and Jackson 1992; Nilsen et al. 1995). This fits in with the magnetotelluric data which show the presence of high resistive bodies (dry salt) in the Bicorb-Quesa Diapir and beneath the main half-graben bounding faults (Fig. 4.6).

4.4.2.2.Overburden structure

4.4.2.2.1.Northern segment (Sácaras Half-graben)

The Sácaras Half-graben system is located northwest of the western end of the Bicorb-Quesa Diapir (Fig. 4.4). It is a half-graben that developed from the extensional motion of the SW-dipping Solana Fault and tilts 10-35º toward the NE of its hanging-wall overburden block (cross-section AA' in Fig. 4.7). As in the other major extensional faults cutting the overburden (the Cazuma and Carroig Faults), this hanging-wall block is deformed close to the fault by a syncline whose geometry indicates that the overburden faulting was preceded by the growth of extensional fault propagation folds. On the other side of the fault, which is the footwall block, the overburden is flexed up with a tilting that increases with the fault displacement (Fig. 4.7 cross-section AA'). This flexure, which is also present in all major overburden-cutting faults, is ascribed to the inflation of Middle-Upper Triassic salt in the reactive diapirs that developed in the fault footwalls. The flexion also produces the bending

of the overlying fault surface.

4.4.2.2.2. Western segment (Juanera half-graben)

The Juanera Half-graben (Fig. 4.4) is bounded on the northwest by a SE-dipping extensional fault. This fault, the Carroig Fault, connects with the western end of the Bicorb-Quesa Diapir and depicts a dip slip which increases eastwards up to 900-1000m close to this connection (cross-sections CC' and DD' in Fig. 4.7). The horizontal arrangement of the Variscan basement top in the magnetotelluric I-I' profile (Fig. 4.6) shows that the Carroig fault is also rooted in the ductile Middle-Upper Triassic layer. However, the higher elevation of the subhorizontal overburden in the Muelas de Cortes platform with respect to the overburden located south of the Juanera Half-graben (cross-sections CC' and DD' in Fig. 4.7) and the profile II-II' in Figure 4.6 suggests that its location is controlled by the motion of an underlying buried basement fault.

The age of the Carroig Fault motion and of the Juanera Half-graben should beplaced between the early-middle Miocene and the post early-middle Miocene period. This is constrained by the presence of early to middle Miocene continental deposits in the hanging-wall fault block adjacent to the fault. These deposits are cut by the Carroig Fault and the related antithetic faults whereas the underlying overburden is folded by the precursor extensional fault-propagation fold (syncline) (cross-sections BB' to DD' in Fig. 4.7).

Earlier than this extensional deformation, no other Alpine deformations have been observed in the area, except close to the Bicorb-Quesa Diapir, where the unconformable arrangement of the lower-middle Miocene deposits over different Upper Cretaceous units (Fig. 4.4) points to the development of an ENE-trending Paleogene to earliest Miocene anticline. This anticline, which is located in the western prolongation of the Bicorb-Quesa Diapir, plunges westwards and disappears beneath the Juanera Half-graben infill (Fig. 4.5).

4.4.2.2.3.Eastern segment (Bicorb and Quesa Half-grabens)

The geological map (Fig. 4.4) and the cross-sections EE' to HH' in Figure 4.7 clearly show that the overburden structure in this rift segment is much more complex. In outline, it corresponds to two opposite-verging half-grabens (the Bicorb and Quesa Half-grabens) flanking a central anticline pierced by the Bicorb-Quesa Diapir.

The southeastern half-graben (the Quesa Half-graben) could be considered as the eastern extension of the Juanera Half-graben (Figures 4-5). The structural polarity

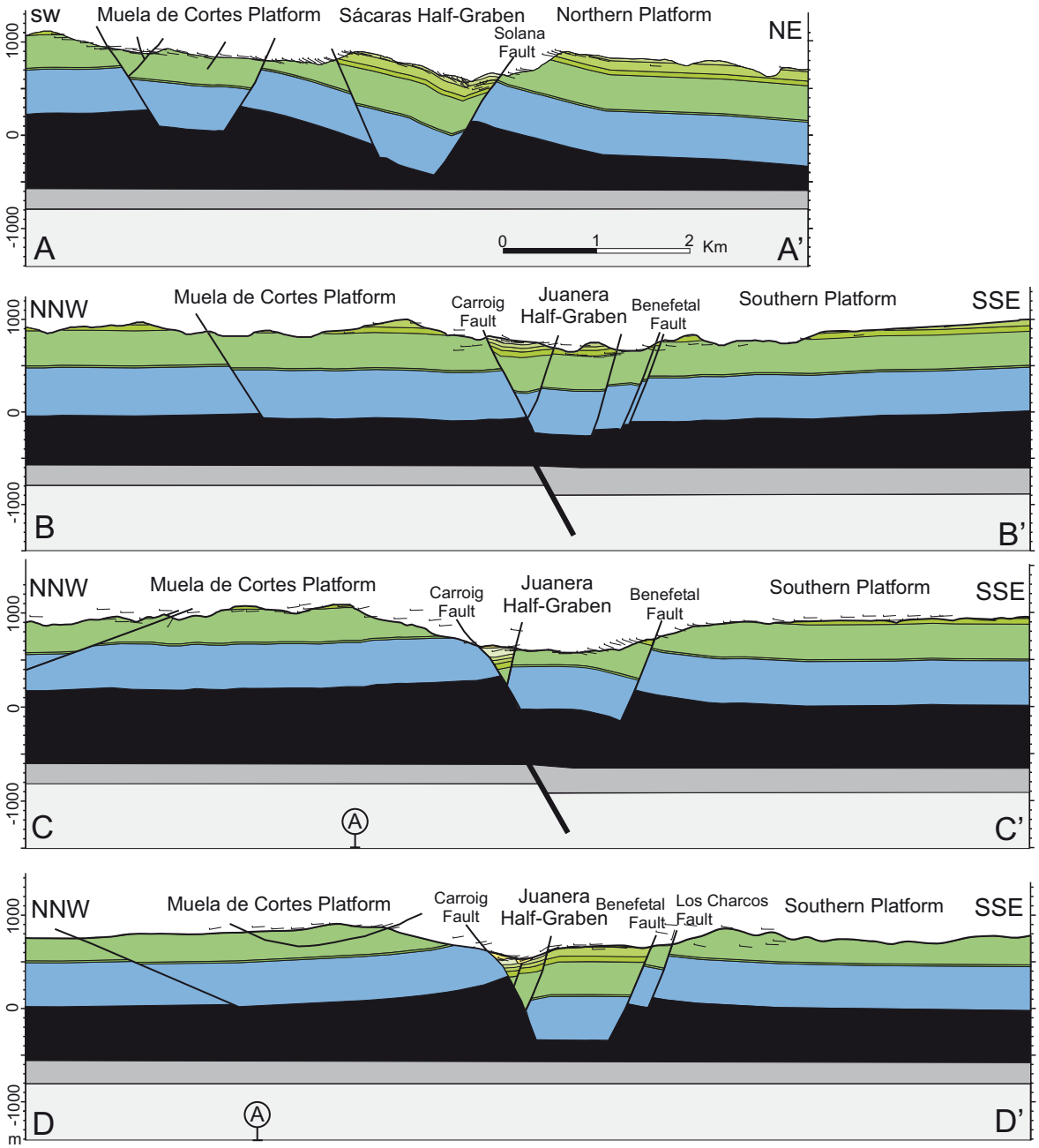

Figure 4.7. Continued on next page

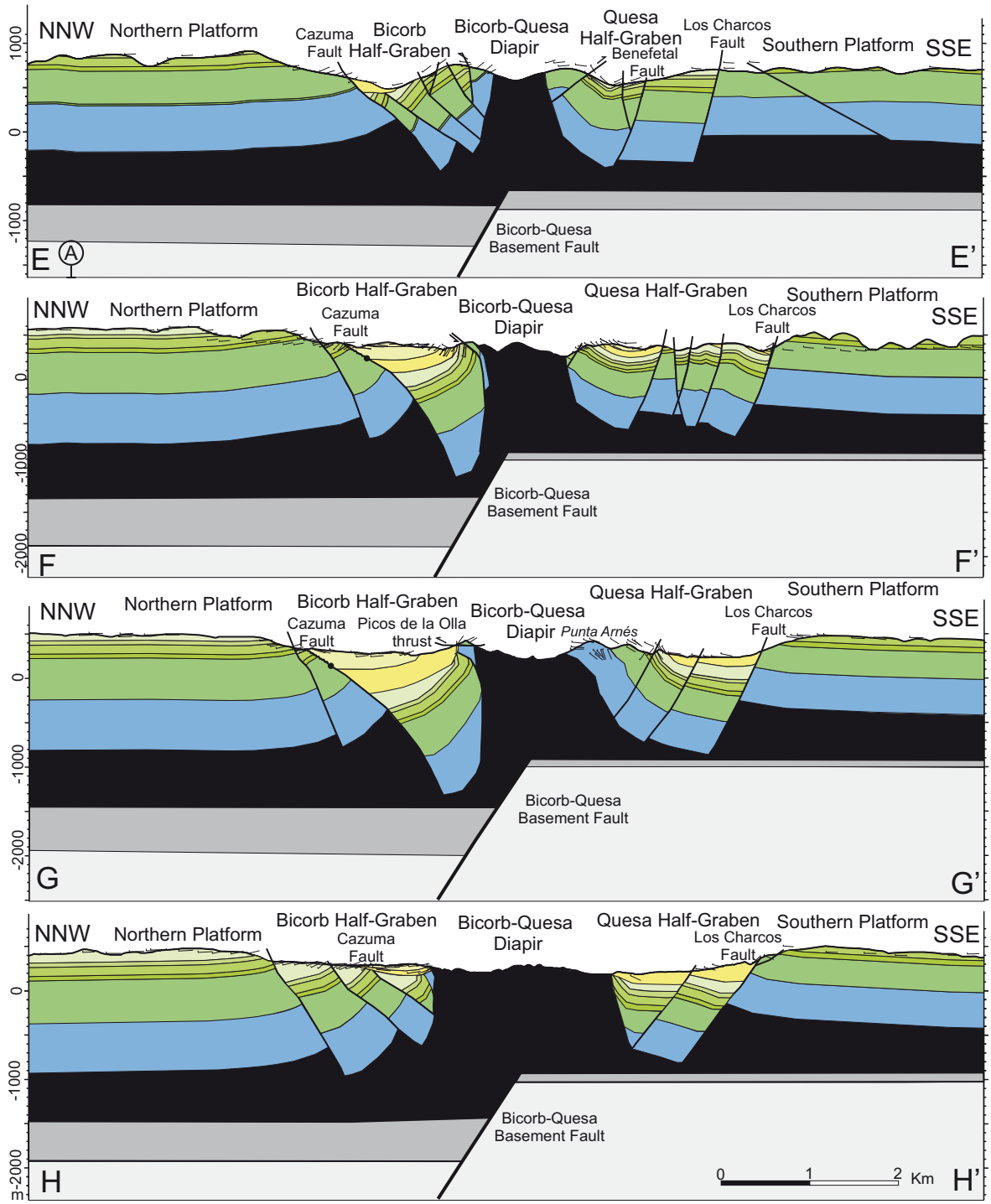

Figure 4.7. West to East serial geological cross-sections through the study area (see Fig. 5 for location) showing the decoupling of the deformation above and below the Middle-Upper Triassic evaporites. Note the Bicorb-Quesa Diapir development on top of an N-dipping extensional basement fault and the overburden complex structure with both contractional and extensional faults on the diapir walls.

of faulting and tiltingis different in the two half-grabens. Unlike the Juanera Half-graben, the overburden here is mainly tilted to the southeast and the main bounding extensional fault is not located in the northwestern margin but in the southeastern one. This main extensional fault (Los Charcos Fault) dips northwestwards and connects westwards with the main antithetic fault of the Carroig Fault (the Benefetal Fault). The Los Charcos Fault increases its vertical throw to the east from 350m to 900m (cross-sections DD' to HH' in Fig. 4.7) while the footwall southeast tilting intensifies. However, in the hanging-wall, the overburden is tilted to the southeast and compartmentalized by many NW-dipping extensional faults, among which is the eastern prolongation of the Benefetal Fault. This overburden, as in the Juanera Half-graben, is also unconformably overlain by Miocene successions. In the Quesa Half-graben, it is possible to distinguish two extensional events. The latter event involves all the Miocene materials, whereas the former involves the Lower-Middle Miocene (dated by Ruiz-Sanchez and Santisteban 2004) (Fig. 4.4 and cross-section FF' in Fig. 4.7).

On the northern side of the Bicorb-Quesa Diapir, the Bicorb Half-graben consists of a NW-tilted block bounded northwards by SE-dipping extensional faults (cross-sections DD' to HH' in Fig. 4.7). The main fault is the ENE-trending Cazuma Fault, which shows a dip slip of about 1000-1300m, and is the highest of the half-graben main faults in the study area. Its large dip slip produces salt unloading below the fault and the rise of a reactive diapir, which folds the materials located above (Vendeville and Jackson 1992). In the footwall, north of the Cazuma Fault, there are minor faults parallel to the main one. These minor faults are less folded and present less displacement (Fig. 4.7 cross-sections FF' and GG'). The Cazuma hanging-wall is NW-tilted and presents some minor extensional faults. On top of the Mesozoic materials, the Miocene sediments are disposed discordantly (Fig. 4.4 and 7 cross-sections EE' to HH'). The lower-middle Miocene sediments are coeval with the extension of Cazuma Fault and with the hanging-wall faults, while the footwall faults are coeval with the upper Miocene sediments (Roca et al. 1996).

The serial cross-sections in Figure 4.7 clearly show that both the Mesozoic and the early-middle Miocene successions of the Bicorb and Quesa Half-grabens are bent up close to the Bicorb-Quesa Diapir. This bending-up is not symmetrical along the two diapir edges. It is much more pronounced along the northern diapir edge where the lower-middle Miocene appears vertical or even overturned. Along this edge, growth-strata geometries date the bending-up as middle Miocene, which is more or less coeval with the emplacement of the Picos de la Olla low-angle thrust (Roca et al. 1996). This NW-directed thrust, which is cut by the diapir, affects the lower-middle Miocene deposits but not the younger ones (Fig. 4.4 and Fig. 4.7 cross-section GG').

Before the development of these early-middle Miocene structures, the subcrop map in Figure 4.8 clearly shows the presence of a pre-early middle Miocene ENE-trending anticline in the present-day location of the Bicorb-Quesa Diapir that had been partially or totally eroded before the sedimentation of the Miocene deposits. This anticline, which is pierced by the Bicorb-Quesa Diapir, depicts a south-verging fold and has its hinge locally preserved on the southeastern flank of the diapir (Punta Arnés and Burriquet Alt; Fig. 4.4). The Jurassic-Cretaceous successions folded by this anticline are thinner than in the rest of the study area and are cut by pre-Miocene faults (Fig. 4.7 cross-sections EE' to HH'). These faults, in the forelimb (=northwestern part of the Quesa Half-graben), are high-angle SE-directed reverse faults formed during or after the anticline development. In contrast, in the backlimb (=southeastern part of the Bicorb Half-graben), they are, apparently, NW-directed reverse faults that are over-rotated faults and that, after unfolding the bent-up lower-middle Miocene deposits, became NW-dipping extensional faults. The age of the formation of these faults is probably assigned to the Mesozoic according to the models of Nalpas and Brun (1993), Vendeville et al. (1995), Withjack and Callaway (2001), Dooley et al. (2003). These models have the same configuration as our study area (basement, salt layer and overburden) and they show the formation of normal faults above the basement fault as well as the thinning of the overburden.

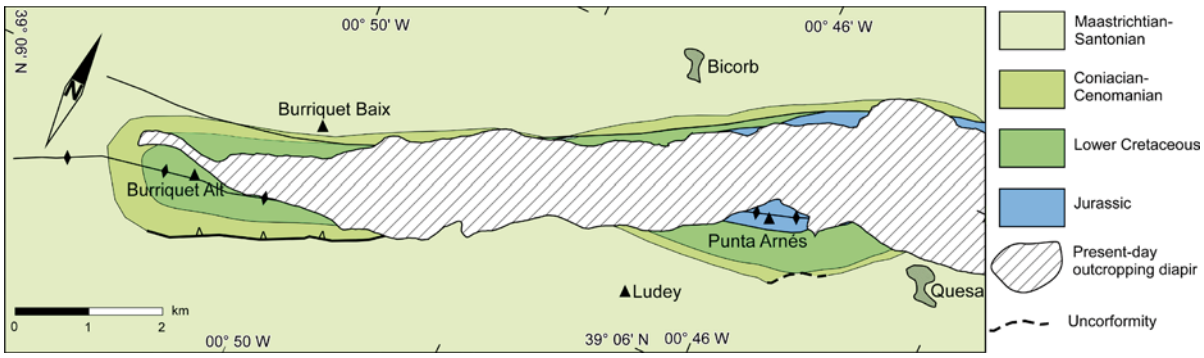

Figure 4.8. Subcrop map of the Miocene showing the pre-diapiric structure of the study area.

4.5.Bicorb-Quesa Diapir evolution

The comparative analysis of the overburden, Middle-Upper Triassic and Variscan basement structure shows that the Bicorb-Quesa Diapir developed above a NNW-dipping extensional basement fault with a complex deformational history that includes both contractional and extensional diapir reactivations. This story begins with the formation of a drape fold above the basement fault, which plays an essential role in the subsequent development of the area structure.

Specifically, our structural observations, combined with the tectono-sedimentary information provided by the Miocene deposits (Roca et al. 1996; Anadón et al. 1998), allow us to establish that the present-day structure of the Bicorb-Quesa Diapir is the result of a complex Alpine evolution with seven major deformational stages. The first three stages are linked to the Mesozoic extensional opening of the Tethys Sea and the other three to the development of the Iberian and Betic thrust-and-fold belts (Fig. 4.9).

4.5.1.Permian-Early Triassic rift stage

This is the first Alpine deformational stage observed in the study area and it corresponds to the extensional stage in which the NNW-dipping Bicorb-Quesa basement fault was formed. The extensional motion of this fault during the Permian-Early Triassic period is evidenced by the variations in thickness of the pre-Jurassic successions which, according to the magnetotellutic data, are much thicker in its hanging-wall (1100m) than in its footwall (600m). The parallel extensional basement fault depicted in Figure 4.2 beneath the Xúquer Diapir probably also formed during this rifting stage.

4.5.2.Late Jurassic-Early Cretaceous synrift stage

Although most of the extensional motion of the Bicorb-Quesa Fault occurred during the Permian-Early Triassic period, variations in thickness of the Mesozoic overburden indicate that this fault also moved extensionally during the sedimentation of the Upper Jurassic-Lower Cretaceous successions. However, this motion, which was much smaller, produced the monoclinal drape folding of the overburden over the basement extensional fault, with salt accommodating the difference in geometry (Fig. 4.9). The extension of this folded overburden probably led to the formation of the extensional fault recognized on the northern flank of the present-day Bicorb-Quesa Diapir. This motion could have generated other extensional faults on the northern flank, but they cannot be identified given that they were rejuvenated in later events. These extensional faults, which developed at the upper hinge of the monoclinal drape fold, would contribute to the formation of an incipient reactive diapir (a salt roller) with salt provided by both the hanging-wall and the footwall (Burliga et al. 2012).

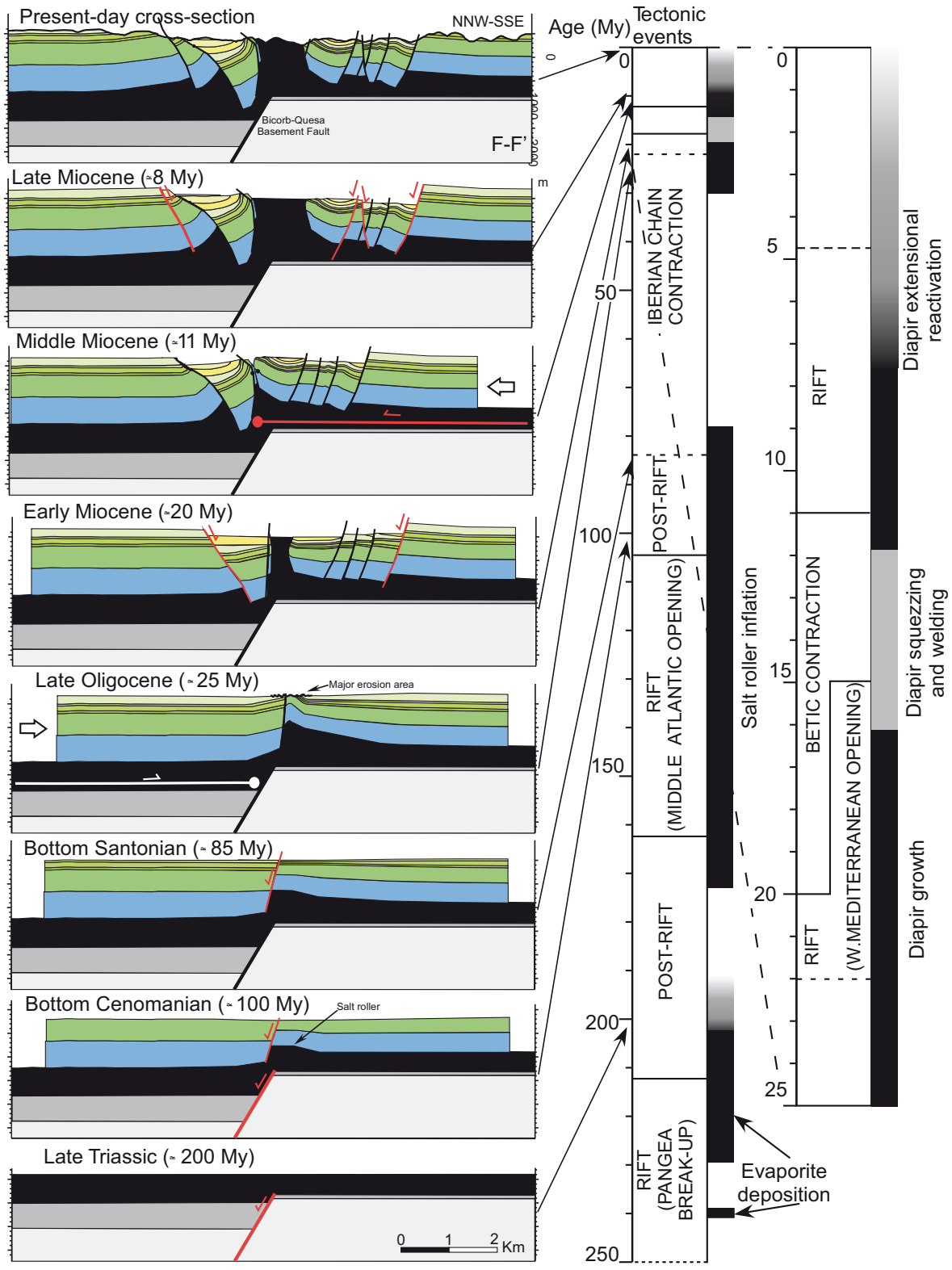

Figure 4.9. Partial restorations of the F-F' transverse cross-section showing the main structural features of the Bicorb-Quesa rift system at the main Alpine deformational stages affecting the eastern Iberian plate (see Fig. 4.5 for location and Fig. 4.3 for legend).

4.5.3.Late Cretaceous postrift stage

The extensional motion of the Bicorb-Quesa Fault fault and the related overburden deformation ended before the start of the Upper Cretaceous. The Cenomanian and Turonian successions are affected only by a slight thinning in the footwall of the active extensional fault that developed at the upper hinge of the previously formed monoclinal drape fold. The Cenomanian-Turonian materials go from the regular thickness of 200m to 80m in this area (Fig. 4.7 cross-section EE' to HH'). Formed in an extensional regional postrift setting (Salas and Casas 1993; Salas et al. 2001), this thinning is interpreted as being driven by a still-working migration of the Middle-Upper Triassic salt because of the overburden load differences (Ge et al. 1997).

4.5.4.Paleogene contractional stage

Between the Senonian (Upper Cretaceous) and the early Miocene, the previous thinning area (the reactive diapir) becomes an S-verging anticline with fairly vertical limbs and a positive relief of between 200m and 400m over the region (Fig 9 and cross-section EE' to FF' in Fig. 4.7). This anticline is well recorded in the lower-middle Miocene subcrop map (Fig. 4.8). It is detached on the Middle-Upper Triassic evaporite layers and had its southern limb cut by S-directed reverse faults. The fold shape, the relief and the presence of the reverse fault rule out the possibility that it was formed by extension, while the lack of active diapirism enables us to conclude that the fold is formed by rejuvenation. These rejuvenation folds are well known in thick-skinned deformations in a contractive event (Letouzey et al. 1995; Krzywiec 2004; Ferrer et al. 2012). Moreover, not far from the study area stands the Iberian Chain (Paleogene and earliest Miocene) (Fig. 4.1). In these nearby areas, the Iberian Chain is formed by a thrust-and-fold system detached above Middle-Upper Triassic salts that propagated southeastwards through time. As shown in the cross-section in Figure 4.2, the location of the deformational front of this part of the Iberian Chain is controlled by the presence of pre-existing basement faults (in this case, the Xúquer basement fault), which cut and displaced the Middle-Upper Triassic detachment level. In this regional scenario, the Paleogene anticline that developed in the Bicorb-Quesa area can be attributed to a further propagation of the Iberian Chain deformation above the Middle-Upper Triassic level of the footwall block of Xúquer basement fault. Further propagation was hampered by the Bicorb-Quesa Fault, which displaced the detachment level, resulting in the formation of a new frontal fold above this sticking point.

4.5.5.Early-middle Miocene diapiric stage

The Bicorb-Quesa Diapir became active and rose to the crest of this anticline just before or at the start of the sedimentation of the lower-middle Miocene detrital deposits. This is evidenced by the petrological composition of the deposits (Roca et al. 1996). The origin of this precursor Bicorb-Quesa Diapir has been explained by thedenudation of extensional faulting caused by the opening of the Valencia Trough (Roca et al. 1996; 2006). However, the diapir risealso seems related to the erosion of the anticline rejuvenated during the Paleogene contractional stage, which was significantly eroded before the deposition of the lower-middle Miocene sequences (Fig. 4.9). The growth of the Bicorb-Quesa Diapir during the early-middle Miocene entailed salt evacuation on the hanging-wall block of the Bicorb-Quesa Fault and, to a lesser extent, in the other diapir areas. This resulted in the sinking of the overlying overburden, which was extensionally faulted and unconformably overlain by relatively thick lower-middle Miocene detrital successions. Coeval with this process the Bicorb and the incipient Quesa and Juanera half-grabens were formed as salt evacuation basins.

4.5.6.Middle Miocene contractional stage

During the Middle Miocene development of the Prebetic folds and thrusts, the pre-existing Bicorb-Quesa Diapir was shortened producing, first, the squeezing of the diapir as indicated in the sedimentary record by a significant rise of evaporitic material (Roca et al. 1996). Then, once the diapir was welded, a contractional deformation occurred in the surrounding overburden and lower-middle Miocene syn-diapir rocks (Roca et al. 1996; 2006; Fig. 4.9). This contractional deformation was focused on the pre-existing diapir because of its weakness, and it consisted of a major NNW-verging anticline cut on its forelimb by the NNW-directed Picos de la Olla low-angle thrust. This contractive event could be responsible for the thrust observed inside the present-day diapir. As in the Paleogene contractional stage, the Middle Miocene contractional deformation did not affect the basement since it was detached from the Middle-Upper Triassic evaporites. However, the deformation during this shortening phase propagated northwards in the footwall of the Bicorb-Quesa basement fault (Fig. 4.9). This different configuration hampers the propagation of Prebetic thin-skinned contractional deformation north of the Bicorb-Quesa basement fault because the detachment level was down-dropped to the north of the fault.

4.5.7.Late Miocene extensional diapir reactivation stage.

This is the last Alpine deformational stage distinguished in the study area. It corresponds to a regional extensional stage in which the Jurassic-Cretaceous subhorizontal platform of the Valencian Domain was extended by means of the formation of several sets of extensional faults detached in the Middle-Upper Triassic evaporites (De Ruig 1992, Roca et al. 1996; Fig. 4.9). In the study area, this extensional overburden deformation produced the extensional reactivation of the squeezed Bicorb-Quesa Diapir and the development, at its western prolongation, of a major SE-dipping extensional fault (the Carroig Fault) (Roca et al. 1996; 2006)

4.6.The role of pre-existing basement faults in the initiation and reactivation of salt diapirs

The reconstruction of the evolution of the Bicorb-Quesa Diapir indicates a complex salt diapir that evolved from a contractional and extensional thin-skinned deformation of an overburden located on top of a pre-existing extensional basement fault. A thin-skinned deformation produced the rejuvenation of a previous reactive diapir, the growth of the Bicorb-Quesa Diapir, the squeezing of the diapir and the reactivation of the diapir.

In each of these stages, cover deformation and diapirism appear strongly influenced by the propagation direction of the deformation above the detachment level, which was previously flexed or truncated on top of the pre-existing basement fault. This propagation, in the compressive stages, was directed toward the basement fault. In the Paleogene contractional stage, it occurred in the hanging-wall, whereas in the middle Miocene it occurred in the footwall. Below we discuss the role played by the pre-existing basement faults in the thin-skinned contractional initiation and reactivation of salt diapirs, focusing on the influence of the propagation direction of the cover deformation.

4.6.1.Contractional diapir initiation

Before addressing contractional deformation, it should be noted that the structural style of overburden and salt-layer deformation above a growing extensional basement fault is strongly dependent on the degree of decoupling between supra- and subsalt deformation (Withjack and Callaway 2000). Thus, if the deformation is coupled, then the deformation style is transferred through the detachment level (Fig.

4.10). By contrast, if the deformation is decoupled, structural styles above and below the salt can be quite different and may result in an overburden drape folding above a basement extensional fault (Jackson and Vendeville 1994). Since the overburden section must extend as much as the basement, this drape folding is accompanied by extensional faulting on the upper hinge of the monoclinal drape fold. This is the area where reactive diapirs can initiate (Fig. 4.10). Also in this decoupled scenario, salt-layer thickness is not constant but changes laterally, accommodating the difference between the supra- and subsalt geometries. As regards this major salt mobility, the salt layer (potential future detachment level of later thin-skinned deformations) usually has lateral continuity above the basement fault, which does not occur in the coupled scenario, where it is simply cut and displaced by the fault (Fig. 4.10).

Shortening of these different thick-skinned salt tectonic structures would promote the growth of different contractional structures (mainly folds) which, in some cases, can enhance diapirism as a result of their erosion and/or fracture weakening (Fig. 4.10). The diapir initiation in these structures would not only depend on the amount of overburden denudation but also on the fold shape and kinematics. This initiation also depends of the following factors: thickness and mechanical behaviour of the overburden, deformation rates, amount of deformation, thickness of the salt, and the pre-existing overburden, salt configuration, etc. Consequently, the possibility of developing contractional-driven diapirism over a pre-existing basement fault will be different if the contractional deformation is developed over a previously coupled or decoupled overburden. The resulting structure will also depend on whether the overburden thin-skinned contractional deformation propagates on top of the hanging-wall or on top of the footwall of the basement fault.

We focus on three possible scenarios: i) a coupled salt layer:ii) a decoupled salt layer with the footwall and hanging-wall salt-layer that is disconnected, iii) a decoupled salt layer that is connected (Fig 4.10a). Thus, if we consider that the salt layer acts as a detachment level, the contractional deformation can be propagated toward the pre-existing extensional basement fault over its hanging-wall or over its footwall (Fig 4.10a).

In the case of a salt-disconnected/hanging-wall propagation, the basement fault acts as a barrier for the propagation of the contractional overburden deformation, leading to the development of buttressing structures (mainly detachment folds and backthrusts) or basement short-cuts. In this setting, the salt-cored structures that developed from contractional structures have a thick overburden and, therefore, are not very suitable for being pierced by salt. The only exception might be the tight buttress anticlines that can be formed against the fault plane (Fig. 4.10a). These

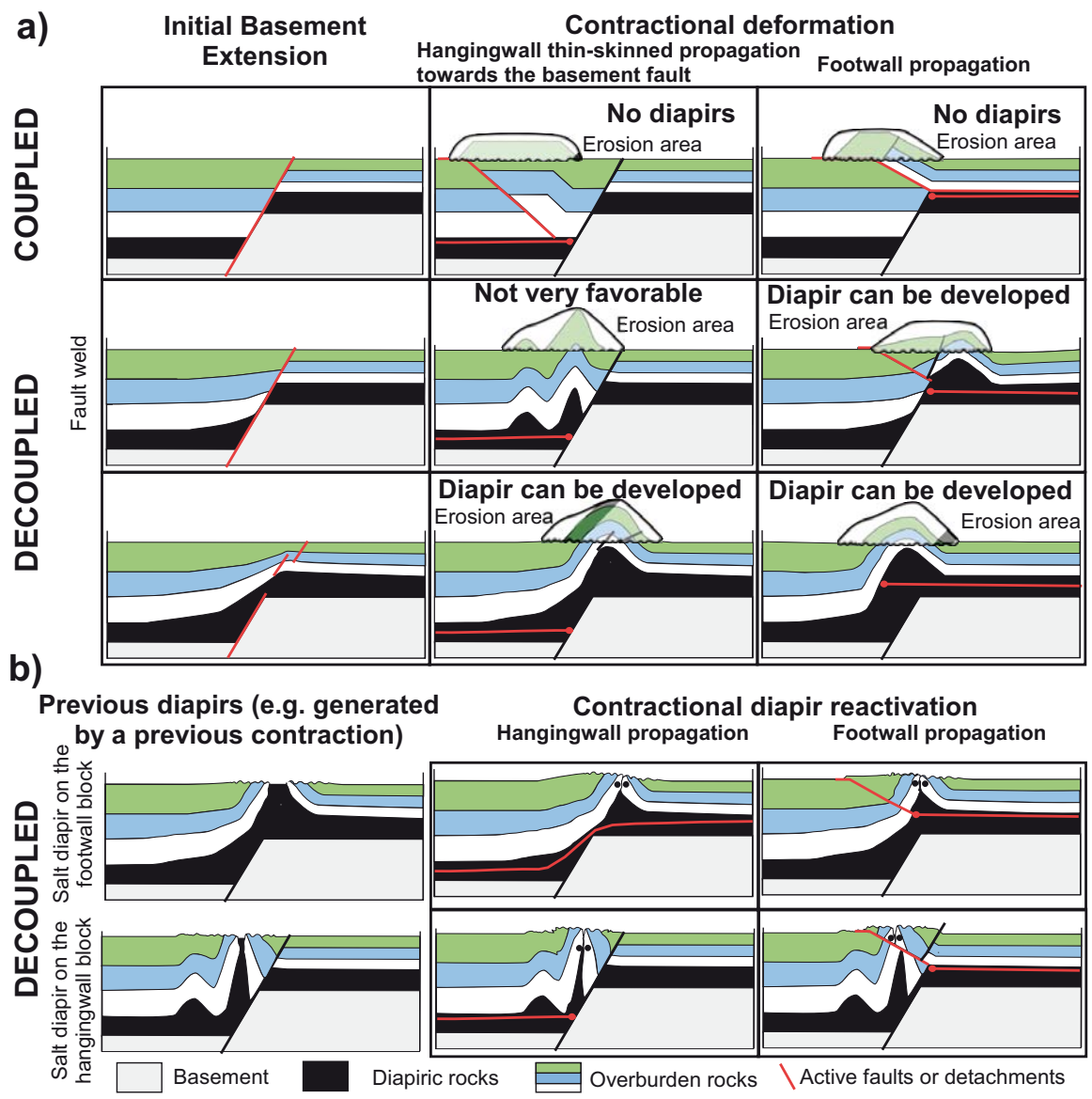

Figure 4.10. Summary diagram of the role of pre-existing extensional basement faults in the cover thin-skinned contractional initiation (a) and reactivation (b) of salt diapirs. The analysed factors are the propagation sense and the degree of coupling or decoupling of the thin-skinned deformation.

anticlines present better conditions for developing a salt diapir since they tend to be taller and have an initial small overburden/salt thickness ratio (see above for more information on a decoupled extensional deformation over a basement extensional fault). Furthermore, if a basement short-cut develops, these anticlines could also be significantly uplifted above the regional level, favouring a deep erosion to an even greater extent.

In the case of a salt-connected/hanging-wall propagation, the overburden contractional deformation can propagate toward the basement fault footwall above the inherited flat-ramp-flat geometry of the upper part of the salt layer. This detachment

geometry leads to the development of a detachment fold on the concave-downward detachment bend, and also to the squeezing of the salt located on the basement fault surface. The salt is expelled upwards toward the generated detachment fold. Note that all these contractional structures develop at or very close to the location of the hinge of the overburden monoclinal drape fold that formed during the older extensional motion of the underlying basement fault. Therefore, contractional anticlines develop at the place where the overburden is thinner and where the salt layer is thicker (Fig. 4.10a). As a result, the formation of diapirs by erosion and salt breakthrough is relatively easy here. An example of this kind of contractional-driven diapir would be the one that developed during the Paleogene-Lower Miocene over the Bicorb-Quesa basement fault.

In the case of a footwall propagation, the contractional deformation would be blocked at the top of the basement fault. The detachment fault would be interrupted by the fault in a salt-disconnected scenario or by the monocline limb of the drag fold in a salt-connected scenario. This would give rise to the formation of a thrust front or detachment anticline at the top of the basement footwall cut-off of the pre-existing extensional fault (Fig 10a). As in the previous case, these contractional structures would be developed at or very close to the hinge of the overburden monoclinal drape fold that formed during the older extensional motion of the underlying basement fault. Consequently, they would also constitute a suitable locationfor the generation of salt diapirs by overburden denudation. The Betic Front at the Xúquer River (Fig. 4.2) provides an example of this kind of situation.

4.6.2.Contractional diapir reactivation and/or squeezing

The propagation direction of an overburden contractional deformation also plays a major role in the contractional reactivation and/or squeezing of a salt diapir developed over an extensional basement fault. Both the geometrical features and the evolutionary trends of shortened diapirs will be rather different depending on whether the contractional deformation propagates toward the diapir over the hanging-wall or over the footwall of the basement fault (Fig. 4.10b).

Indeed, if contractional deformation propagates above the salt layer lying over the hanging-wall block, the entire pre-existing diapir narrows, forcing a large volume of salt to flow upwards. This results in an acceleration of the extrusion of diapiric materials or, in the case of a buried diapir, in its rejuvenation. With increased shortening, the diapirs close along secondary welds or generated “Q-tip” structures (Rowan

and Vendeville 2006; Dooley et al. 2009). Folds and thrusts form at the squeezed diapir limb with a predominant vergence that will depend on the basement fault dip. Note that this evolution is only valid if the overburden contractional deformation can propagate up to the salt diapir location above a continuous detachment salt layer (see discussion on the propagation of overburden deformation above a basement fault in the previous section). In the other cases, diapir reactivation will be more difficult and complex (e.g., diapirs developed over the basement fault but disconnected from the source layer by a primary weld) or it may never occur (diapirs developed over the basement footwall block in a pre-contractional configuration in which the detachment salt layer has a high-angle dip above the basement fault).

In the case where contractional overburden deformation has propagated on the basement footwall block, all pre-existing salt diapirs can be easily reactivated provided that primary welds were formed on their flanks (Fig. 4.10b). The pattern of the contractional reactivation in pre-existing diapirs is similar to the pattern described in the previous scenario with the exception of diapirs that developed over the basement fault surface. In these scenarios, not all the diapir is shortened but only part of the feeding stem located above the detachment level of the regional footwall of the basement fault. Moreover, the post-diapir welding thrusts and folds in these diapirs show a preference for vergence toward the foreland, with the development of forethrusts in the diapir forelimb (Fig. 4.10). It is interesting to note that the preservation of the lower part of the feeding stems in these diapirs can favour later diapir reactivation, even where the upper part of the diapir was completely welded. An example of this kind of later reactivation is the Bicorb-Quesa Diapir, which was contractionally welded during the middle Miocene and reactivated during the late Miocene by extensional thinning of the overburden above the welded stem or feeder.

4.7.Conclusions

Detailed analysis of structural surface data in addition to available and new magnetotelluric data enabled us not only to recognize the structure and Alpine evolution of the Bicorb-Quesa Diapir but also to propose a new model for contractional diapir initiation and reactivation over a pre-existing extensional basement fault.

In the study area, the geometric analysis of the available data indicates that the Alpine structure of the Bicorb-Quesa area is strongly conditioned by the presence of a ductile and diapiric Middle-Upper Triassic level. The evaporite-detrital level decouples the deformation of the Iberian basement from the one affecting the Jurassic

to Miocene overburden. This leads to a structural style of deformation of the basement (thick-skinned) and overburden (thin-skinned) that is completely different from the structural style especially during Cenozoic times, when contractional and extensional deformations only affected the overburden.

The Bicorb-Quesa Diapir is a salt wall formed above a NNW-dipping extensional basement fault with a complex deformational history that includes both contractional and extensional diapir reactivations. The extensional basement fault formed during Permian-Early Triassic times and still slightly active up to the beginning of the Late Cretaceous produced the development of a monoclinal drape fold in the Jurassic-Cretaceous overburden as well as the formation of a reactive diapir on the hinge of the drape fold. After the Late Cretaceous, the Jurassic-Cretaceous overburden was affected by thin-skinned contraction related to the formation of the Iberian Chain and Betics. These deformations led to the polyphase development of the Bicorb-Quesa Diapir because of the erosion of a Paleogene rejuvenated reactive diapir on top of the basement fault, and because of the early Miocene extension. This diapir was contractionally deformed during the middle Miocene and extensionally reactivated during the late Miocene.

The role played by pre-existing basement faults in thin-skinned contractional initiation and reactivation of salt diapirs was analysed using the information provided from this reconstruction. This analysis highlights the role played by the geometric relationship between the propagation direction of the cover deformation and the dip direction of the basement fault. In this regard, it shows that 1) the propagation of an overburden contractional deformation over a basement footwall block results in the development of detachment folds on top of the basement fault which, with a thin cover, are propitious for the formation of a salt diapir by erosion, and 2) the propagation of an overburden contractional deformation over the basement hanging-wall block, is not very favourable to the formation of salt diapirs since it generally induces the generation of buttressing structures that involve a thicker hanging-wall sequence that resists piercement. This general working model, however, is not without its exceptions. The main exception is attributed to the presence of a thick salt layer beneath the monocline drape fold. A thick salt layer, when squeezed by a hanging-wall compressive deformation, can displace salt to the footwall block and pump up the reactive diapir, allowing the diapir to grow.

As for diapir reactivation, when a contractional deformation propagates toward a pre-existing diapir over the hanging-wall, it will result in the entire narrowing of pre-existing diapirs over the basement fault but not in the entire narrowing of the ones located over the basement footwall block. By contrast, a footwall propagation of the

contractional deformation will generate the entire narrowing of all pre-existing diapirs over the footwall block, but only a portion of the diapirs formed over the basement fault. Specifically, in these diapirs, the lower part of the stems remains almost undeformed, creating a situation very propitious for a subsequent diapir reactivation even if the upper part of the diapir is completely welded.

Chapter 5

Application of Paleomagnetism to kinematic analysis in Salt Tectonics: the Bicorb-Quesa and northern Navarrés salt wall segments case (Prebetic Zone, SE Spain)

Resum del Capítol (Summary in Catalan)

Aquest capítol conté el tercer article del compendi que forma la tesis. En aquest capítol es presenten les dades de paleomagnetisme i l'estructura interna de la paret salina. Les dades de paleomagnetisme ens proporcionen una informació molt valuosa sobre les rotacions que han tingut lloc a l'àrea d'estudi i del temps en què aquestes s'han produït. Les dades de l'estructura interna del diapir ens informa sobre com ha crescut la paret salina però també ens proporciona informació sobre antigues deformacions.

Per l'estudi paleomagnètic s'han mostrejat tant els materials diapírics com la cobertora, obtenint resultats a ambdós llocs. Els materials del Keuper mostren dos components estables, un component datada com a Triàsic i una altre com a Cretàcic Superior-Paleocè que han sofert una rotació antihorària. A la cobertora trobem els materials que han rotat horàriament entre el Miocè Superior i l'actualitat i que no han sofert rotacions al sud de la paret salina.

La paret salina mostra estructures de diverses edats, les més modernes corresponents al creixement de la paret salina actual es corresponen amb dos grans bulbs nucleats amb K1 que estan limitats per zones de cisalla i falles inverses, entre aquests i les parets del diapir trobem materials de les unitats K2-K5 formant uns plecs longitudinals que es disposen tallant uns plecs perpendiculars. L'anàlisi d'eixos de plecs menors ens informa de la presència de dos plecs tipus cortina en les zones dels bulbs de K1 i de plecs tipus baina a les zones de K2-K5. També hi destaca la presència de les restes d'un antic diapir a la paret nord de la paret diapírica.

Tota aquesta informació ens ha dut a conèixer millor l'evolució del diapir sabent

que va estar afectat per una etapa de rotació antihorària dels materials diapirics durant la compressió Iberica (Paleocè), i que després durant la pròpia compressió Paleocena i/o durant la compressió Bètica (Miocè Mig), es produeix la formació del dúplex i/o plecs en el Keuper. L'estudi posa de manifest també que el diapir és reactiva durant el Miocè superior, primer formant un diapir reactiu que genera plecs longitudinals i després mitjançant el creixement dels bulbs. Aquest darrer creixement és causat per un desplaçament cap al sud de la cobertora amb una rotació horària de 20º que deixa lloc a un nou diapir per créixer.

Summary

This chapter contains the third article of the thesis. This chapter presents the paleomagnetic data and the internal structure data of the salt wall. The data of paleomagnetism provide valuable information about rotations that have occurred in the study area and the time when these occurred. In turn, the internal structure data supply information about the diapir rise structures and also give us information about older deformations.

Samples from salt wall and overburden were taken for the paleomagnetic study obtaining results in both places. The Keuper shows two temperatures, one primary, dated as Triassic and the other dated as Upper Cretaceous-Paleocene both affected by a counter-clockwise rotation. The overburden materials are clockwise rotated between the Upper Miocene and the present south of the diapir and are not affected by rotations southward the diapir.

The most modern diapir structures correspond to the salt wall rise of two bulbs formed by K1 which are limited by reverse faults and shear zones. Between the SWS walls and the bulb the K2-K5 materials predominate forming longitudinal folds that cut diapir perpendicular to the folds. The analysis of minor fold axes points out the presence of curtain in the bulbs area and sheath folds in the areas formed by K2-K5. It also highlights that the presence of the ancient diapir remains located on the north wall diapir.

All this information has led to a better understanding of the evolution of the salt wall which was affected by a counter-clockwise rotation phase during the Iberian Chain emplacement (Paleocene). Then, during this stage and/or during the Betic compression (Middle Miocene) duplex and folds were formed in the Keuper materials. Also, during the Late Miocene, the reactivation of the salt wall first generates longitudinal folds as a reactive diapir and then the diapir rise as bulbs. This latter

reactivation occurs because of the southwards translation of the overburden with a rotation of 20° which generates the space necessary to the diapir rise.

Application of Paleomagnetism to kinematic analysis in Salt Tectonics: the Bicorb-Quesa and northern Navarrés salt wall segments case (Prebetic Zone, SE Spain)

M. Rubinat[1], E. Beamud[2], R. Soto[3], and E. Roca[1]

1 Institut GEOMODELS - Group of Geodynamics and Basin Analysis, Departament de Geodinàmica i Geofísica, Facultat de Geologia, Universitat de Barcelona, 08028-Barcelona, Spain.

2 Laboratori de Paleomagnetisme (CCiT UB-CSIC). Institut de Ciències de la Terra "Jaume Almera", Solé i Sabarís, s/n, 08028 Barcelona, Spain.

3 Instituto Geológico y Minero de España (IGME), Unidad de Zaragoza. C/ Manuel Lasala, 44, 9B, 50006 Zaragoza, Spain. e-mail:∗Mrubinat@ub.edu

Abstract: *Paleomagnetism together with a detailed analysis of the internal structure of the Bicorb-Quesa and Navarrés salt wall segments and their overburden, within the Prebetic zone in SE Spain, have been used in this work to constrain their kinematics and driving mechanisms. Paleomagnetic data from Upper Triassic red beds interlayered with evaporites ourcropping inside the selected salt-related structures and Miocene rocks belonging to adjacent syn-diapiric half-grabens were interpreted. These data revealed a stable primary component for both the Upper Triassic and Miocene materials, and an additional secondary component in the Upper Triassic samples, that have permitted to unravel the occurrence of vertical-axis rotations on the diapiric sequence predating the salt wall development probably linked to regional deformation events and also, 20º clockwise vertical-axis rotations affecting only the southern cover block and related to the Middle-Late Miocene salt wall development that responds to a thin-skinned extensional fault deformation strongly controlled by basement normal faults. This approach represents a powerful tool to analyse the kinematics of salt-related structures and driving mechanisms.*

5.1.Introduction

Salt-related structures play an important role in the spatial and temporal distribution of sedimentary geological reservoirs as well as in the generation, migration and entrapment of hydrocarbons. Most of the major world petroleum provinces (i.e., Gulf of Mexico, Zagros, North Sea and offshore Atlantic margins of Brazil and West Africa) are located in areas deformed by salt tectonics. Moreover, in the field of waste geological storage, salt-structures have been profusely prospected as favorable sites to confine both CO_2 and nuclear products. Deformation of salt-related structures is controlled by the rheology and properties of the salt rock (halite) which deforms plastically and is less dense and much weaker and viscous than most rocks (Jackson and Talbot, 1986; Jackson and Vendeville, 1994). This different behavior implies the generation of high complex 3D structures and has hampered their structural characterization since the beginnings of Structural Geology. However, during the last three decades, understanding of the geometry and mechanics of salt-related structures and associated strata has taken a huge step forward from advances in five main areas: experimental and numerical modeling (e.g. Jackson and Talbot 1989, Zaleski and Julien 1992, Vendeville and Jackson, 1992, Podladchikov et al 1993, Chemia et al 2008, Dooley et al 2009), field studies (e.g. Jackson et al 1990; Sans 2003), reflection seismic imaging (e.g. Netzeband et al 2006, Fiduk and Rowan 2012), structural restoration (e.g., Worrall and Snelson, 1989; Hossack, 1995; Rowan and Ratlift, 2012) and potential field geophysical methods (e.g. Al-Zoubi and ten Brink 2001; Nagihara and Hall 2001; Pinto et al 2005; Key et al., 2006; Rubinat et al 2010).

From these advances, it has been possible to define the general patterns of salt deformation and characterize the formation and evolution of most of the observed salt-related structures. In practically all developed structural models, the tridimensional nature of salt deformation is emphasized as well as the presence of rotations along vertical, horizontal or inclined axes affecting single or various structures. Nevertheless, when applied to real cases, few are the studies (i.e., Talbot and Aftabi, 2004; Rowan and Vendeville, 2006) that take into account the presence of non horizontal-axis rotations or that quantify them both in the inner parts of the salt structures and adjoining overburden. This anachronism is, to a large extend, due to the difficulty of detecting them with most geophysical methods and from mapping field data. Vertical-, horizontal- and inclined-axis rotations are usually defined and quantified by means of Paleomagnetism which has been reported as a powerful tool to unravel not only the motion histories of continental plates but also the kinematics of crustal deformations. In this way, paleomagnetism has been successfully used in characterizing the kinematics of fold-and-thrust belts (e.g. Grubbs and Van der Voo, 1976; Pueyo et al., 2002;

Arriagada et al., 2003; Roperch et al., 2006), extensional (e.g., Nagy, 2000; Mattei et al., 2004; Cifelli et al., 2007) and strike-slip fault systems (e.g., Ron et al., 1984; Zhan et al., 1996) as well as middle-lower crustal ductile deformations (e.g., Lefort et al., 2001). However, paleomagnetism has not been widely applied to salt structures and it has been mainly restricted to diapir emplacement studies. In such studies, the paleomagnetic data are not used to reconstruct vertical- and inclined-axis rotations but mainly to obtain the layer polarity of diapiric and overburden rocks (Weinberger et al. 1995; 1997; Henry et al. 2000). This deficiency could be related to the remote or offshore location of most salt outcropping structures (see Hudec and Jackson, 2007 compilation), but mainly deals with the poor magnetic signal of the evaporites and the highly complex internal architecture of many salt structures.

In this setting, the salt diapiric structures of SE Spain, specifically the Bicorb-Quesa and Navarrés ones, fulfill the characteristics that made them ideal candidates to carry out a study to test the utility of paleomagnetism in the kinematic characterization of salt-related structures. They are good outcropping salt wall segments with a relatively simple internal diapir structure depicted by layered evaporitic sequences with red mudstones interlayers suitable for paleomagnetic analyses (Ortí, 1974). Furthermore, they pierce a carbonate overburden overlain by halokinetic continental successions that allow to date and characterize not only the shape and vertical diapir evolution (Roca et al., 1996; 2006; Rubinat et al 2010; 2012) but also, to perform a paleomagnetic study designed to recognize vertical-axis rotations (VAR) there.

Under these favorable conditions, the paleomagnetic study carried out in both the diapiric and the halokinetic successions allows identifying VARs that provide a set of constraints in the kinematics of the Bicorb-Quesa and Navarrés salt wall segments not previously considered. Thus, a new kinematic model of the Late Miocene opening of these diapirs, together with the characterization of the internal diapir structure, are presented taking into account these constraints. This study denotes that paleomagnetism must be considered as a powerful technique to improve our understanding on the kinematics of salt-related structures.

5.2.Geological Setting

The studied Bicorb-Quesa and Navarrés salt wall segments (Fig. 5.1) are located in the eastern part of the Prebetic Zone, the outermost zone of the Betic Chain (Blumenthal, 1927; Vera, 1983). The Prebetic Zone belongs to the inner platform parts of the Mesozoic Tethys Ocean and its present-day structure mainly

consists of a thin-skinned thrust-and-fold belt of Jurassic to middle Miocene rocks detached from the Iberian basement on the Middle and Upper Triassic evaporites (Vera, 1983). Emplaced towards the NNW during the early-middle Miocene (Azéma et al., 1979; García-Hernández et al., 1980; De Ruig, 1992), the structure of the Prebetic thrust-and-fold belt is rather complex and includes box-fold anticlines, steep dipping faults and salt diapirs cored by the Triassic evaporites (Fig. 5.1). The trend of these structures is predominantly ENE-WSW although other orientations (mainly NNW-SSE) are also present (De Ruig 1992; Roca et al. 2006; ter Borght et al. 2011).

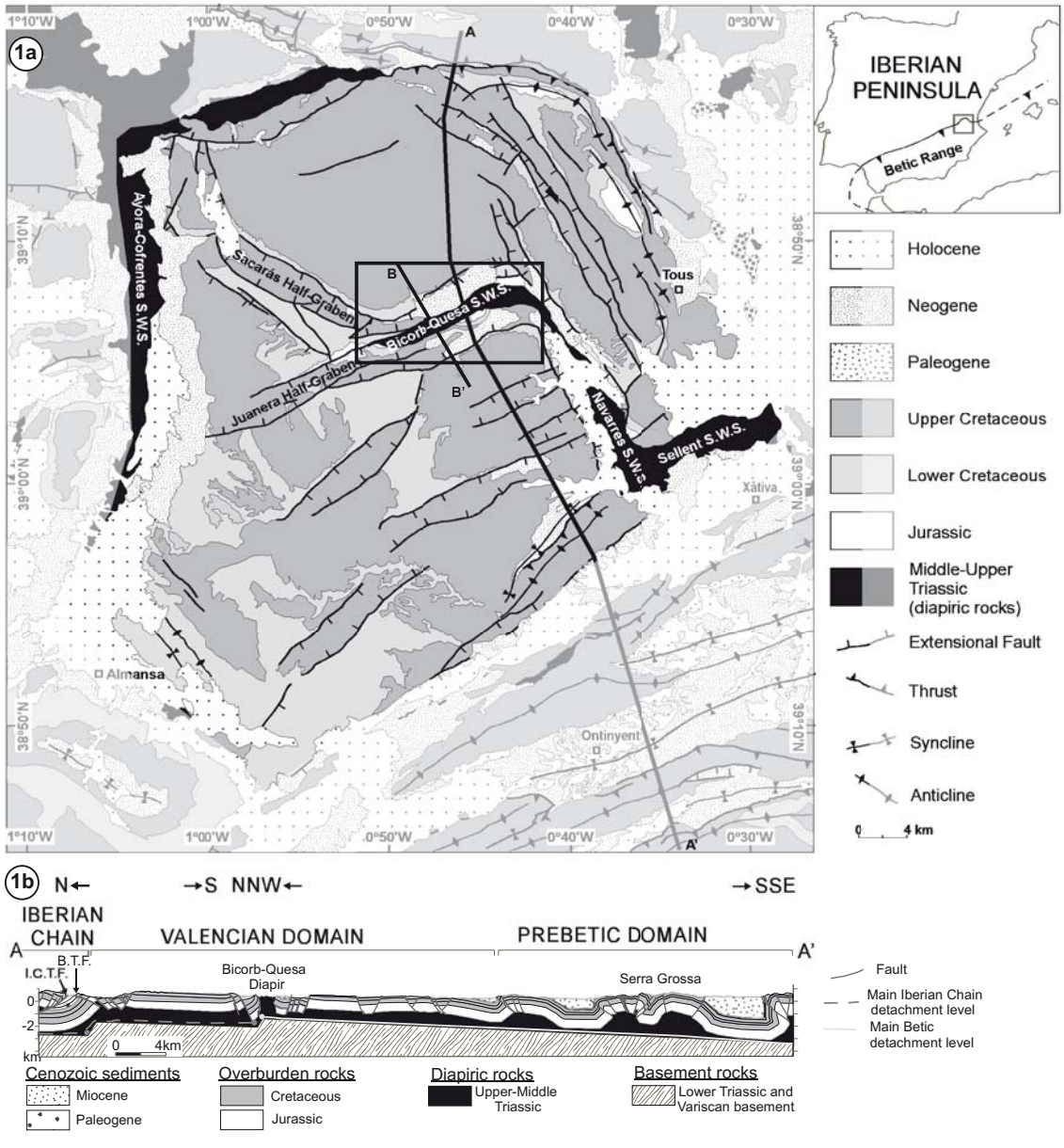

Figure 5.1 A. Geological map of the Valencian Domain and adjoining Iberian Chain and external Prebetics fold-and-thrust belts. Note the location of the Bicorb-Quesa, Navarrés and Sellent salt wall segments (SWS) at the center of Valencian Domain and their relationships with extensional faults. Non-diffused frames and lines: Valencian Domai; B-B': location of the cross-section shown in Fig. 3. Black box: location of study area (Fig. 2). **B.** Regional NNW-trending cross-section through the Valencian Domain.

In this regional setting, the Bicorb-Quesa and Navarrés salt wall segments are located in the northern and outermost parts of the Prebetic thrust-and-fold belt which consists of a thrust sheet 40 km wide with less than 2 km of northwards displacement (Roca et al. 2006). This thrust sheet, called Valencian Domain, is made up by a 1000-1500 m thick succession of Jurassic to Upper Cretaceous carbonate rocks that only exhibit a significant contractional deformation in its NNW and ENE-trending thrust front (Fig. 5.1). In the rest, the Jurassic to Upper Cretaceous cover is predominantly subhorizontal and appears deformed by elongated salt diapirs and extensional faults with both ENE- and NNW-trends. Most of these extensional structures developed during the Late Miocene after the thrust emplacement (Moissenet 1985; 1989), although some of them are older (early Miocene). It should be noted that the distribution and orientation of the extensional faults is not homogeneous within the thrust sheet. As shown in the map of Fig. 5.1, the Bicorb-Quesa and Navarrés salt wall segments delimit domains in which deformation shows different features. Southwards of these salt wall segments, the cover appears cut by ENE-trending extensional faults parallel to the Bicorb-Quesa segment, whereas northwards it is cut by extensional faults with a NNW orthogonal trend, parallel to the Navarrés segment trend. Moreover, the extensional faulting in the northern domain is not homogeneous, as north of the Bicorb-Quesa Diapir the Jurassic and Cretaceous carbonates are unfaulted. This regional pattern of the extensional deformation inside the Valencian Domain evidences that both the Bicorb-Quesa and the Navarrés salt wall segments played as transfer zones during the late Miocene extensional deformation which, as will be shown, is crucial to interpret the observed kinematics deduced from paleomagnetism.

5.3.The Bicorb-Quesa and Navarrés salt wall segments

The Bicorb-Quesa and Navarrés salt wall segments, together with the Sellent one (see Fig. 5.1), constitute a continuous kinked salt wall of Middle to Upper Triassic evaporites that crosses the central part of the Valencian Domain from its SE corner to the junction with the NW-trending Sácaras Half-graben and the ENE-trending Juanera Half-graben in the central part of the domain (Fig. 5.1). The ENE-trending segment located in the westernmost part of this wall is the so-called Bicorb-Quesa Diapir and the NNW-trending one, the so-called Navarrés Diapir (Fig. 5.1). The Bicorb-Quesa salt wall segment is about 12 km long and widens progressively eastwards up to be almost 2 km width at its eastern end (Fig. 5.2), where it joins with the northern end of the NNW-trending Navarrés salt wall segment. The Navarrés Diapir spreads 15 km southwards with a constant width of 1 km up to join with the western end of the ENE-trending Sellent Diapir (Fig. 5.1).

The kinked shape of these salt walls and also the shape of the Valencia Domain thrust front (see Fig. 5.1) could be related to the presence and motion of the ENE and NNW-trending basement extensional faults beneath the detached thrust sheet (Carbó, 1982)This is clear in the Bicorb-Quesa salt wall segment where recent field studies and magnetotelluric surveys have depicted the existence of a basement ENE-trending fault, the Bicorb-Quesa fault (Fig. 5.3), beneath the salt wall (Rubinat et al., 2010; 2012). The Bicorb-Quesa fault sinks the NNW fault block with a vertical throw that decreases progressively westwards from about 1000 meters up to disappear close to the western end of the present-day outcropping salt wall. In the Navarrés salt wall segment, the presence of an underlying basement fault is not so well documented due to the lack of magnetotelluric surveys and detailed structural studies. However, it has been inferred from: 1) the gravimetric data that show the presence of a basement anomaly along the salt wall trace (Carbó, 1982), and 2) the different topographic elevation of the subhorizontal Jurassic-Cretaceous successions on both sides of the wall. These data point to the existence of a basement fault beneath the Navarrés salt wall segment which would dip southwestwards with a throw increasing towards the SSE.

Over this basement fault pattern, the Bicorb-Quesa and Navarrés salt wall segments appear flanked by parallel half-grabens developed on the Jurassic to Cretaceous carbonate overburden (Figs. 2 and 3). These half-grabens, bounded by extensional faults dipping to the diapir wall, are filled by Miocene sediments deposited during the salt wall development (Santisteban et al., 1989; Anadón et al., 1994; 1996). From the observation of these sediments and the structure of the overburden close to the salt walls it has been inferred a complex deformational history for the Bicorb-Quesa Diapir that includes both contractional and extensional diapir reactivations (Roca et al., 1996; 2006; Rubinat et al., 2012). In such history, the Bicorb-Quesa basement extensional fault formed during the Permian-Early Triassic times and, still slightly active up to the beginning of the Late Cretaceous, produced the development of a monoclinal drape fold of the Jurassic-Cretaceous overburden, with Middle-Upper Triassic salt accommodating the difference between both fault blocks. After a Late Cretaceous tectonic quiescent activity, the Jurassic-Cretaceous overburden was affected by the Iberian Chain and Betic related contractional and extensional thin-skinned deformations. These deformations led to the development of the Bicorb-Quesa Diapir from the early Miocene erosion of a Paleogene contractional fold formed on top of the basement fault, and then its middle Miocene contractional squeezing and late Miocene extensional reactivation. This complex and polyphase history has not been described in the Navarrés segment where the widespread presence of flat lying Quaternary terraces over most of the diapir and adjoining rocks greatly hampers

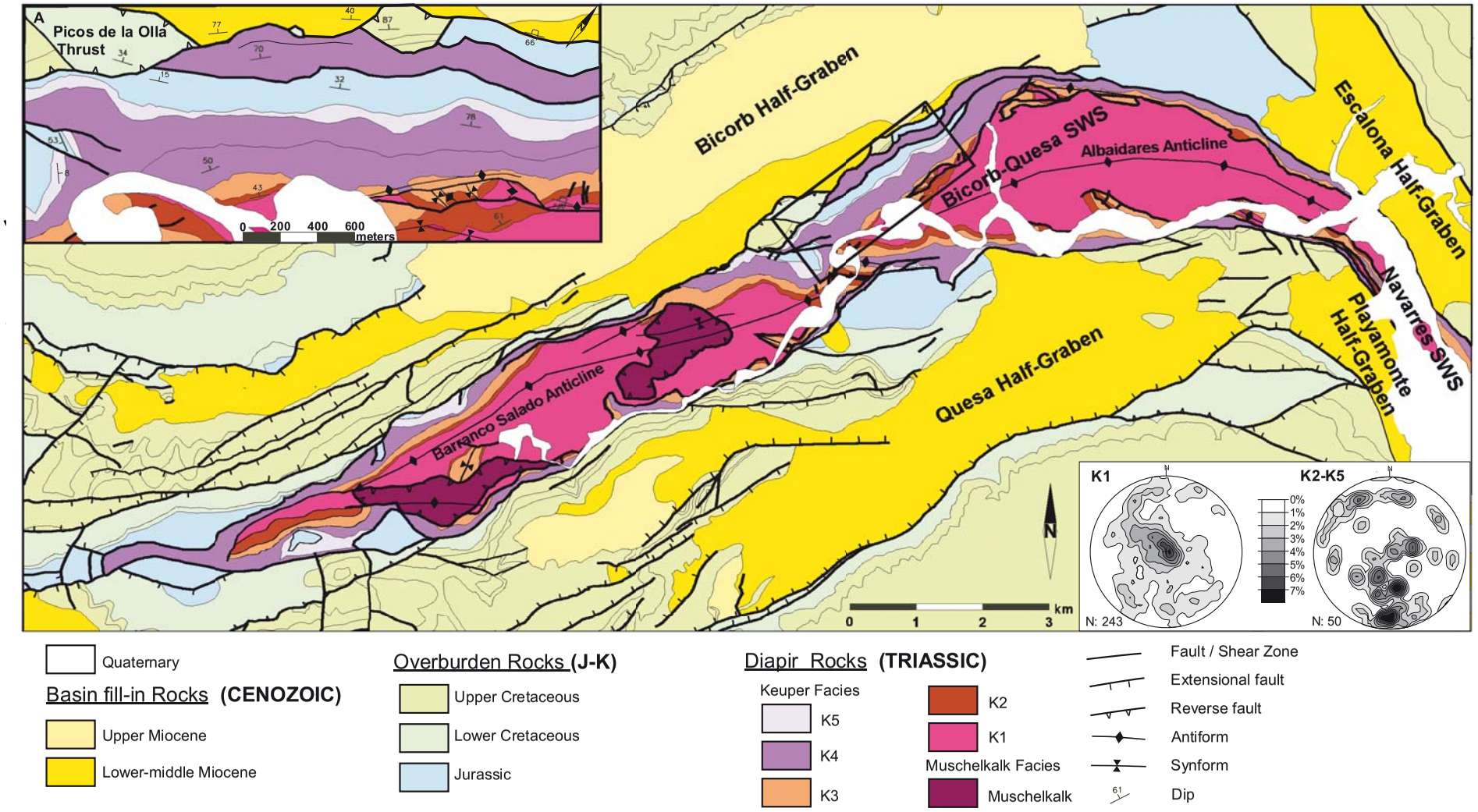

Figure 5.2 Geological map of the study area depicting the main structural features of the Bicorb-Quesa and northern Navarrés salt wall segments. The represented stereoplots are lower hemisphere equal angle stereographic projections of fold axes measured in the Middle-Upper Triasic rocks. I: fold axes measured in the K1 unit coring the Barranco Salado and Albaidares anticline culminations; II: fold axes measured in the K2 to K5 units as well in the K1 unit outcrops located at the periclinal ends. Black box: location of study inset area A. **A.** Map inset showing the detailed structure of the northern flank of the Bicorb-Quesa segment northwest of the Albaidares Anticline.

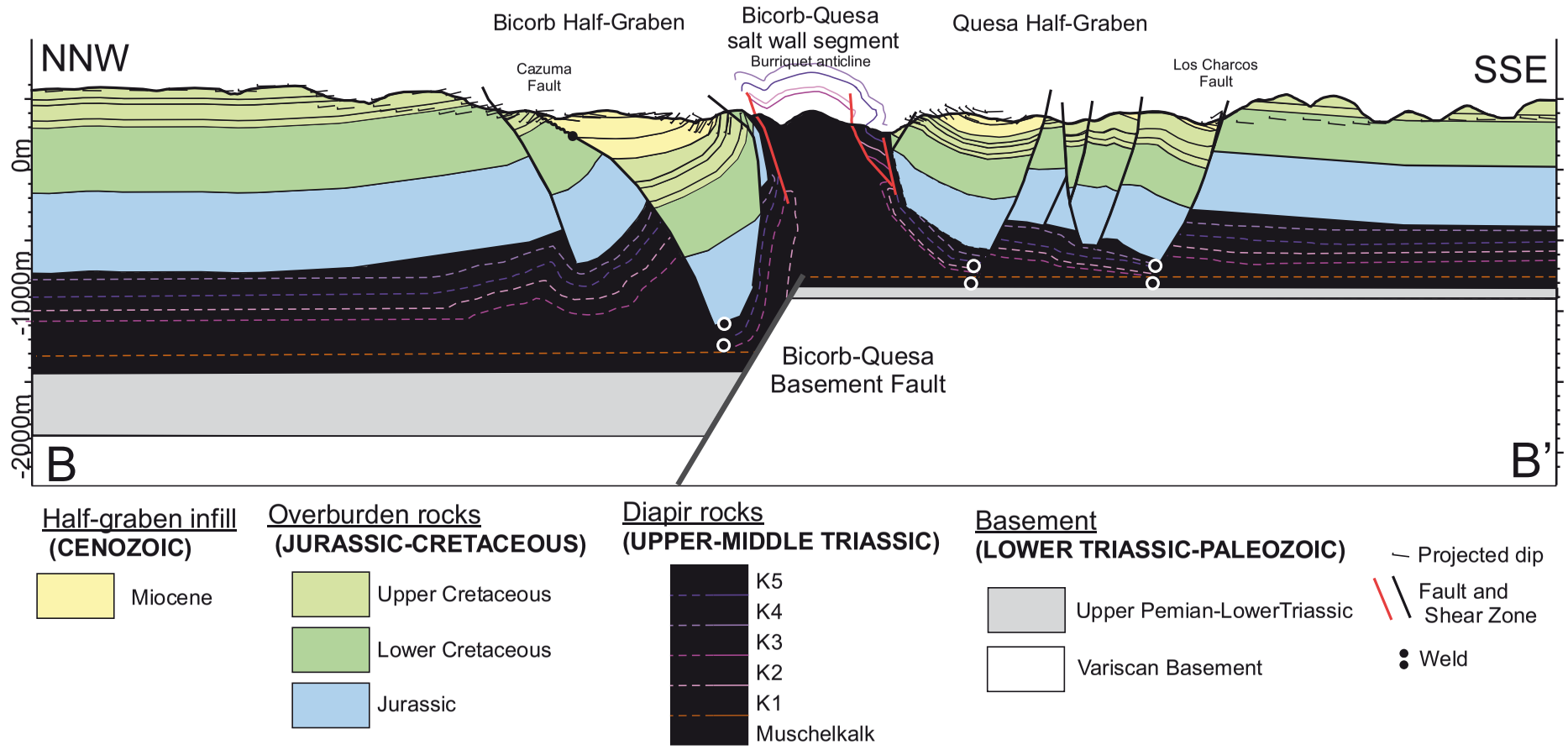

Figure 5.3. Cross-section through the central part of the Bicorb-Quesa salt wall segment showing the main of the basement, overburden and inner salt wall structure (modified from Rubinat et al. in press). Dashed lines: poor constrained stratigraphic boundaries. For cross-section location see Fig. 1.

to decipher its history. However, we can assume that it was not very different by observing the structure of the outcropping diapir, its overburden and Miocene syn-diapiric rocks. These data also indicate the development of this salt wall segment during the early Miocene and a later extensional reactivation during the late Miocene. It should be noted that this late extensional reactivation comes out as the responsible for the present-day salt wall configuration as well as the formation of most extensional faults observed in the Valencian Domain.

5.3.1. Internal structure of the Bicorb-Quesa salt wall segment

The internal structure of the Bicorb-Quesa salt wall segment has been characterized thanks to the variable and distinctive stratigraphy depicted by the Middle to Upper Triassic rocks that constitute the diapirs and salt walls of the study area (Fig. 5.4). Actually, oil well data and surface geological studies show that salt-related structures in southeastern Spain are cored by a thin basal evaporite layer (Röt facies), a 50-200 m thick succession of Middle Triassic carbonates (Muschelkalk facies; Suarez Alba, 2007) and a 600-700 m thick succession of continental evaporites and fine clastics Upper Triassic in age (Keuper facies) (Bartrina et al., 1990; De Torres and Sánchez, 1990). Five stratigraphic units have been distinguished in the Keuper facies, based on the predominant lithology (Figs. 5.2 and 5.3) (Ortí, 1974; De Torres and Sánchez, 1990; Ortí and Pérez-Lopez, 1994): K1, a thick (250 m) salt layered sequence with thin interbeds of grey gypsiferous marls, sandstones and carbonates; K2, a 70 m thick msuccession of fine-grained red sandstones; K3, about 130 m of massive red and green mudstones; K4, a 150 m thick package of red and, locally, grey gypsiferous mudstones with interbeds of salt; and K5, a 50 m thick succession of laminated gypsum. Although all these units are included in the diapir and salt wall bodies, the development of the salt-related structures seems to be mainly driven by the salt flow of the K1 unit, the thickest salt layered sequence. Thus, in the Bicorb-Quesa salt wall segment, surface mapping (Fig. 5.2) and magnetotelluric data (Rubinat et al., 2010) clearly show that the dry salt coring the salt wall correlates at surface with the intensely folded and sheared sequences of the Keuper K1 unit.

The geological mapping of K1 and the other easily distinguishable diapir-integrating units evidence that the internal structure of the Bicorb-Quesa and the northern Navarrés salt wall segments is rather complex with variably oriented folds, shear zones and faults cut by the sheared salt wall edges (Fig. 5.2). More precisely, the mapping shows that these salt wall segments are constituted by two folded and sheared anticlines cored by Muschelkalk facies and/or diapiric K1 unit: the Barranco

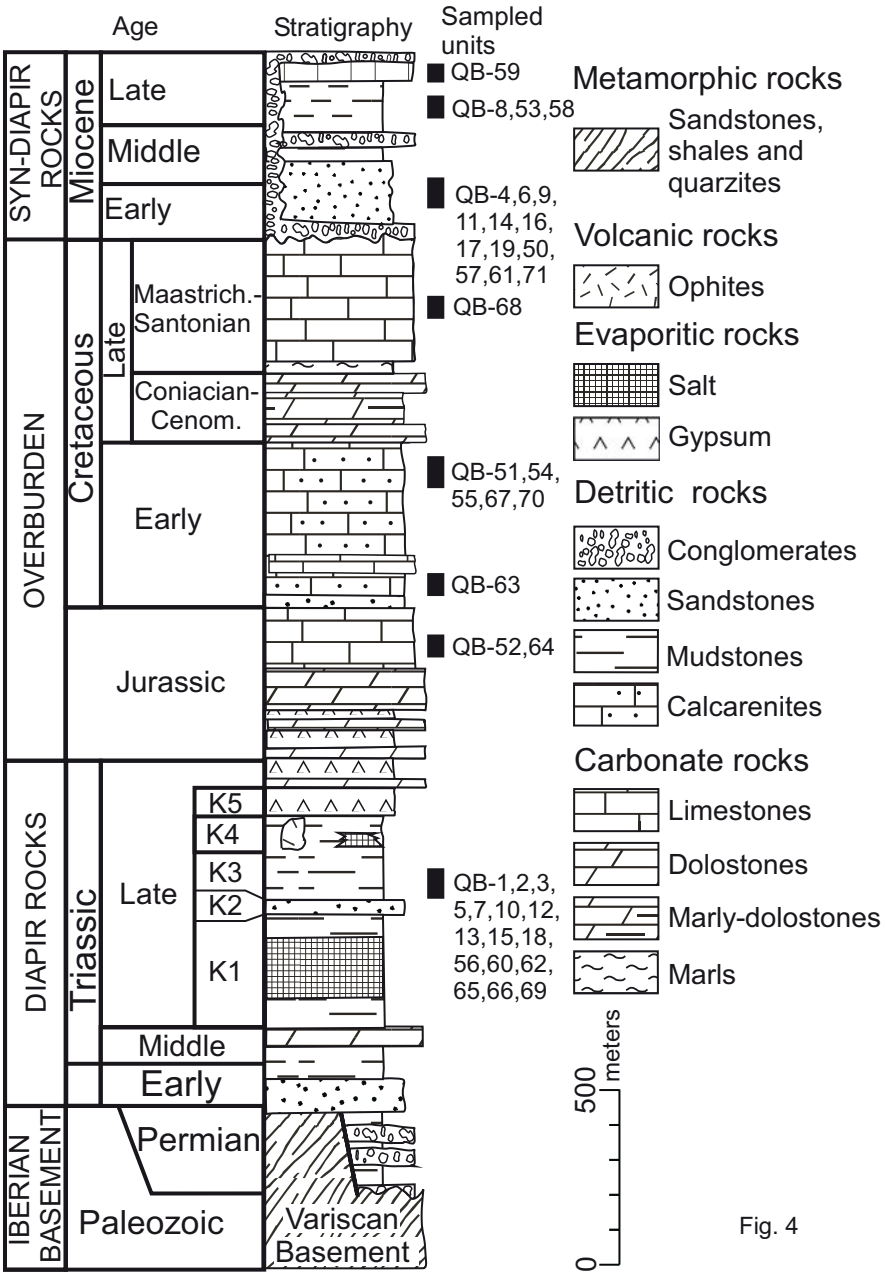

Figure 5.4. Synthetic stratigraphic chart of the study area. Stratigraphic location of the paleomagnetic sampled sites are indicated with black squares and rectangles on the right of the lithological section (see table 1 in supplementary material, for data details).

Salado and Albaidares anticlines (Fig. 5.2). These two anticlines are arranged along the Bicorb-Quesa Salt Wall axis and are separated by an ESE-trending syncline in which extensionally faulted upper Keuper (K2 to K5) and lowermost Jurassic successions crop out (Fig. 5.2).

The structure of the Barranco Salado and the Albaidares anticlines is very similar (Fig.2 and 3). They are double-plunging folds fringed by outward verging synclines that disappear towards the periclinal anticline ends. Also, both anticlines are

affected by the same kind of faults and shear zones: NNE-SSW trending faults that develop inside the diapiric K1 unit and located along the western boundary of the outward verging synclines and others faults parallel to the salt wall axis that get in contact the inner parts of the anticline (mainly K1 and Muschelkalk) with the folded "non-diapiric" upper successions K2 to K5. These last longitudinal faults and shear bands are located close to the salt wall edges and disappear at the anticline ends. These faults show a reverse geometry in the center of the anticlines; bordered by synclines meanwhile on the periclinal have normal fault geometries and the synclines are absent.

The double-verging geometry of the central parts of the Barranco Salado and Albaidares anticlines as well as the presence of both kinds of bounding shear bands denote the development of the Bicorb-Quesa salt diapir with incipient bulbs. The development of these salt diapirs is evidenced by the existence of salt springs in these areas and the presence of chaotic brecciated bodies affected by dissolution collapse landforms inside the K1 unit that can be interpreted as cap rocks. It is also corroborated by the analysis of 293 minor-scale fold and shear band data collected mainly in the diapiric K1 unit. This dataset shows that the fold axes and planes dip few degrees in the periclinal anticline ends but not in the central anticline parts where they are mainly vertical or highly dipping (Fig. 5.2). This fold pattern denotes a sharp change in the salt flow along the anticlines from horizontal in the periclinal anticline ends to vertical in the anticline parts fringed by outward verging synclines. It should be noted that the transition between both anticline portions with different salt flow coincides with the described NNW-trending shear zones which can be consequently interpreted as boundaries of the anticline diapiric areas.

Besides of these curtain folds derived from the vertical salt flow, the Keuper successions of the Barranco Salado and Albaidares anticlines are also deformed by other fold sets with low-dipping axes. Among them, the set of NNW- to WNW-trending folds affecting the upper Keuper K2 to K4 successions of the anticline limbs appears clearly depicted in the map of Fig. 5.2. These folds mainly plunge northwestwards and are cut by both the Bicorb-Quesa salt wall edges and the longitudinal faults and shear bands formed along the anticline limbs (Fig. 5.2). Consequently, they must be interpreted as folds that probably formed before or during the earlier stages of the Bicorb-Quesa salt wall development.

The Barranco Salado and Albaidares anticlines, however, are not exactly alike. The Barranco Salado Anticline includes Muschelkalk rocks in its outcropping inner part, not observed in the Albaidares Anticline. Moreover, the Albaidares Anticline appears flanked by a set of parallel narrow upright tight to isoclinal folds absent in the

Barranco Salado Anticline (Fig. 5.2). These last folds also deform the oblique WNW to NW-trending folds and, affecting the entire Keuper succession, have sometimes overturned limbs cut by thrusts or shear zones.

Regarding the Muschelkalk carbonates cropping out in the Barranco Salado Anticline, they constitute two isolated sheets that rest upon the K1 and, locally, K2 and K3 Keuper units (Fig. 5.2). Consequently, they belong to the remains (klippes) of the hanging wall of a major thrust that placed the Muschelkalk over folded Keuper units. The emplacement age of this thrust is well constrained by the geometry of these Muschelkalk klippes that are both folded by the Barranco Salado and related longitudinal folds and cut by the longitudinal faults and shear zones developed along the southern anticline limb (Fig. 5.2). These geometric relationships indicate that the emplacement of this thrust took place before the development of the present-day diapir salt wall but after an older folding stage of the Keuper units. Taking into account this relative chronological age, the regional deformational history and the adjoining overburden structure, Roca et al (1996; 2006) suggested that this thrust emplacement occurred during the middle Miocene development of the Prebetic fold-and-thust belt just after the closure of an older diapir.

The existence of this older diapir is proved by: a) the stratigraphical and structural features of the sediments filling the Bicorb Half-graben (Roca et al., 1996; Anadón et al., 1998); and b) the presence of a squeezed diapiric stem on the northern flank of the Bicorb-Quesa salt wall segment (locally represented by a secondary weld). This squeezed stem is represented by the anastomosed body of Upper Triassic rocks that crops out northwestwards of a narrow stripe of Jurassic and K5 materials at the northwest limb of the Albaidares Anticline (Fig. 5.2). Bounded by two ENE-trending shear zones, this strongly deformed body is constituted by a mélange of Keuper units thrusted by the Cretaceous successions of the Picos de la Olla Thrust (Fig.2). This thrust also affects the lower Miocene fill of the Bicorb Half-graben (Anadón et al., 1998; Rubinat et al., 2012) and is cut by the ENE-trending shear zone that constitutes the northwestern edge of the late Miocene Bicorb-Quesa salt wall segment. Accordingly the formation of the underlying mélange of Keuper units must be placed during the early-middle Miocene when the sedimentary record of the Bicorb Half-graben denotes an increase of salt extrusion (Anadón et al., 1998) that has been associated with a contractional diapir reactivation.

5.4.Paleomagnetic sampling and laboratory procedures

A total of 41 paleomagnetic sites were sampled inside the Bicorp-Quesa and northern Navarrés salt wall segments and through the adjacent Mesozoic overburden and syn-diapiric Miocene deposits (Fig. 5.2). As shown in Figure 5.4, sampling focused on: (1) the red mudstones and fine grained sandstones of the K3 Keuper unit (16 sites), (2) the grey and white Jurassic and Cretaceous limestones (9 sites) and, (3) the white, grey, orange and red mudstones and fine grained sandstones of the Miocene half-grabens infills (16 sites, 12 in the lower Miocene and 4 in the upper Miocene). Paleomagnetic samples were obtained with a portable drill cooled with water. Soft rocks (mudstones and fine grained sandstones) were drilled with an electrical power drill, whereas a gas power drill was used to sample harder materials (limestones). Ten to twelve samples per site were drilled along 2-5 meters of stratigraphic succession in order to average the geomagnetic field secular variation. All samples were oriented *in situ* with a compass placed on a core orienting device with inclinometer.

Paleomagnetic analyses were carried out in the Paleomagnetic Laboratory of Barcelona (CCiT UB-CSIC). They consisted in stepwise thermal demagnetization and subsequent measurement of the Natural Remanent Magnetization (NRM) of 8 paleomagnetic specimens per site. Thermal demagnetization was conducted in thermal demagnetizers TSD-1 (Schonstedt) and MMTD-80 (Magnetic Measurements) and the NRM was measured in a superconducting rock magnetometer SRM 755R (2G Enterprises). Upper Triassic red beds were heated up to 700 ºC, Jurassic and Cretaceous limestones up to 570 ºC and Miocene samples up to either 570 or 690 ºC depending on their lithology. Demagnetization data were represented in vector-end point orthogonal diagrams also known as Zijderveld diagrams (Zijderveld, 1967) (Fig. 5.5). Magnetic components were calculated by principal component analysis (Kirschvink, 1980) after visual inspection of the Zijderveld diagrams. Linear regression techniques were used to calculate the directions of the observed components which were classified in class 1, 2 or 3 according to the following criteria. Directions showing straight trajectories directed towards the origin and maximum angular deviations (MADs) of the linear regression lower than 10 were classified as first class. When the demagnetization plots were also well directed towards the origin but more scattered or the calculated direction got MAD greater than 10, they were classified as second class directions. Finally, scattered directions not directed towards the origin were classified as third class directions and were discarded for additional analyses (Table supplementary material). The site mean directions and dispersion parameters (k and a95) were obtained following Fisher's statistics (Fisher, 1953) (Fig. 5.6). Site mean

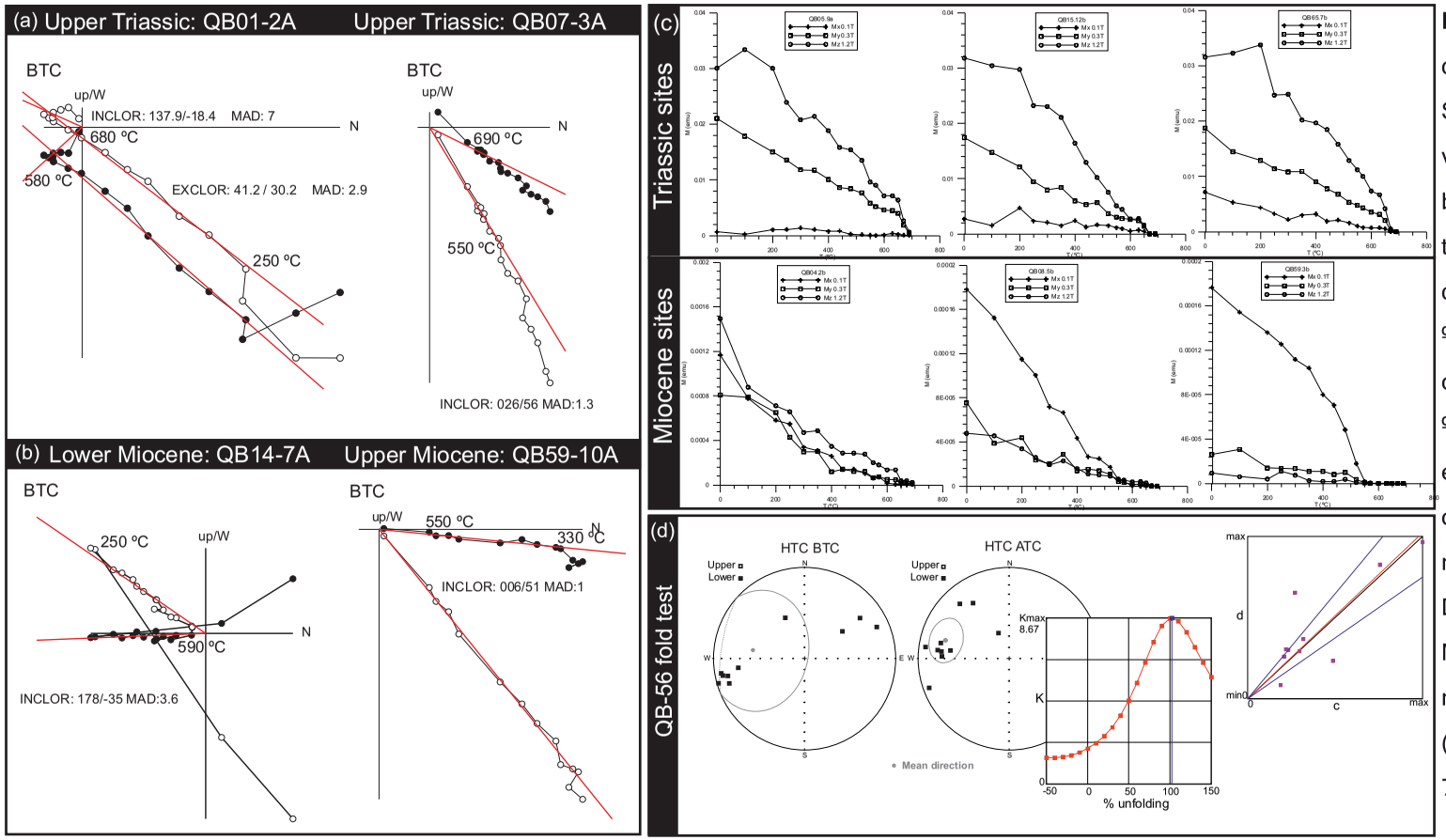

Figure 5.5.(a) Demagnetization diagrams of Triassic samples. Sample QB01-2A shows a viscous component erased below 250 ºC, an intermediate temperature component (ITC) defined between 300 and 580 ºC and a high temperature component (HTC) up to 680 ºC. Sample QB07-3A only exhibits a HTC. The calculated characteristic components are represented as red lines. (b) Demagnetization diagrams of Miocene samples, showing normal and reverse polarities (samples QB59-10A and QB14-7A, respectively). (c) Thermal demagnetization of 3 axis IRM for Triassic and Miocene samples. Triassic samples show a mixture of hematite and medium coercivity magnetite with very low content of low coercivity magnetite. For Miocene sites, Upper Miocene samples (QB08-5B and QB59-3B) show a predominance of low coercivity magnetite, whereas Lower Miocene sample QB04-2B exhibits a higher proportion of hematite and similar contents of low and medium coercivity magnetite. (d) Fold test for site 56 (Watson and Enkin, 1993). Individual directions for ITC and HTC are represented in stereographic projection before and after tectonic corrections. A best grouping can be observed for the HTC component. Variation of k with rate of unfolding for the HTC components is also represented. The highest k is attained close to the 100% of unfolding, resulting in a positive fold test.

Site	Age	s0	comp.	N	Dg	Ig	k	α95	Ds	Is	k	α95
Bicorb-Quesa Diapir												
QB1	Tk	290/50	ITC	8(8)	047	42	54	7.6	344	44	54	7.6
			HTC	6(8)	194	52	3.9	38.8	230	33	3.9	38.8
QB2	Tk	053/39	ITC	7(8)	038	22	5.2	29.2	011	-16	5.2	29.2
			HTC	5(8)	343	20	8.9	27.2	322	03	8.9	27.2
QB3	Tk	329/83ov	ITC	5(8)	083	29	37.4	12.7	301	24	37.4	12.7
			HTC	7(8)	099	63	3.2	36.8	340	24	3.2	36.8
QB5	Tk	026/52ov	ITC	8(8)	028	11	23.4	11.7	131	41	23.4	11.7
			HTC	6(8)	050	30	25.1	13.6	112	18	25.1	13.6
QB7	Tk	325/50	HTC	7(8)	013	31	146.7	5.0	005	-06	146.7	5.0
QB10	Tk	051/67	ITC	8(8)	286	24	19.6	12.8	334	40	19.6	12.8
			HTC	7(8)	300	24	17.1	15.0	337	27	17.1	15.0
QB12	Tk	155/49	ITC	8(8)	330	15	7.5	21.7	334	64	7.5	21.7
			HTC	6(8)	159	23	11.7	20.4	348	26	11.7	20.4
QB13	Tk	165/49	HTC	7(8)	347	15	3.8	32.7	10	62	3.8	32.7
QB56	Tk3	fold	ITC	5(18)	045	02	39.2	12.4	321	40	27.6	14.8
			HTC	10(18)	280	42	1.9	51.1	286	28	8.7	17.4
QB60	Tk3	028/64	ITC	5(8)	340	20	38.3	12.5	338	-25	38.3	12.5
			HTC	5(8)	185	05	83.7	8.4	338	-60	83.7	8.4
QB65	Tk3	004/79ov	ITC	7(8)	246	29	55	8.2	344	29	55	8.2
			HTC	6(8)	094	-37	142.1	5.6	335	06	142.1	5.6
Navarrés Diapir												
QB15	Tk	055/60	HTC	8(8)	314	12	58.2	7.3	330	15	74.7	6.4
QB18	Tk	185/48	ITC	8(8)	243	-29	16.5	14.1	336	42	16.5	14.1
			HTC	7(8)	276	-33	31.2	11	313	21	31.3	11
QB62	Tk3	144/25	ITC	8(8)	295	32	26	11	281	53	26	11
			HTC	7(8)	144	23	32	11	324	02	32	11
QB69	Tk3	069/60	HTC	8(8)	160	13	9.6	18.8	328	-07	9.6	18.8
Bicorb Half-Graben												
QB6	Mio-	330/55	HTC	8(8)	083	25	14.3	15.2	050	33	14.3	15.2
QB8	Mio+	335/30	HTC	6(8)	008	57	25.4	13.6	354	25	25.4	13.6
QB57	Mio-	123/86ov	HTC	8(8)	063	22	48.5	8.0	006	26	48.5	8.0
QB58	Mio+	340/07	HTC	8(8)	348	52	24.4	11.4	347	45	24.4	11.4
QB59	Mio+	318/03	HTC	7(8)	004	54	1069.1	1.8	001	52	1069.1	1.8
Quesa Half-Graben												
QB4	Mio-	149/45	HTC	5(8)	020	21	67.5	11.3	046	42	67.5	11.3
QB17	Mio-	163/10	HTC	6(8)	024	34	19.1	15.7	029	41	19.1	15.7
QB19	Mio-	108/17	HTC	7(8)	005	38	21.7	13.3	019	40	21.7	13.3
QB53	Mio+	124/06	HTC	6(8)	019	47	29.8	12.5	025	48	29.8	12.5
Escalona Half-Graben												
QB16	Mio-	063/56	HTC	8(8)	312	39	16.7	14	359	35	16.7	14
QB71	Mio-	281/13	HTC	6(8)	022	47	167.1	5.2	008	48	167.1	5.2
QB61	Mio-	010/48	HTC	8(8)	280	70	6.5	21.9	343	39	6.5	21.9
Juanera Half-Graben												
QB11	Mio	015/10	HTC	6(8)	345	55	153.7	5.4	350	46	153.7	5.4
Playamonte Half-Graben												
QB14	Mio-	221/13	HTC	6(8)	354	47	32	12	341	55	32	12

Table 1: *Paleomagnetic* results.

directions (Table 5.1) were also classified in three qualities based on the following criteria: sites with a95 lower than 10 were qualified as first class, second class sites were defined for a95 between 10 and 25 and finally third class sites correspond to sites with a95 higher than 25. Third class sites were considered unreliable and were discarded for further interpretations.

Additionally to thermal demagnetization, isothermal remanent magnetization (IRM) acquisition up to 1.2 T and 3 axes IRM (in fields of 1.2, 0.3 and 0.1 T) demagnetization according to Lowrie (1990) were applied to 10 selected samples to characterize the magnetic carriers of the different sampled lithologies (Fig. 5.5). IRM acquisition was performed with a pulse magnetizer IM10-30 (ASC Scientific) and thermal demagnetization was conducted on a thermal demagnetizer TSD-1 (Shondstedt).

5.5.Paleomagnetic results

5.5.1.First and second class Upper Triassic (K3) sites

Initial NRM intensities of the Upper Triassic samples ranged from 406• 10^{-6} to 15887•10^{-6} A/m with average values around 4000•10^{-6} A/m. Up to 18 thermal demagnetization steps were applied between 100 and 700ºC. The obtained demagnetization diagrams revealed a low temperature viscous component (usually erased around 250ºC) parallel to the recent magnetic field before any tectonic correction. Above this temperature, most samples showed two stable components with both normal and reverse polarities (Fig. 5.5 and Table 5.1). The first component is defined between 250 and 520ºC, pointing to magnetite as its main remanence carrier. This component has been called "Intermediate temperature component (ITC)" and has been observed in 11 Upper Triassic sites. The other stable component, the so-called "High temperature component (HTC)", is defined between 550ºC and 690ºC and has been identified in 12 sites. These maximum unblocking temperatures suggest hematite as the main remanence carrier of this last component (Fig. 5.5). IRM acquisition and thermal demagnetization of 3 axes IRM (Lowrie, 1990) (Fig. 5.5) also reinforce the presence of a mixture of magnetite and hematite as principal magnetic carriers in the Keuper K3 mudstones and fine sandstones.

Mean directions per site have been obtained for the ITC and HTC before and after tectonic correction (Table 5.1). Tectonic correction of both ITCs and HTCs has been carried out following two different tilt corrections depending on the location of the site with respect to the internal structural elements inside the salt wall. Thus, in areas where the structure is relatively simple and consists on parallel sets of non-plunging upright folds (sites QB10, QB15, QB62, QB69), the tectonic correction has been done by simple restoration of bedding to the horizontal. In areas with superimposition of 2 different-oriented trains of folds, we have corrected following two steps. The first step unfolds the later vertical growth of the salt wall restoring to the horizontal the general dip shown by the flanks of the salt wall around each analysed site. This results in a new orientation for both bedding attitude and ITC and HTC components that would correspond to the end of the first folding phase stage. The second step consists on unfolding the resulting directions by means of a simple restoration of beds to the horizontal with the new bedding orientation. The validity of this two-step tectonic correction is proven since the internal structure of the studied salt walls has been analysed in detail. Site mean directions before and after tectonic correction were represented in stereographic diagrams and compared to the Late Triassic and Miocene reference directions for stable Iberia (Fig. 5.6). The Late Triassic reference mean direction has been calculated from the Iberian Ranges, Alcazar de San Juan,

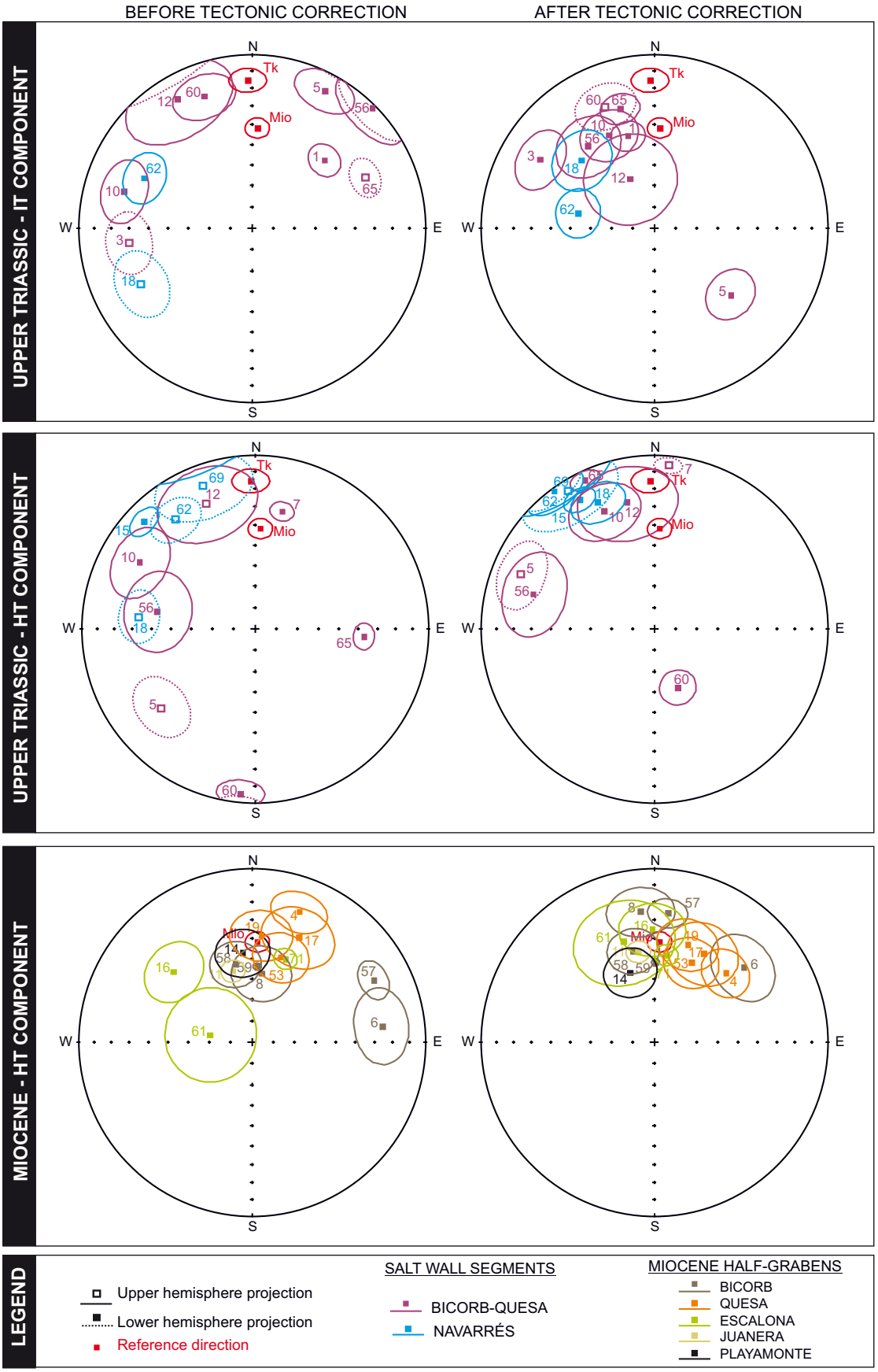

Figure 5.6. Stereographic projections of site mean directions. Open (closed) symbols and dashed (solid) lines correspond to projections onto the upper (lower) hemisphere. Reference directions are represented in red (Tk: Upper Triassic; Mio: Miocene).

Alcazar South Meseta and Ayllon directions as compiled by Osete et al (1997) and Osete and Palencia (2006). The Miocene reference has been calculated from the Calatayud, Esteban/Sora and Bardenas magnetostratigraphic sections (Krijgsman et al, 1996; Pérez-Rivarés et al, 2004 and Larrasoaña et al, 2006; respectively). Both directions were relocated to the geographic coordinates of the studied area by the via pole conversion method (Noel and Batt, 1990), obtaining a reference mean direction of 358.4/15.6 (a_{95}=7) for the Late Triassic and 003.1/41.6 (a_{95}=5.2) for the Miocene.

For the ITC, the mean directions of each site show variable clustering with *k* values ranging between 5.2 and 55 and a_{95} ranging from 7.6 to 29.2 (Table 5.1). Before tectonic correction, the ITC mean site directions show scattered NE to North to NW to SW declinations with low-medium (2-42º) inclinations (Fig. 5.6). Once the tectonic correction is applied, the clustering of the mean directions improves significantly (Fig. 5.6), showing a general NW declination (286-344ºN) with moderate inclinations (23-64º). In average, these inclinations are higher than the Late Triassic reference one (I=15.6º) and lower than the inferred for the Miocene reference direction (I=41.6º). Accordingly, the ITC component is interpreted as a non primary component acquired prior to the total tilting of beds in relation with salt wall development. The normal and inverse polarity of this component (Table 5.1) suggests that it might respond to various remagnetization events or to a large one, which age and/or ages are difficult to constrain.

Regarding the HTC, site mean directions also show variable clustering with *k* values ranging between 3.9 and 146.7 and a_{95} ranging from 5.0 to 38.8 (Table 5.1). The mean directions also show a very scattered distribution before tectonic correction with general moderate inclinations (5-63º), and, as the ITC components, their clustering significantly improves after tectonic correction (Fig. 5.6). In particular, all HTC site mean directions become NW-directed (292-352º) with inclinations that, except in site 60, are similar or slightly lower than the inclination of the Late Triassic reference direction (Fig. 5.6). This suggests a pre-tilting magnetization for the HTC component. The primary character of both components has been tested by means of a fold test (following Watson and Enkin, 1993) in site 56, which present a metric fold and samples were sampled on both flanks (Fig. 5.5). For the ITC no significant improvement of mean direction statistic parameters is achieved and an undetermined fold test is obtained after tectonic correction. Conversely, the HTC individual directions tend to cluster when applying the tectonic correction diminishing a95 and increasing k, with the best grouping attained close to the 100% of untilting (Fig. 5.5), confirming the prefolding origin of this magnetization. Consequently, the angular differences between the tectonic-corrected HTC site mean directions and the expected Late Triassic reference direction can be used to define the VARs affecting the sampled Upper

Triassic materials (K3 unit). As shown in the stereoplots of Fig. 5.6 and the map in Figure 5.7, these VARs are always counter-clockwise with an average value of 15-30º. However, there are few exceptions to this general trend. Site 7 depicts a small clockwise VAR (8º) that is non-significant because its confidence angle is slightly overlapped to the one of the reference direction. Site 5 yields a deviant direction after tectonic correction, WNW declination with negative inclination. It should be noted that the ITC mean direction of this site also yields an outsider direction when compared to the rest of sites denoting an anomalous behavior. Finally, site 56 reveals about 70º of counter-clockwise VAR and site 60 also shows an anomalous mean direction.

After tectonic correction, the distribution of most mean directions of both ITC and HTC components displays a similar pattern with NW declinations (Fig. 5.6). This implies that the VARs affecting the HTC (i.e. the primary Upper Triassic component) probably also affect the ITC (i.e. the secondary component which age of acquisition is unknown), that is, the counter-clockwise VARs affecting the Upper Triassic rocks probably occurred after the acquisition of the ITC. The grouping of the ITC mean directions after tectonic correction (Fig. 5.6) suggests that this secondary component was acquired before the tilting of beds related to salt wall inflation. Thus, the timing of the deduced VARs is bracketed after the acquisition age of the ITC, and therefore before the tilting of beds related to the final salt wall development.

5.5.2.Jurassic and Cretaceous sites

Jurassic and Cretaceous samples yielded erratic demagnetization diagrams due to low NRM intensities and unstable behavior at relatively low temperatures (Table 5.1, supplementary material). Thus, the paleomagnetic data from the 9 Jurassic and Cretaceous sites were not taken into account for further interpretations.

5.5.3.First and second class Miocene sites

Initial NRM intensities ranged from $40 \cdot 10^{-6}$ to $3717 \cdot 10^{-6}$ A/m with average values around $500 \cdot 10^{-6}$ A/m. These values are valid for all sites, except QB11 which exhibits much higher NRM intensities with values ranging from $23616 \cdot 10^{-6}$ to $42061 \cdot 10^{-6}$ A/m. 14 thermal demagnetization steps were applied between 100 and 570ºC for the white and grey samples and from 100 up to 690ºC for the orange and red samples. Overall, the demagnetization diagrams show the presence of two components (Fig. 5.5). The first one is a low temperature viscous component parallel to the present

day geomagnetic field generally removed below 200 ºC. After removing this viscous component, samples show a well-defined component with either normal or reversed polarity which has been considered as the characteristic remanent magnetization (ChRM). This component is usually defined between 300-550ºC in the pale samples (Fig. 5.5) pointing to (titano) magnetite as the main remanence carrier. Red samples got characteristic components usually defined between 300-550 ºC and 450-670 ºC pointing to a mixture of (titano) magnetite and hematite as the remanence carriers. IRM acquisition and thermal demagnetization of 3 axis IRM (Fig. 5.5) also show the presence of a mixture of magnetite and hematite with predominance of low coercivity magnetite in Upper Miocene sites (QB8 and 59) and a higher proportion of hematite in Lower Miocene sites (QB04). Mean directions per site for the ChRM component before and after bedding correction were represented in stereographic diagrams to compare them to the Miocene reference direction for the Iberian Peninsula, 003.1/41.6 (a_{95}=5.2) (Fig. 5.6).

From Fig. 5.6 it can be observed that the mean directions of the ChRM component show a better grouping after bedding correction which, together with the presence of both normal and reverse polarity components at the site level, suggests that it is a primary magnetization. Northwards the Bicorb-Quesa salt wall (i.e. inside the Bicorb Half-graben), the mean directions of all sites, except site QB6 that exhibits a significant clockwise VAR of 47º, show overlapping of their confidence limits with the confidence angle of the Miocene reference direction, revealing no significant VARs there (Fig. 5.7). On the contrary, all sites located south of the Bicorb-Quesa salt wall (i.e. inside the Quesa Half-graben) show clockwise VARs; 43º in site QB-4 and 15-26º in the other sites (QB17, QB19 and QB53), although the confidences angles of these sites are slightly overlapped with the Miocene reference direction one (see Fig. 5.6). At the Juanera and Playamonte half-grabens (sites QB11 and QB14, respectively), counter-clockwise VARs of 10-19º are deduced. All sites located at the Quesa basin show a similar VAR pattern and the youngest site (QB53) was done in Middle-Upper Miocene rocks, therefore, VARs affecting rocks from this basin must be at least post-Middle Miocene, probably linked to the development of the present salt-wall during the Late Miocene.

5.6.Driving mechanism for the late Miocene salt wall development

Paleomagnetic data together with sedimentological and structural data provide fundamental information that allows to characterize the mechanism controlling the development of the Bicorb-Quesa and Navarrés salt wall segments during the late

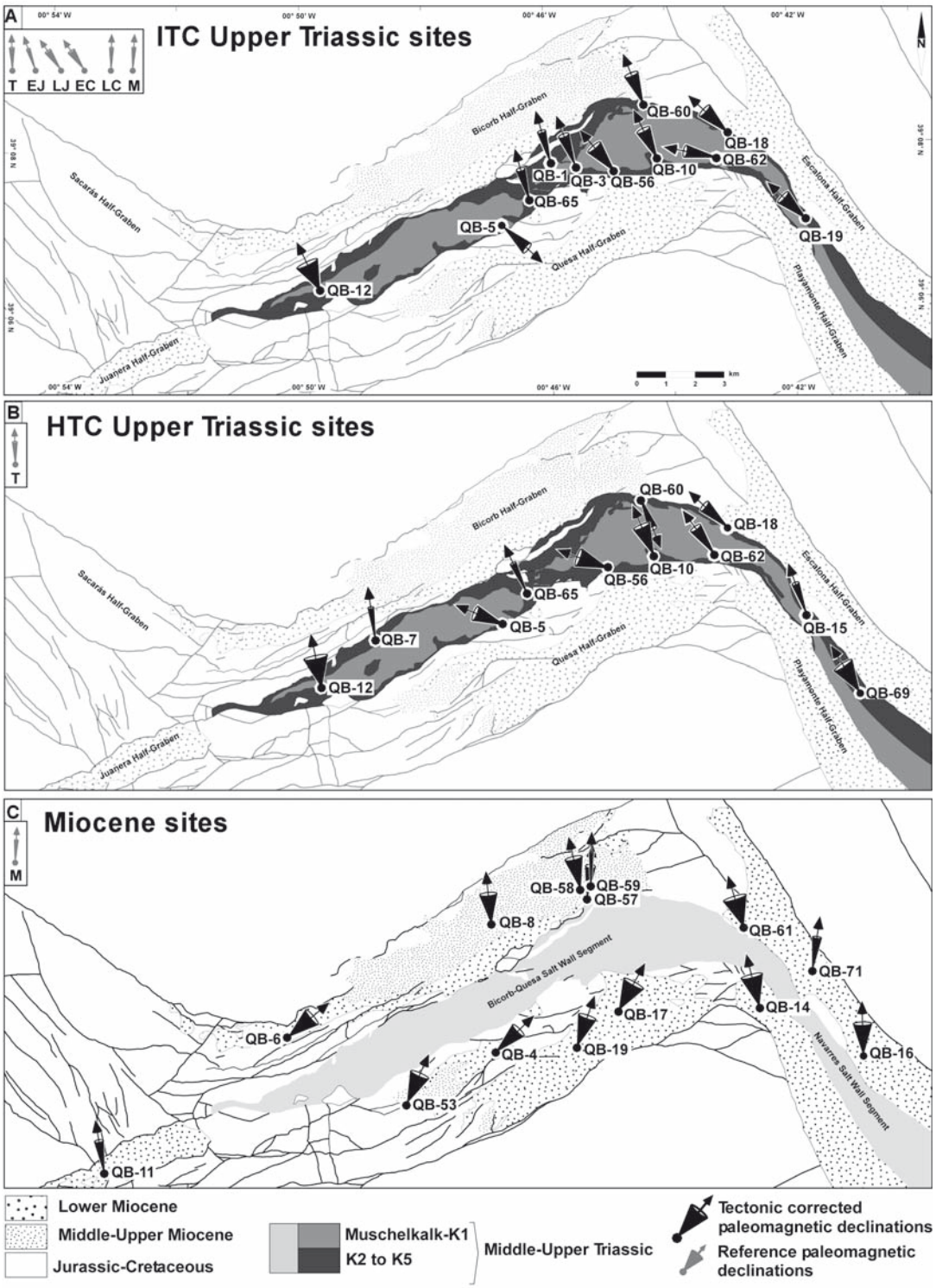

Figure 5.7. Simplified geological map of the study area with the tectonic corrected declinations of the measured paleomagnetic sites, where the keuper ofthe Navarres SWS is an aproximation. Cones represent the α_{95} of the mean directions. Within the black box is located the reference paleomagnetic declination of Triassic (T), Early Jurassic (EJ), Late Jurassic (LJ) Early Cretaceous (EC), Late Cretaceous (LC) and Miocene (M). **A**. Declinations of the intermediate temperature components (ITC) measured in the Upper Triassic red and grey mudstones (K2 and K3 units); **B**. Declinations of the high temperature components (HTC) measured in the Upper Triassic red mudstones (K2 and K3 units). Note that only the first and second class sites are represented. **C**. Declinations of the Miocene sites;

Miocene. Previously, the available structural, geophysical and sedimentological data suggested that the Bicorb-Quesa Diapir corresponds to a salt wall formed above a NNW-dipping extensional basement fault. Besides they also allowed understanding the driving mechanisms that formed this salt wall segment during the early Miocene and its later middle Miocene contractional squeezing (Roca et al., 1996; Rubinat et al., 2010; 2012). However, they were insufficient to decipher the features of the mechanisms that led the extensional reactivation during the late Miocene and that were responsible for the present-day salt wall geometry.

Our paleomagnetic study provides two crucial data to understand this last evolutionary stage. The first one is the ascertainment that, before the growth of the actual salt wall, the Keuper roof acted as a regional detachment level decoupling Triassic materials affected by a generalized counter-clockwise VAR from a Jurassic to Miocene cover probably unrotated. And the second one is that the salt wall separates a northern domain (i.e. Bicorb basin) with unrotated Miocene sediments from a southern domain (i.e. Quesa basin) in which these materials are affected by VARs mainly clockwise and also a small counter-clockwise VAR following to the west the Bicorb-Quesa salt wall (i.e. Juanera basin) (Fig. 5.7). Both data denote that the formation of the present-day Bicorb-Quesa and Navarrés salt walls is related to a differentiated displacement of the southern cover block bounded northwards by these salt wall segments. This displacement was south-southwest directed and included a clockwise vertical-axis rotation component.

According to regional and structural data (De Ruig, 1995; Martínez del Olmo, 1999; Roca et al., 2006), the origin of this displacement, must be linked to a thin-skinned extensional deformation developed on top of the Keuper detachment level, which compartmentalizes the Prebetics Valencian Domain in several blocks bounded by ENE and NNW-trending extensional faults. The geometry and arrangement of these faults are strongly controlled by the underlying Bicorb-Quesa, Navarrés and Xúquer basement faults that shift and/or cut the Keuper detachment level (Fig. 5.8). Indeed, it can be observed from the maps in figures 1 and 2, that: 1) the orientation of the extensional faults affecting the cover is different on both sides of these basement faults; 2) the salt wall segments (sectors where the major extensional deformation in the cover level occurs) are located precisely upon the detachment level steps that generate these basement faults; and 3) the northern boundary of the extensionally deformed cover area is not rectilinear but formed by two nearly NW-trending border faults linked by a north to northeast-trending faulted relay ramp which coincides with the trace of the Bicorb-Quesa basement fault. This relay ramp becomes an accommodation zone to the southwest and separates an eastern domain extensionally displaced south-southwestwards from a western domain where this displacement, at

the same transverse, is null or significantly smaller. Consequently, it is part of an extensional faulted transfer zone in which there is a relative right-lateral strike-slip motion between the adjoining blocks. It should be noted that this relative strike-slip motion does not take place along strike-slip faults (see map in Fig. 5.1) but diffusely along a 2 to 8 km wide stripe where the Jurassic to Miocene cover is sheared and rotated clockwise. The clockwise rotation observed in the Miocene Quesa basin infill would reflect this kind of deformation since, as shown in Figure 5.8, it develops over the cover block located at the northern end of the accommodation zone where the rotation would be maximum. The clockwise VAR observed in the western end of the Bicorb Basin (site QB-6) could have also the same origin. In relation to the <10-20º counter-clockwise VAR recorded in the Juanera and Playamonte half-grabens (QB11 and QB14, respectively), they are placed out of the accommodation zone and probably record small lateral changes in the south- southwestwards displacement of the Jurassic to Miocene cover over the extensional fault system.

Accordingly with this proposed late Miocene deformation scenario, the salt walls would be formed in the most extended areas. This is, in the relay border fault that, located in the northern end of the accommodation zone, produces a significant displacement with a clockwise VAR of its hangingwall (Bicorb-Quesa segment); and over the detachment flexure formed upon the Navarrés basement fault (Navarrés segment). The origin of the Bicorb-Quesa salt wall segment by south to southwest displacement with rotation of the cover underlying the Quesa basin fill is coherent with the plan-view shape of the salt wall that disappears west of the proposed transfer zone and becomes progressively wider eastwards until its junction with the Navarrés salt wall segment (Fig. 5.2).

5.7.Internal salt wall kinematics

In this regional setting, the structural and paleomagnetic data collected in the outcropping Triassic rocks reveal that the internal structure of the salt walls not only records their late Miocene diapiric development but also an older deformation history. Specifically they show that, previously to the salt wall growth, the outcropping Triassic rocks were affected, first, by a generalized counter-clockwise VAR and, then, by the development of a train of tight WNW to NNW-trending folds. The pre-diapiric age of these deformations is defined by: 1) the cross-cutting relationships between these last folds and the longitudinal salt wall shear-bands and thrusts which, associated to the salt wall formation, clearly cut the folds; 2) the rather constant and oblique orientation of the WNW to NNW-trending folds in relation to the differently oriented salt wall

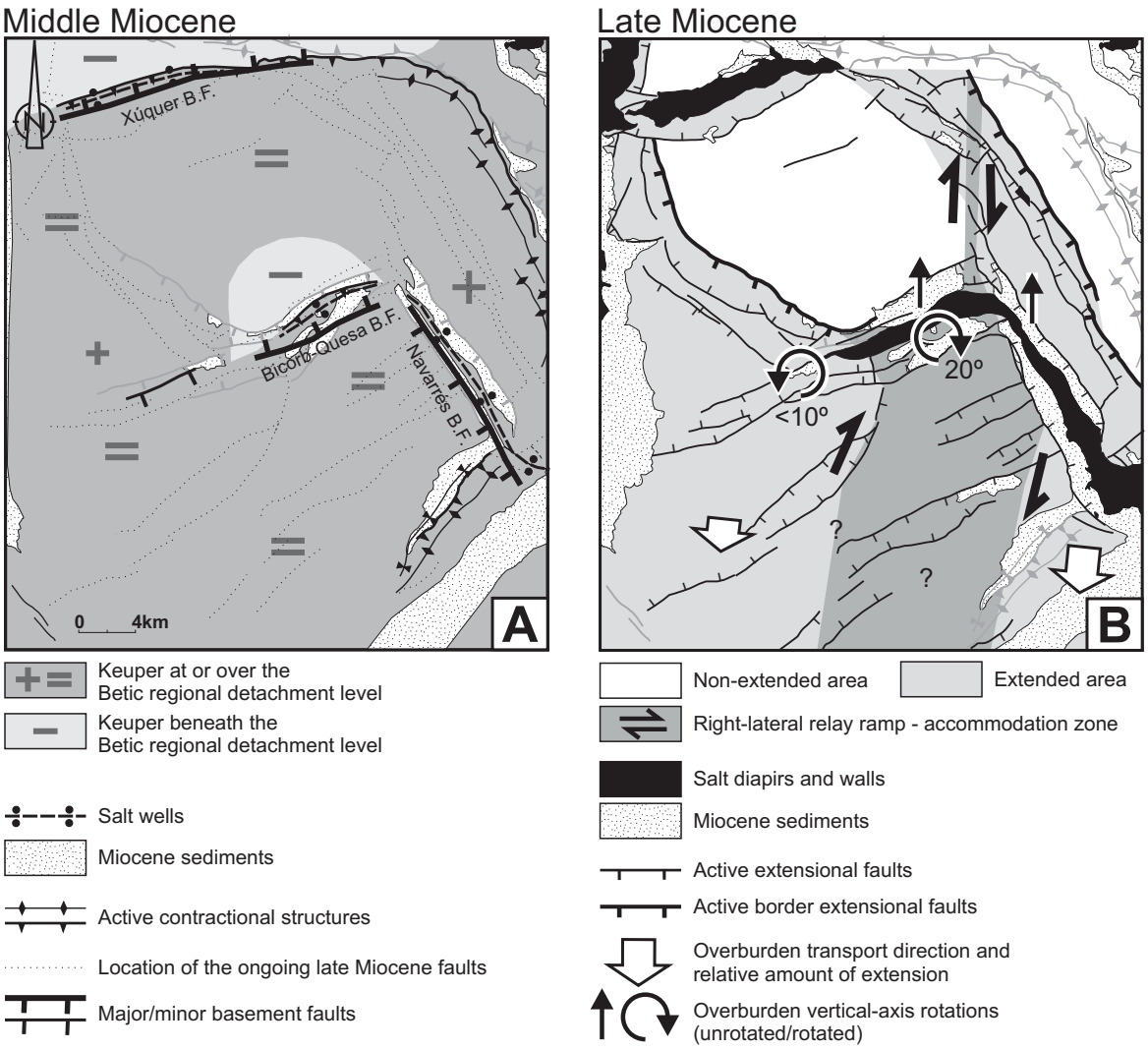

Figure 5.8 A. Structural map of the Valencian Domain at the end of the north-propagating middle Miocene contractional deformation. Note the arrangement of the pre-existing basement faults and how they control de cover deformation and the geometry of the Upper Triassic detachment level. **B.** Structural map of the Valencian Domain at the end of the late Miocene extensional deformation with the paleomagnetic rotations recorded in our sampled Miocene deposits. This second map denotes that the Bicorb-Quesa salt wall segment developed in a relay border fault that produced a significant displacement with a vertical-axis clockwise rotation of its hangingwall; and the Navarrés salt wall segment formed over a pre-existent detachment flexure. In both maps, active structures are in black and the inactive older ones in grey.

flanks; and 3) regarding the counter-clockwise VAR, by its pre-folding signature. With the available data, however, it is difficult to constrain the precise age of these two deformations. We can assert that the counter-clockwise VAR affecting the Triassic rocks occurred before the Miocene, since Miocene materials are not affected, and after the acquisition of the ITC, interpreted to be occurred before the tilting of beds. Regarding the timing of the folds, they are constrained between the VAR event (as VARs are pre-folding) and the late Miocene.

Taking into account these constraints and the regional deformation history of this sector, the counter-clockwise VARs observed in the Upper Triassic rocks must be associated to the Paleogene-earliest Miocene contractional stage related to the development of the Iberian Chain. Meanwhile the WNW to NNW-trending folds may be formed during the development of the Iberian Chain or the Betic Chain. These two contractional fold-and-thrust belts affected the study area and generated the horizontal displacement of the Mesozoic cover over an autochthonous Lower Triassic-Paleozoic basement (Roca et al., 1996; Rubinat el al., 2012). This displacement, in both cases, could be accompanied by VAR and was able to form duplexes and detachment folds between the top of Buntsandstein and upper Keuper detachment levels. The thrusting of the Muschelkalk carbonates over the Keuper observed at the Barranco Salado Anticline (Fig. 5.3) would be an example of this kind of Triassic internal deformation developed during the contraction building of the Paleogene-earliest Miocene Iberian Chain or middle Miocene Prebetics.

The rest of structures observed in the Bicorb-Quesa salt wall segment, clearly younger, can be directly related with the rise of the salt wall and together allow establishing a pattern of the formation and later kinematic evolution of the external Prebetics salt walls. In this history, younger VARs are not detected and two stages can be distinguished. The first one corresponds to reactive growth of the salt wall and it is characterized by the formation of a set of large double-plunging anticlines along the developing salt walls, often flanked by minor parallel upright folds. These folds, commonly with parallel thrusts or shear zones cutting the vertical to overturned limbs, are cored by inflated masses of the diapiric K1 unit which apparently are more shortened. The structural features of this train of longitudinal folds are consequently coherent with the beginning of the salt inflation process along the salt walls with salt flowing from the bottom of the salt wall flanking Miocene half-grabens to the core of the axis salt wall anticlines. With a probably heterochronous transition along the walls, the second stage records, in turn, the active to passive growth of the salt walls. Therefore it corresponds to the stage in which the folded Triassic pierces the overburden and generates the present-day salt wall geometry. In this second stage, the formation of small extruding diapirs piercing the anticline culminations combined with the lack of these structures in the saddles denotes that the amount of salt inflation continues to not being uniform along the salt walls. This gives rise to a longitudinal migration of the salt in the K1 unit from the saddles to the culminations which produces the observed extensional collapse of the anticline saddles in advanced evolutionary stages. It should be noted that in this stage, such changes in the amount of salt inflation are not gradual but rather sharp in such a way that they occur along more or less vertical shear zones oblique to the salt wall flanks. This kind of shear

zones, also present along the salt wall flanks, produces a vertical stretching of the affected successions and, in the case of passive markers as paleomagnetic data, might deform the initial paleomagnetic vector. This is evident in site QB-57 which shows an anomalous high paleomagnetic inclination (Fig. 5.6). This site was sampled in lower Miocene materials strongly deformed by the shear zone that limits the Bicorb-Quesa salt wall segment to the north. Also, such local shearing deformation can be invoked to explain the major counter-clockwise VAR and the deviated inclinations from the Triassic reference one in the Upper Triassic sites QB-5, QB-56 and QB-62, all of them located against the southern flank of the Bicorb-Quesa salt wall segment (Fig. 5.7).

5.8.Conclusions

This work demonstrates that paleomagnetism represents a powerful technique not only to characterize the internal structure of the salt-related structures but also to improve our understanding on their kinematics and driving mechanisms. Thus, this technique carried out in the diapiric rocks and overburden of the selected examples, the Bicorb-Quesa and Navarrés salt wall segments (Prebetic Zone), together with a detailed analysis of their internal structure, have permitted to constrain their kinematics providing fundamental data to understand their evolutionary stage.

The outcropping Upper Triassic diapiric rocks were affected firstly, by generalized counter-clockwise VAR (ranging between 15-30º) and, afterwards, by a train of tight WNW to NNW-trending folds. These VARs, only affecting Upper Triassic rocks (data from the Jurassic and Cretaceous overburden were not satisfactory), are probably associated to the thin-skinned Paleogene-earliest Miocene contractional stage related to the building of the Iberian Chain. Meanwhile the folding is related to this same event or the Middle Miocene contractional stage related to the Betic Chain emplacement.

The origin of the Bicorb-Quesa and Navarrés salt wall segments during the Late Miocene is linked to a thin-skinned extensional fault deformation that, developed on top of the Keuper detachment level, compartmentalized the Valencian Domain of the Prebetics in several cover blocks bounded by ENE and NNW-trending extensional faults. The geometry and arrangement of these faults were strongly controlled by underlying basement faults that shifted and/or cut the Keuper detachment level. In this regional scenario, the Bicorb-Quesa and Navarrés salt wall segments formed by the differential south to southwest displacement with a 20º clockwise VAR of their southwards cover block.

During this Late Miocene salt wall development, the Upper Triassic diapiric succession was not affected by significant VARs, but it was deformed first by a set of longitudinal large double-plunging anticlines, often flanked by minor parallel upright folds, and then by a complex set of shear zones. These shear zones bounded areas with different amount of salt inflation and induced internal deformation that deformed the paleomagnetic vector of sites located close to the flanks of the salt wall segments.

Chapter 6

Discussion and Conclusions

6.1.Bicorb-Quesa Salt Wall Segment evolution

The integrated study of the present-day subsurface, surface and rotations of the Bicorb-Quesa Salt Wall Segment (SWS) and its surroundings has allowed us to better understand the evolution of this area. The basement geometry, provide by the magnetotelluric profiles is a key feature to understand the first evolutionary stages of the diapir. In turn, the paleomagnetic data is essential for a detailed study of the last diapir rise. This information joined to the structural observations and the tectono-sedimentary information provided by the Miocene deposits (Roca et al. 1996; Anadón et al. 1998), allow us to distinguish seven deformational stages. The first three stages are related to Mesozoic extensional stages. The four last stages are related to the development of the Iberian and Betic thrust-and-fold belts.

6.1.1.Permian-Early Triassic rift stage

The paleomagnetic data show an important thickness variation on the pre-Jurassic successions located below the Bicorb-Quesa SWS and no variations below the Juanera and Sacaràs Half-grabens. This points out the first deformational stage observed in the study corresponding to an initial stage of intracontinental rifting related to the break-up of Pangea and the divergence of between Eurasia and Africa (Dewey et al 1989; Malod and Mauffret 1990; Pèrez-Lòpez, 1991; Hanne et al 2003). This extensional stage generated a NNW-dipping Bicorb-Quesa basement fault where the sedimentation at this time is thicker in its hanging-wall (1100m) than in its footwall (600m). We suggest that the parallel extensional basement fault depicted in Fig. 2.3 beneath the Xúquer SWS probably also formed during this rifting stage. The different attitude of the platforms located eastwards and westwards the Navarres SWS also led to think in the presence of an east dipping basement fault located below this salt wall.

6.1.2.Late Jurassic-Early Cretaceous synrift stage

This second stage of deformation took place in the area connected to the opening of the Atlantic Ocean (García-Hernández et al. 1980; Klitgorg and Schouten 1986; Ziegler 1989; Arias Abellán et al. 1996). In the study area, this extensional motion is recorded as thickness variations within the Late Jurassic-Early Cretaceous overburden, indicating that this fault also moved extensionally during the sedimentation on these materials. The Paleomagnetic and the geologic data show a thickness of 1000m of the Upper Jurassic-Lower Cretaceous successions on the the Bicorb-Quesa Fault footwall and 700m on its hangingwall. This motion produced a forced fold in the overburden over the basement extensional fault, with the salt level accommodating the difference in geometry (Nalpas and Brun 1993; Jackson and Vendeville 1994; Vendeville et al. 1995; Withjack et al. 2000; Fig. 6.1). The extension of this folded overburden probably led to the formation of the extensional fault recognized on the northern flank of the present-day Bicorb-Quesa SWS. It is possible that it also generated other extensional faults on the northern flank, but it is difficult to distinguish which ones because they were rejuvenated in later events. An incipient reactive diapir would be formed on the basement fault footwall, close to the upper hinge of the monoclinal forced fold (Nalpas and Brun 1993; Withjack et al. 2000) with salt provided by both the hanging-wall and the footwall (Burliga et al. 2012). This incipient reactive is recorded on the Upper Jurassic-Lower Cretaceous succession close to the southern flank of the Bicorb-Quesa SWS (Fig. 2.11 and 2.13 cross-section E-E' to HH') with thicknesses of 500-600m.

6.1.3.Late Cretaceous postrift stage

According to the constant thickness of the Upper Cretaceous materials in the study area, the extensional motion of the Bicorb-Quesa Fault and the related overburden deformation ended before the beginning of the Upper Cretaceous. The Cenomanian and Turonian successions are affected only by a slight thinning in the footwall of the active extensional fault developed at the upper hinge of the previously formed monoclinal forced fold. The Cenomanian-Turonian materials decrease from a regular thickness of 200m down to 80m in this area (Fig. 2.13 cross-section EE' to HH'). A thinning is also recognizable on hangingwall of the Carroig fault, where this unit is 120m. thick (Fig. 2.13 cross-section BB' and CC') This suggest that the movement of the Carroig Fault during this time, was produced by the forced fold induced by the basement fault (Fig. 6.1). These structures were generated during an extensional regional postrift stage (Salas and Casas 1993; Salas et al. 2001). This thinning is interpreted as being driven by a migration of the Middle-Upper Triassic salt due to the differences in the overburden load differences (Ge et al. 1997).

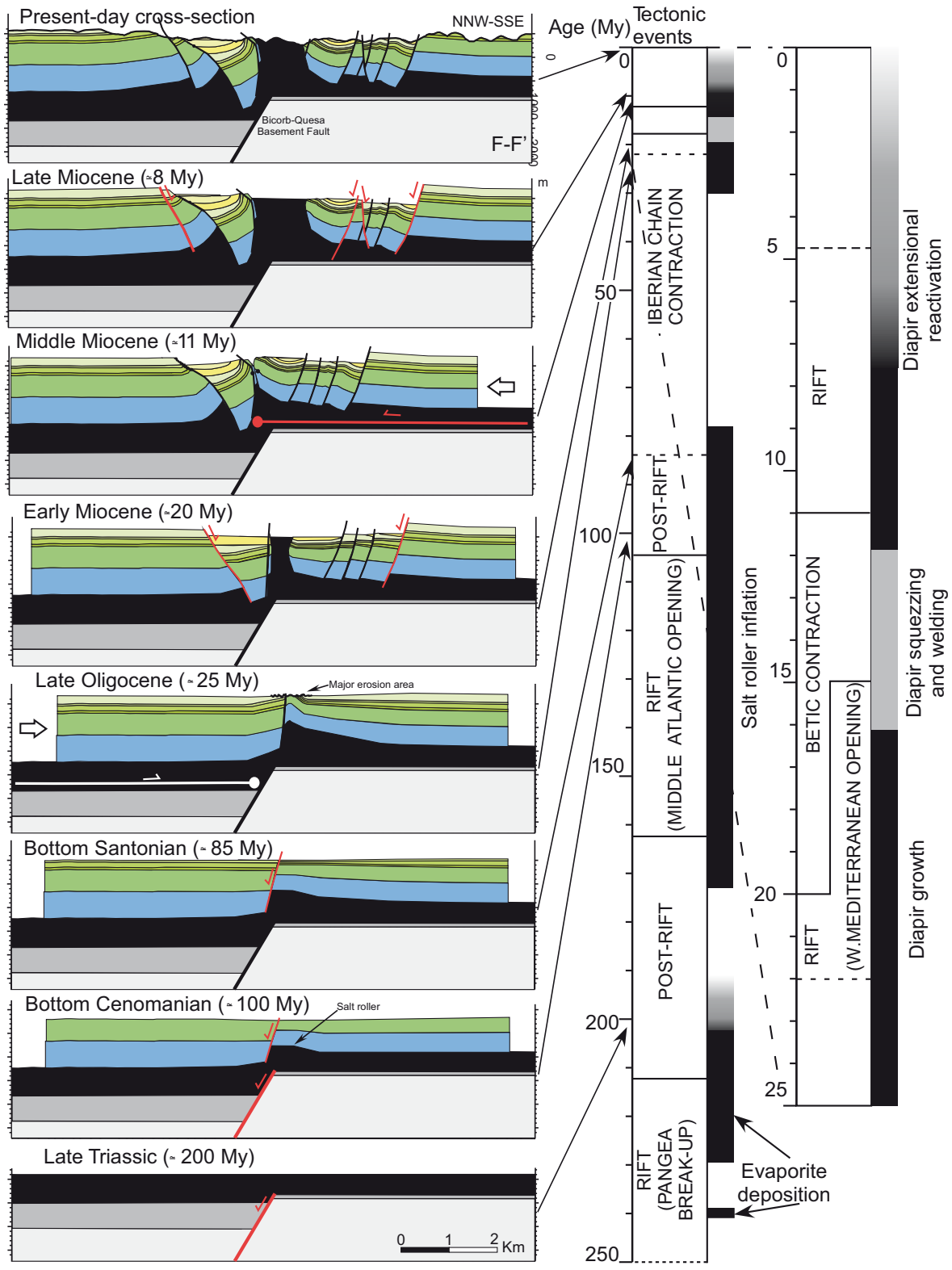

Figure 6.1. Partial restorations of the F-F' transverse cross-section showing the main structural features of the Bicorb-Quesa rift system at the main Alpine deformational stages affecting the eastern Iberian plate (see Fig. 4.5 for location and Fig. 4.3 for legend).

6.1.4.Paleogene contractional stage

Between the Senonian (Upper Cretaceous) and the early Miocene, the previous thinning area (the reactive diapir) becomes an south verging anticline with nearly-vertical limbs and a positive relief between 200m and 400m above the region (Fig 6.1. and cross-section EE' to FF' in Fig. 7). This anticline is well preserved in the lower-middle Miocene subcrop map (Fig. 6.2). It is detached on the Middle-Upper Triassic evaporite layers. Its southern limb is cut by south directed reverse faults. The fold geometry, the relief and the presence of reverse faults discard the possibility that this anticline was formed by extension, whereas the lack of active diapirism enables us to conclude that the fold is formed by rejuvenation of the reactive diapir. These rejuvenation folds are well known in thick-skinned contractive deformation events (Letouzey et al. 1995; Krzywiec 2004; Ferrer et al. 2012). Also, not far from the study area stands the Iberian Chain (Paleogene and earliest Miocene) (Fig. 2.3). In these nearby areas, the Iberian Chain is formed by a thrust-and-fold system detached above Middle-Upper Triassic salts that propagated southeastwards through time. As shown in the cross-section in Figure 2.4, the location of the deformational front of this part of the Iberian Chain is controlled by the presence of pre-existing basement faults (in this case, the Xúquer basement fault), which cut and displaced the Middle-Upper Triassic detachment level. In this regional scenario, the Paleogene anticline that developed in the Bicorb-Quesa area can be interpreted as a result of a further propagation of the Iberian Chain deformation above the Middle-Upper Triassic level on the footwall block of the Xúquer basement fault. Further propagation was hampered by the Bicorb-Quesa Fault, which displaced the detachment level again, resulting in the formation of a new frontal fold above this sticking point.

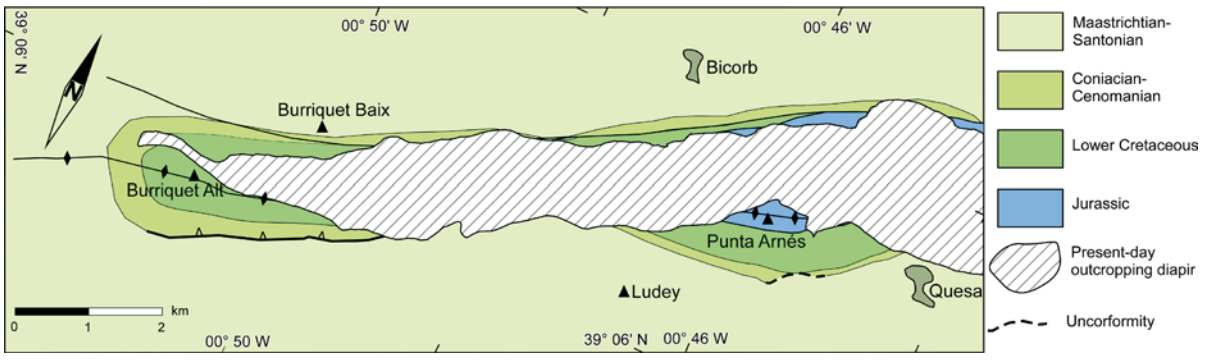

Figure 6.2. Subcrop map of the Miocene showing the pre-diapiric structure of the study area.

The Paleomagnetic data also indicate that this salt movilized the materials and rotated counter-clockwise 15-30º. This rotation is probably produced at this time since it occurred after the remagnetitzacion of the IMT but before the NW-directed

fold formation. These folds are better preserved on the non-diapiric materials (K2 to K5) (Fig. 2. 11) , and are cut by the longitudinal folds, vertical folds, shear-bands and thrusts generated on the salt wall rise denoting been previous to the actual diapir. These folds could be produced during the Paleogene-Early Miocene Iberian Chain or to Middle Miocene Prebetics. The thrust observed whitin the present-day diapir, exhibiting Muschelkalk materials in its hangingwall (Fig 2.11) above K1 to K3 formations is a duplex formed on the evaporitic levels. As happen with previous folds the relations of this unit with respect to the others do not allow to discriminate in which contractive event was produced.

6.1.5.Early-middle Miocene diapiric stage

The Bicorb-Quesa SWS became active and rose to the crest of the anticline produced by the reactive diapir. This rise caused the beginning of the sedimentation of the lower-middle Miocene detrital deposits dating this rise. This is supported by the petrological composition of the deposits (Roca et al. 1996). The origin of this previous Bicorb-Quesa SWS has been explained by extensional faulting denudation caused by the opening the Mediterranean (Roca et al. 1996; 2006), but it also seems to be related to the erosion of the rejuvenated anticline during the Paleogene contractional stage (Fig.6.1.). The growth of the Bicorb-Quesa SWS during the Early-Middle Miocene caused the salt evacuation in the hanging-wall block of the Bicorb-Quesa Fault and, to a lesser extent, in the other surrounding diapir areas. This resulted in the sinking of the overlying overburden, which was extensionally faulted and unconformably overlain by relatively thick Lower-Middle Miocene detrital successions. It is in this process when the Bicorb and the incipient Quesa and Juanera half-grabens formed as salt evacuation basins.

6.1.6.Middle Miocene contractional stage

During the Middle Miocene development of the Prebetic fold-and-thrust system, the pre-existing Bicorb-Quesa SWS was shortened (Roca et al 1996; 2006), first produzing the squeezing of the diapir as indicated in the sedimentary record by a significant rise of evaporitic material (Roca et al. 1996; Anadon et al. 1998). Then, once the diapir was welded, contractional deformation occurred in the surrounding overburden and Lower-Middle Miocene syn-diapir rocks were folded (Roca et al. 1996; 2006; Fig. 6.1). This contractional deformation focused in the pre-existing diapir area because of its weakness, it consisted of a NNW-directed Picos de la Olla low-angle

thrust that cut the folded Lower-Middle Mioce materials. The deformation during this shortening phase propagated northwards in the footwall of the Bicorb-Quesa basement fault (Fig. 9). This different configuration difficult the propagation of Prebetic thin-skinned contractional deformation north of the Bicorb-Quesa basement fault because the detachment level was down-dropped to the north of the fault.

6.1.7.Late Miocene extensional diapir reactivation stage

This is the last Alpine deformational stage distinguished in the study area and therefore the best preserved one. It corresponds to a regional extensional stage in which the Jurassic-Cretaceous subhorizontal platform of the Valencian Domain was extended by the formation of several sets of extensional faults detached on the Middle-Upper Triassic evaporites (De Ruig 1992; Roca et al. 1996; Fig. 6.1). In the study area, this extensional overburden deformation produced the extensional reactivation of the squeezed Bicorb-Quesa SWS and the development, at its western prolongation, of a major SE-dipping extensional fault (the Carroig Fault) (Roca et al. 1996; 2006) This deformation is well recorded within the diapiric materials, the overburden and the paleomagetic data.

The present day cartography of the diapir shows the growth of the salt wall, characterized by the formation along the developing salt walls of a set of kilometer-scale double-plunging anticlines, often flanked by minor parallel upright folds. These folds, commonly showing parallel thrusts or shear zones cutting the vertical to overturned limbs, are cored by inflated masses of the diapiric K1 unit that apparently are more shortened. The structural features of this train of longitudinal folds are consequently coherent with the beginning of the salt inflation process along the SWS with salt flowing from the bottom of the Miocene half-grabens to the core of the axis salt wall anticlines. The rest of the structures observed in the Bicorb-Quesa SWS, are clearly younger, and can be directly related to the rise of the salt wall. The K1 unit advanced in evolutionary stages and produces the changes in the amount of salt inflation, these are not gradual in a such a way that they occur along more or less vertical shear zones oblique to the salt wall flanks. This kind of shear zones, also present along the salt wall flanks, produces a vertical stretching of the affected successions which, in the case of the performed paleomagnetic measurements, would result in changes of the initial declination and/or inclination angles. This is evident in the site QB-57 where the lower Miocene, strongly deformed by the shear zone that limits the Bicorb-Quesa salt wall segment to the north, shows an anomalous high paleomagnetic inclination (Fig. 6.3). Also, such a local shearing deformation can be

invoked to explain the major counter-clockwise rotation of the measured paleomagnetic component shown at sites QB-5, QB-56 and QB-62, all of them located near the southern flank of the same salt wall segment.

According to regional and structural data (De Ruig, 1995; Martínez del Olmo, 1999; Roca et al., 2006), the origin of this displacement, must be linked to a thin-skinned extensional deformation developed on top of the Keuper detachment level, which compartmentalizes the Prebetics Valencian Domain in several blocks bounded by ENE and NNW-trending extensional faults. The geometry and arrangement of these faults are strongly controlled by the underlying Bicorb-Quesa, Navarrés and Xúquer basement faults that shift and/or cut the Keuper detachment level (Figure 6.4). Indeed, it can be observed from the maps in figures 2.3 and 2.11, that: 1) the orientation of the extensional faults affecting the cover is different on both sides of these basement faults; 2) the salt wall segments (sectors where the major extensional deformation in the cover level occurs) are located precisely upon the detachment level steps that generate these basement faults; and 3) the northern boundary of the extensionally deformed cover area is not rectilinear but formed by two nearly NW-trending border faults linked by a north to northeast-trending faulted relay ramp which coincides with the trace of the Bicorb-Quesa basement fault. This relay ramp becomes an accommodation zone to the southwest and separates an eastern domain extensionally displaced south-southwestwards from a western domain where this displacement, at the same transverse, is null or significantly smaller. Consequently, it is part of an extensional faulted transfer zone in which there is a relative right-lateral strike-slip motion between the adjoining blocks. It should be noted that this relative strike-slip motion does not take place along strike-slip faults (see map in Fig. 2.11) but diffusely along a 2 to 8 km wide stripe where the Jurassic to Miocene cover is sheared and rotated clockwise (Fig 6.4). The clockwise rotation observed in the Miocene Quesa basin infill would reflect this kind of deformation since, as shown in Figure 6.4, it develops over the cover block located at the northern end of the accommodation zone where the rotation would be maximum. The clockwise vertical axis rotation (VAR) observed in the western end of the Bicorb Basin (site QB-6) could have also the same origin. In relation to the <10-20º counter-clockwise VAR recorded in the Juanera and Playamonte half-grabens (QB11 and QB14, respectively), they are placed out of the accommodation zone and probably record small lateral changes in the south- southwestwards displacement of the Jurassic to Miocene cover over the extensional fault system. The origin of this displacement, according to the regional and structural data (De Ruig, 1995; Martínez del Olmo, 1999; Roca et al., 2006) must be linked to a thin-skinned extensional deformation, which developed on top of the Keuper detachment level, compartmentalizing the Valencian Domain in several blocks

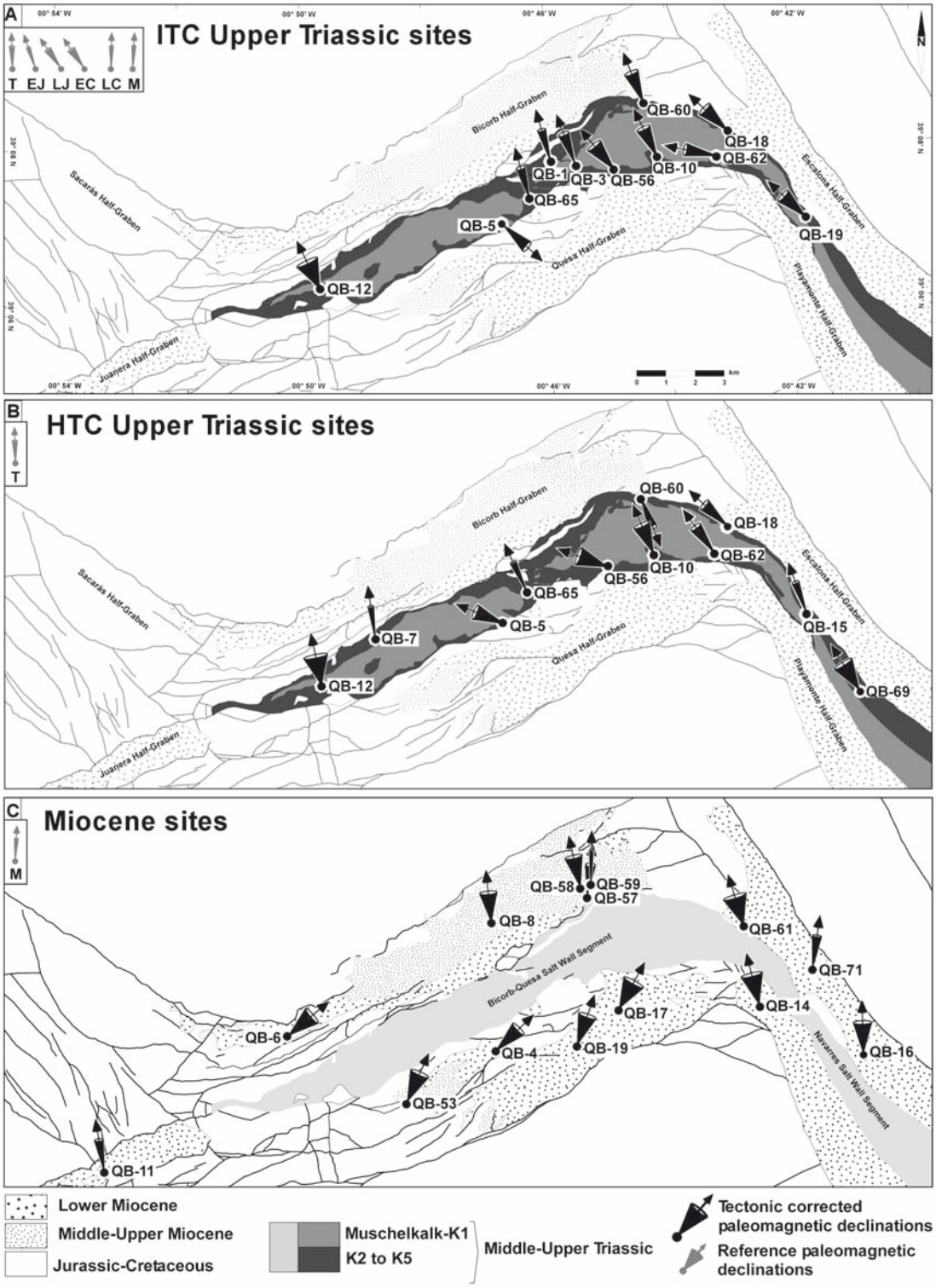

Figure 6.3. Simplified geological map of the study area with the tectonic corrected declinations of the measured paleomagnetic sites, where the keuper ofthe Navarres SWS is an aproximation. Cones represent the α_{95} of the mean directions. Within the black box is located the reference paleomagnetic declination of Triassic (T), Early Jurassic (EJ), Late Jurassic (LJ) Early Cretaceous (EC), Late Cretaceous (LC) and Miocene (M). **A**. Declinations of the intermediate temperature components (ITC) measured in the Upper Triassic red and grey mudstones (K2 and K3 units); **B**. Declinations of the high temperature components (HTC) measured in the Upper Triassic red mudstones (K2 and K3 units). Note that only the first and second class sites are represented. **C**. Declinations of the Miocene sites;

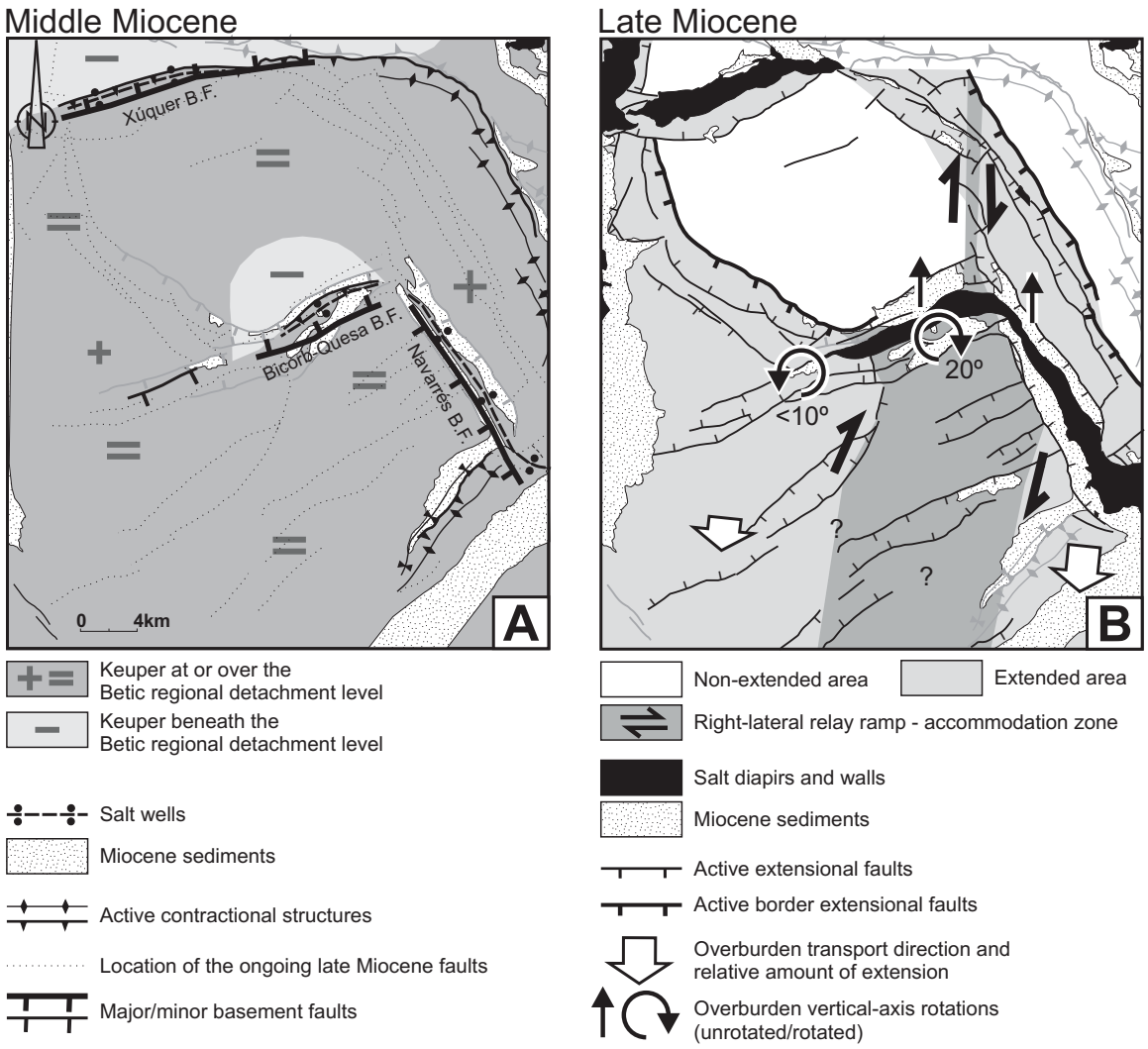

Figure 6.4. Structural map of the Valencian Domain at the end of the north-propagating middle Miocene contractional deformation. Note the arrangement of the pre-existing basement faults and how they control de cover deformation and the geometry of the Upper Triassic detachment level. **B.** Structural map of the Valencian Domain at the end of the late Miocene extensional deformation with the paleomagnetic rotations recorded in our sampled Miocene deposits. This second map denotes that the Bicorb-Quesa salt wall segment developed in a relay border fault that produced a significant displacement with a vertical-axis clockwise rotation of its hangingwall; and the Navarrés salt wall segment formed over a pre-existent detachment flexure. In both maps, active structures are in black and the inactive older ones in grey.

bounded by ENE and NNW-trending extensional faults.

According to this proposed late Miocene deformation scenario, the salt walls would be formed in the most extended areas. This occurs in the relay border fault that, located in the northern end of the accommodation zone, produces a significant displacement with a vertical-axis clockwise rotation of its hangingwall (Bicorb-Quesa segment); and over the detachment flexure formed upon the Navarrés basement fault (Navarrés segment). The origin of the Bicorb-Quesa SWS due to a south to southwest

displacement with rotation of the cover underlying the Quesa basin fill is coherent with the plan-view geometry of the salt wall that disappears west of the proposed transfer zone and becomes progressively wider eastwards until its junction with the Navarrés salt wall segment (Fig. 2.11).

6.2.The role of pre-existing basement faults in the initiation and reactivation of salt diapirs

The reconstruction of the evolution of the Bicorb-Quesa SWS therefore, indicates that we are facing a complex salt diapir that developed from an extensional and contractional thin-skinned deformation of an overburden located on top of a pre-existing extensional basement fault. A thin-skinned deformation produced the rejuvenation of a previous reactive diapir, the growth of the Bicorb-Quesa SWS, its squeezing and finally its reactivation.

In each of these stages, cover deformation and diapirism appear strongly influenced by the propagation direction of the deformation above the detachment level, which was previously flexed or truncated on top of the pre-existing basement fault. This propagation, in the compressive stages, was directed toward the basement fault. In the Paleogene contractional stage it occurred in the hanging-wall, whereas in the middle Miocene it occurred in the footwall. Next we present a discussion on the role played by the pre-existing basement faults in the thin-skinned contractional initiation and reactivation of salt diapirs, focusing on the influence of the propagation direction of the cover deformation.

6.2.1.Contractional diapir initiation

Prior to discussing the contractional deformation, it should be emphasized that the structural style of overburden and salt-layer deformation above a growing extensional basement fault is strongly dependant on the degree of decoupling between supra- and subsalt deformation (Withjack and Callaway 2000). Thus, if the deformation is coupled, then the deformation style is transferred through the detachment level (Fig. 6.5). In contrast, if the deformation is decoupled, structural styles above and below the salt can be quite different and may result in an overburden drape folding above a basement extensional fault (Jackson and Vendeville 1994). As the overburden section must extend as much as the basement, this drape folding is accompanied by extensional faulting in the upper hinge of the monoclinal drape fold. This is the area where reactive diapirs can initiate (Fig. 6.5). Also in this decoupled scenario, salt-layer thickness is not constant but changes laterally, accommodating the difference between the supra- and subsalt geometries. With respect to this major salt mobility, the salt layer (potential future detachment level of later thin-skinned deformation) usually

has lateral continuity above the basement fault. This does not occur in the coupled scenario, where it is simply cut and displaced by the fault (Fig. 6.5).

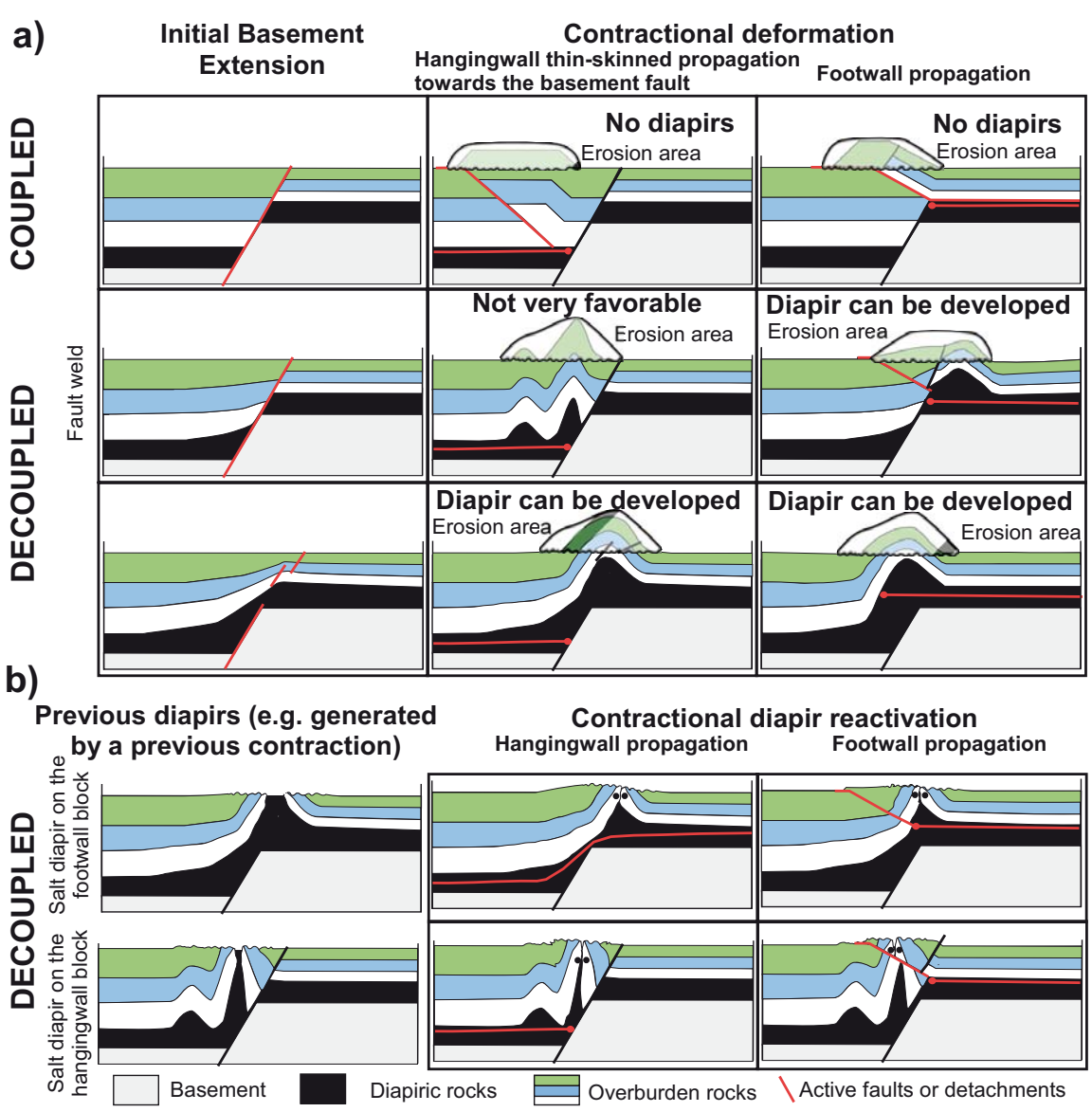

Figure 6.5. Summary diagram of the role of pre-existing extensional basement faults in the cover thin-skinned contractional initiation (a) and reactivation (b) of salt diapirs. The analysed factors are the propagation sense and the degree of coupling or decoupling of the thin-skinned deformation.

Shortening of these different thick-skinned salt tectonic structures would produce the growth of different contractional structures (mainly folds) which, in some cases, can enhance diapirism as a result of their erosion and/or fracture weakening (Fig. 6.5). The diapir initiation in these structures would be strongly dependent on the amount of overburden denudation but also on the fold shape and kinematics, which in

turn are also dependent on a number of factors, including thickness and mechanical behaviour of the overburden, deformation rates, amount of deformation, salt thickness, and the pre-existing overburden and salt configuration. Consequently, the possibility of developing contractionaly driven diapirism over a pre-existing basement fault will vary if the contractional deformation is developed over a previously coupled or decoupled overburden, and also whether the overburden thin-skinned contractional deformation propagates on top of the hanging-wall or on top of the footwall of the basement fault.

We focus on three possible scenarios: i) a coupled salt layer:ii) a decoupled salt layer with the footwall and hanging-wall salt-layer that is disconnected, iii) a decoupled salt layer that is connected (Fig 6.5a). Thus, if we consider that the salt layer acts as a detachment level, the contractional deformation can be propagated toward the pre-existing extensional basement fault over its hanging-wall or over its footwall (Fig 6.5a).

In the salt-disconnected/hanging-wall propagation case, the basement fault acts as a barrier for the propagation of the contractional overburden deformation, inducing the development of buttressing structures (mainly detachment folds and backthrusts) or basement short-cuts. In this setting, the salt-cored structures that developed from contractional structures have a thick overburden and, therefore, are not very suitable for being pierced by salt. The only exception might be the tight buttress anticlines that can be formed against the fault plane (Fig. 6.5a). These anticlines present better conditions for developing a salt diapir since they tend to be taller and have an initial small overburden/salt thickness ratio (see above for wider explanation on a decoupled extensional deformation over a basement extensional fault). Furthermore, in the case of a basement short-cut developing, they could also be significantly uplifted above the regional level, favouring a deep erosion to an even greater extent.

In the salt-connected/hanging-wall propagation case, the overburden contractional deformation can propagate toward the basement fault footwall above the inherited flat-ramp-flat geometry of the upper part of the salt layer. This detachment geometry leads to the development of a detachment fold on the concave-downward detachment bend, and also to the squeezing of the salt located on the basement fault surface. The salt is expelled upwards toward the generated detachment fold. Note that all these contractional structures develop at or very close to the location of the hinge of the overburden monoclinal drape fold that formed during the older extensional motion of the underlying basement fault. Therefore, contractional anticlines develop where the overburden is thinner and the salt layer is thicker (Fig. 6.5a). As a result, the formation of diapirs by erosion and salt breakthrough is relatively easy here. An example of this kind of contractionally driven diapir would be the one that developed

during the Paleogene-Lower Miocene over the Bicorb-Quesa basement fault.

In a footwall propagation case, the contractional deformation would be blocked at the top of the basement fault. The detachment fault would be interrupted by the fault in a salt-disconnected scenario or by the monocline limb of the drag fold in a salt-connected scenario. This would give rise to the formation of a thrust front or detachment anticline at the top of the basement footwall cut-off of the pre-existing extensional fault (Fig 6.5a). As in the previous case, these contractional structures would develop at or very close to the hinge of the overburden monoclinal drape fold that formed during the older extensional motion of the underlying basement fault. Consequently, they would also be favourable places for the generation of salt diapirs by overburden denudation. The Betic Front at the Xúquer River (Fig. 2.3) provides an example of this kind of situation.

6.2.2.Contractional diapir reactivation and/or squeezing

The propagation direction of an overburden contractional deformation also plays a fundamental role in the contractional reactivation and/or squeezing of a salt diapir developed over an extensional basement fault. Both the geometrical features and the evolutionary trends of shortened diapirs will be rather different depending on whether the contractional deformation propagates toward the diapir over the hanging-wall or over the footwall of the basement fault (Fig. 6.5b).

Effectively, if contractional deformation propagates above the salt layer lying over the hanging-wall block, the entire pre-existing diapir narrows, forcing a large volume of salt to flow upwards. This results in an acceleration of the extrusion of diapiric materials or, in the case of a buried diapir, to its rejuvenation. With increased shortening, the diapirs closed along secondary welds or generating “Q-tip” structures (Rowan and Vendeville 2006; Dooley et al. 2009). Next, folds and thrusts form at the squeezed diapir limb with a predominant vergence that will depend on the basement fault dip. Note that this evolution is only valid if the overburden contractional deformation can propagate up to the salt diapir location above a continuous detachment salt layer (see discussion on the propagation of overburden deformation above a basement fault in the previous section). In the other cases, diapir reactivation will be more difficult and complex (e.g., diapirs developed over the basement fault but disconnected from the source layer by a primary weld) or it may even possibly never occur (diapirs developed over the basement footwall block in a pre-contractional configuration in which the detachment salt layer has a high-angle dip above the basement fault).

In the case in which contractional overburden deformation has propagated on the basement footwall block, all pre-existing salt diapirs can be easily reactivated provided that primary welds were formed at their flanks (Fig. 6.5b). The pattern of the contractional reactivation in pre-existing diapirs is similar to the pattern described in the previous scenario, with the exception of diapirs that developed over the basement fault surface. In these last ones, not all the diapir is shortened but only the part of the feeding stem located above the detachment level of the regional footwall of the basement fault. Moreover, the post-diapir welding thrusts and folds in these diapirs show a preference for vergence toward the foreland, with the development of forethrusts in the diapir forelimb (Fig. 6.5). It is interesting to note that the preservation of the lower part of the feeding stems in these diapirs can produce a situation very favourable to any kind of later diapir reactivation, even if the upper part of the diapir was completely welded. An example of this kind of later reactivation is the Bicorb-Quesa SWS which, contractionally welded during the middle Miocene, was reactivated during the late Miocene by extensional thinning of the overburden above the welded stem or feeder.

6.3. Conclusions

• The magnetotelluric data and the Paleomagnetic data have been proved as very useful in the study of diapirs. More specifically the magnetotelluric data has provided insights from the different resistivity areas at depth. This image allows us to distinguish the basement geometry, the thickness of the different units and the present salt location. The paleomagnetic data, in turn, provided valuable information about the rotations occurred on both the overburden and the diapir. Thanks to this information as well as the detailed cartography of the overburden and diapir and the available information about the syndiapiric materials, a detailed restoration and evolutionary model of the area has been done.

• The Paleomagnetic data demonstrate that the Bicorb-Quesa Salt Wall was formed above a NNW-dipping extensional basement fault. This salt wall has a complex deformational history that comprehends contractional and extensional diapir reactivations. The extensional basement fault formed during Permian-Early Triassic times and, still slightly active until the beginning of the Late Cretaceous, produced the development of a forced fold in the Jurassic-Cretaceous overburden, as well as the formation of a reactivated diapir on the top of the forced fold. After the Late Cretaceous, the Jurassic-Cretaceous overburden was affected by thin-skinned contraction related to the formation of the Iberian Chain and the Betics. These

deformations led to the polyphase development of the Bicorb-Quesa Diapir from the erosion of a Paleogene rejuvenated reactivated diapir on top of the basement fault, and also the early Miocene extension. This diapir was contractionaly squeezed during the middle Miocene and extensionally reactivated later during the late Miocene.

• This last extension compartmentalizes the Valencian Domain of the Prebetics in several blocks bounded by ENE and NNW-trending extensional faults. In this regional scenario, the salt wall segments appear formed by the differentiated displacement of the cover block bounded northwards by the Bicorb-Quesa and Navarrés basement fault. This displacement was south-southwest directed and included a vertical-axis clockwise rotation component of 20º.

• The role played by pre-existing basement faults in thin-skinned contractional initiation and reactivation of salt diapirs has been analysed using the information provided by this reconstruction. The analysis also highlights the role played by the geometric relationship between the propagation direction of the cover deformation and the basement fault. In this regard, it shows that the propagation of contractional deformation over a basement footwall block results propitious to form a salt diapir by erosion. In contrast, hangingwall propagation is not supportive to develop salt diapirs, at least that body salt was connected.

• In a contractional deformation context with a pre-existing diapir, this will be squeezing. However, in the case of a footwall propagation of the contractional deformation is possible to reactivate the diapir after the contraction because the lower part of the stem remains almost undeformed, creating a propitious situation for a later diapir reactivation, even if the upper part of the diapir has been completely welded.

References

Al-Zoubi, A., ten Brink, U.S. 2001. Salt diapirs in the Dead Sea basin and their relationship to Quaternary extensional tectonics. Marine and Petroleum Geology, 18, 779-797.

Alavi, M. 2007 Structures of the Zagros fold-thrust belt in Iran. American Journal of Science 307, 1067-1095.

Álvaro, M., Capote, R., Vegas, R. 1979. Un modelo de evolución geotectónica para la Cadena Celtibérica. Acta Geològica Hispànica 14, 172-177.

Anadón, P., Robles, F., Roca, E., Utrilla, R., Vázquez, A., 1994. Evolución tectonosedimentaria de la cuenca miocena de Bicorp (Macizo de Carroig, Valencia). Comunicaciones. II Congreso del Grupo Español del Terciario, Jaca, Simposio (IGCP 324), pp. 227-229.

Anadón, P., Robles, F., Roca, E., Utrilla, R., Vázquez, A. 1998. Lacustrine sedimentation in the diapir-controlled Miocene Bicorb basin, eastern Spain. Palaeogeography, Palaeoclimatology, Palaeoecology, 140, 217-243.

Anadón, P., Utrilla, R., Vázquez, A. 2000. Use of charophyte carbonates as proxy indicators of subtle hydrological and chemical changes in marl lakes: example from the Miocene Bicorb Basin, eastern Spain. Sedimentary Geology, 133,325-347.

Arche, A., Lopez-Gomez, J. 1996. Origin of the Permian-Triassic Iberian Basin, central-eastern Spain. Tectonophysics 266:443-464.

Arche A., Diez, J.B., López-Gómez, J. 2007. Identification of the Early Permian (Autunian) in the subsurface of the Ebro Basin, NE Spain, and its paleogeographic consequences. Journal of Iberian Geology, 33(1),125-133.

Arias Abéllan, C., Masse, J.P., Vilas, L. 1996. Relaciones tectónica-sedimentación en el Aptiense de Sierra, Larga Jumilla (Murcia). Geogaceta 20, 43-46.

Arias Abellán, C., Elizaga, E., Vilas, L. 1979. Distribución de las facies del Cretácico inferior en el SE de la provincia de Albacete. Sus relaciones. Journal of Iberian Geology, 5, 453-466.

Arriagada, C., Roperch, P., Mpodozis, C., Dupont-Nivet, G., Cobbold, P. R., Chauvin, A., Cortés, J., 2003. Paleogene clockwise tectonic rotations in the forearc of central Andes, Antofagasta region, northern Chile. Journal of Geophysical Research, 108(B1), 2032.

Aurell M., Meléndez G., Olóriz F. 2002. Jurassic in Gibbons W., Moreno T., (eds.) The Geology of Spain Bath, UK, The Geological Society London, 213-253.

Azéma, J., Foucault, A., Chauve, P., Fourcade, E., García-Hernández, M., González-Donoso, J.M., Linares, A., Linares, D., López-Garrido, A.C., Rivas, P., Vera J.A. 1979. Las microfacies del Jurásico y Cretácico de las Zonas Externas de las cordilleras Béticas. Publicaciones Universidad de Granada, 83 p and 46 thin sections.

Azañón, J.M., Galindo-Zaldívar, J., García-Dueñas, V., Jabaloy, A., 2002. Alpine tectonics II: Betic Cordillera and Balearic Islands. In: Gibbons, W., Moreno (eds) The Geology of Spain. Geological Society , London 401-416.

Banks C.J., Warburton J. 1991 Mid-crustal dettachment in the Betic system of southeast Spain. Tectonophysics, 191 275-289.

Bartrina, T., Hernández, E., Serrano, A., 1990. Estudios de subsuelo del Trías salino en la depresión Intermedia. In: Ortí, F. Salvany J.M. (Eds) Formaciones evaporíticas de la Cuenca del Ebro y cadenas periféricas, y de la Zona de Levante. ENRESA- Universitat de Barcelona, 232-238.

Baumgartner, T.R., Van Andel, T.H., 1971. Diapirs of the Continental Margin of Angola, Africa. The Geological Society of America Bulletin, 82, 793-802.

Beets, C.J. and De Ruig, M.J. 1992. 87Sr/86Sr dating of coralline algal limestones and its implications for the tectono-stratigraphic evolution of the eastern Prebetic (Spain). Sedimentary Geology, 78: 233-250.

Blumenthal, M. 1927. Versuch einer tektonischen gliederung der betischen cordilleren

von Central, und Sud-West Andalusien. Eclogae Geologicae Helvetiae, 20,487-592.

Burliga, S., Koyi, H., Chemia, Z. 2012. Analogue and numerical modelling of salt supply to a diapiric structure rising above an active basement fault. In: Alsop GI, Archer SG, Hartley AJ, Grant NT, Hodgkinson R. (Eds) Salt Tectonics, Sediments and Prospectivity, vol 363, Geological Society, London, Special Publications, pp 395-408

Cagniard, L. 1953. Basic theory of the magnetotelluric method of geophysical prospecting. Geophysics, 18, 605-635.

Callot, J.P., Jahani, S., Letouzey, J. 2007. The role of pre-existing diapirs in fold and thrust belt development. In: Lacombe O, Lavé J, Roure F, Verges (Eds) Thrust belts and foreland basins: from fold kinematics to hydrocarbon systems. Springer, Berlin, 309-325

Calvo, J.P., Elizaga, E., Lopez-Martinez, N., Robles, F., Usera, J. 1978. El Mioceno superior continental del Prebético externo: Evolución del estrecho nord-bético. Boletín Geológico y Minero, 89(5) 407-426

Canérot, J., Hudec, M.R., Rockenbauch, K. 2005. Mesozoic diapirism in the Pyrenean orogen: Salt tectonics on a transform plate boundary. American Association of Petroleum Geologists Bulletin, 89, 211-229.

Carbó, A. 1980. Investigación geotectónica en el borde suroriental de la Cordillera Ibérica (prov. de Valencia y Albacete), basada en determinaciones gravimétricas. Tesis Doctoral. Universidad Complutense, Madrid.

Carbó, A. 1982. Estructura cortical del Levante Español en base a datos gravimétricos. Real Academia Ciencias Exactas Física Natural 76(2), 365-378.

Castaño, S., Carbó, A. 1995. Los afloramientos triásicos de la zona de confluencia de las Cordilleras Ibérica y Bética. Aportes de la gravimetría a su interpretación. Cuadernos de Geología Ibérica,19, 235-248.

Castro, J.M., Gea, G.A., de, Ruiz-Ortiz, P.A., Nieto, L.M., 2008. Development of carbonate platforms on an extensional (rifted) margin: the Valanginian-Albian record of the Prebetic of Alicante (SE Spain). Cretaceous Research 29, 848-860.

Chapple, W.M. 1978. Mechanics of thin-skinned fold-and-thrust belts. Geological

Society of America Bulletin, 89,1189-98

Chemia, Z., Koyi, H., Schmeling, H., 2008. Numerical modelling of rise and fall of a dense layer in salt diapirs. Geophysical Journal International, 172, 798-816.

Cifelli F., Rossetti F., Mattei M., 2007. The architecture of brittle postorogenic extension: Results from an integrated structural and paleomagnetic study in north Calabria (southern Italy). Geological Society of America Bulletin, 119(1), 221-239.

Costa, E., Camerlenghi, A., Polonia, A., Cooper, C., Fabretti, P., Mosconi, A., Murelli, P., Romanelli, M., Sormani, L., Wardell, N. 2004. Modeling deformation and salt tectonics in the Eastern Mediterranean Ridge accretionary wedge. Geologic Society of American Bulletin,. 116, 880-894.

Costa, E., Vendeville, B.C. 2002. Experimental insights on the geometry and kinematics of fold-and-thrust belts above weak, viscous evaporitic décollement. Journal of Structural Geology, 24,1729-1739.

Coward, M., Stewart, S. 1995. Salt-influenced structures in the Mesozoic-Tertiary cover of the southern North Sea, UK. In Jackson MPA, Roberts DG, Snelson S (Eds), Salt tectonics: A global perspective, Vol 65. American Association of Petroleum Geologists Memoir pp 229-250

Davis, D.M. Engelder T. 1985. The role of salt in fold-and-thrust belts Tectonophysics, 119, 67-88.

De Ruig M.J. 1990. Fold trends and stress deviation in the Alicante fold belt, southeastern Spain. Tectonophysics, 184. 393-403

De Ruig, M.J. 1992. Tectono-sedimentary evolution of the Prebetic fold belt of Alicante (SE Spain) A study of stress fluctuations and foreland basin deformation: PhD thesis, Structural Geology and Tectonics Group, Vrije Universiteit, Amsterdam.

De Ruig, M.J., 1995. Extensional diapirism in the eastern Prebetic foldbelt, southeastern Spain. In. Jackson, M.P.A., Roberts, D.G., Snelson, S. (Eds), Salt tectonics: a global perspective: American Association of Petroleum Geologists Memoir, 65, 353-367.

De Ruig, M.J., Mier, R.M, Stel, H. 1987: Interference of compressional and wrenching tectonics in the Alicante region, SE Spain. Geol. Mijnbouw, 66: 201-212.

De Torres, T., Sanchez, A. 1990. Espesores de las Facies Keuper en la Rama Castellana de la Cordillera Ibérica y en el Dominio Prebético. In: F.Ortí & J.M. Salvany (eds) Formaciones evaporíticas de la Cuenca del Ebro y cadenas periféricas, y de la Zona de Levante. ENRESA- Universitat de Barcelona, 212-218.

Dewey, J.F., Helman, M.L., Turco, E., Hutton, D.H.W., Knott, S.D. 1989. Kinematics of western Mediterranean. In: Coward, M.P.,Dietrich, D., Park, R.G. (Eds.), Alpine Tectonics. Special Publications, 45. Geological Society, London, pp. 265-283.

Dooley, T., McClay, K.R., Pascoe, R. 2003. 3D analogue models of variable displacement extensional faults: applications to the Revfallet Fault system, offshore mid-Norway. In: Nieuwkand DA (Ed), New Insights into Structural Interpretation and Modelling, Vol 212. Geological Society, London, Special Publications, pp 151-167

Dooley, T., McClay, K.R., Hempton, M., Smit, D. 2005. Salt tectonics above complex basement extensional fault systems: results from analogue modeling. In: Doré A.G., Vining B.A. (Eds), Petroleum Geology: North-West Europe and Global Perspectives-Proceedings of the 6th Petrol Geol Conference. Geol Soc Lond, pp 1631-1648

Dooley, T.P., Jackson, M.P.A., Hudec, M.R. 2009. Inflation and deflation of deeply buried salt stocks during lateral shortening. Journal of Structural Geology, 31, 582-600.

Egeler, C.G., Simon, O.J. 1969. Orogenic evolution of the Betic Zone (Betic Cordilleras, Spain), with emphasis on the nappe structures. Geologie en Mijnbouw, 48: 296-305

Ferrer, O., Jackson, M.P.A., Roca E, Rubinat, M. 2012. Evolution of salt structures during extension and inversion of the Offshore Parentis Basin (Eastern Bay of Biscay). In: Alsop G.I., Archer S.G., Hartley A.J., Grant N.T., Hodgkinson R. (Eds) Salt Tectonics, Sediments and Prospectivity, vol 363, Geological Society, London, Special Publications, pp 361-380

Ferrer, O., Roca, E., Jackson, M.P.A., Muñoz, J.A. 2009. Effects of Pyrenean contraction on salt structures of the offshore Parentis Basin (Bay of Biscay). Trabajos de Geología, 29, 299-303.

Fiduk, J.C., Rowan M.G., 2012. Analysis of folding and deformation within layered evaporites in Blocks BM-S-8 & -9, Santos Basin, Brazil In: Alsop G.I., Archer

S.G., Hartley A.J., Grant N.T., Hodgkinson R. (Eds) Salt Tectonics, Sediments and Prospectivity, vol 363, Geological Society, London, Special Publications, pp 471-487.

Fisher, R., 1953. Dispersion on a sphere. Proceedings of the Royal Society of London A, 217, 295-305.

Fourcade, E. 1970. Le Jurassique et le Crétacé aux confins des Chaînes bétiques et ibériques (Sud-Est de l'Espagne). PhD thesis, Université de Paris, 427pp.

García, A., García, L., Muelas, A. et al. 1981. Mapa geológico de España 1:50.000, Llombay. IGME, Madrid

Garcia-Duenas, V, Balanya, J.C., Martinez-Martinez, J.M. 1992. Miocene extensional detachments in the outcropping basement of the northern Alboran basin (Betics) and their tectonic implications. Geo-Marine Letters, 12, 88-95.

García-Hernández, M., López-Garrido, A.C., Rivas, P., Sanz de Galdeano, C., Vera, J.A. 1980. Mesozoic paleogeographic evolution of the Externals Zones of the Betic Cordillera (Spain). Geologie en Mijnbow, 59, 155-168.

García Rodrigo, B. 1960. Sur la structure du Nord de la province d'Alicante. Bulletin de la Société géologique de France, 7, 273-277.

Ge, H., Jackson, M.P.A., Vendeville B.C., Maler, M.O., Handschy, J.W. 1997. Deformation of prograding wedges over a ductile layer - applications of physical models to geologic examples. Gulf Coast Assoc. Geol. Soc. Trans., 47:177-184

Groom, R.W., Bailey, R.C. 1989. Decomposition of the magnetotelluric impedance tensor in the presence of local three-dimensional galvanic distortion. Journal of Geophysical Research, 94, 1913-1925.

Grubbs, K.L., Van der Voo, R., 1976. Structural deformation of the Idaho-Wyoming overthrust belt (USA), as determined by Triassic paleomagnetism. Tectonophysics, 33, 321-336.

Guimerà J., Álvaro M. 1990. Structure et evolution de la compresion alpine dans le Chaine Iberique et la Chain Cotiere Catalan (Espagne). Bulletin de la Société Geologique de France, 8, 339-340.

Guimera J, De Vicente G, Rodriguez Pascua MA. 2004. La Rama Castellano-

Valenciana. In: Vera JA (Ed) Geología de España. SGE-IGME, Madrid, 610-612.

Hanne, D., White, N., Lonergan, L. 2003. Subsidence analyses from the Betic Cordillera, southeast Spain. Basin Research, 15, 1-21.

Henke, Chr., Schober, J., Weber, U., Gholami, F., Tabatabai, H. 2005. Exploring the High Zagros (Iran): a challenge for geophysical integration: First Break, 23, November 31-42.

Henry, B., Rouvier, H., Le Goff, M., Smati, A., Hatira, N., Laatar, E., Mansouri A., Perthuisot, V., 2000. Paleomagnetism as a structural polarity criterion: application to Tunisian diapirs. Journal of structural Geology, 22, 323-334.

Hossack, J.R., 1995. Geometrical rules of section balancing of salt structures. In: Jackson, M.P.A., Roberts, D.G., Snelson, S. (Eds.), Salt Tectonics: a Global Perspective. American Association of Petroleum Geologists Memoir, 65, 29-40.

Hoversten, G.M., Constable, S.C., Morrison, H.F. 2000. Marine magnetotellurics for base salt mapping: Gulf of Mexico Field Test at the Gemini Structure. Geophysics, 65, 1476-1488.

Hudec, M.R., Jackson, M.P.A., 2006. Advance of allochthonous salt sheets in passive margins & orogens. American Association of Petroleum Geologists Bulletin, 90, 1535-1564.

Hudec, M.R., Jackson, M.P.A., 2007. Terra infirma: Understanding salt tectonics. Earth-Science Reviews, 82, 1-28.

Jackson, M.P.A. 1995. Retrospective salt tectonics. In: Jackson, M.P.A., Roberts, D.G., & Snelson, S. (eds) Salt tectonics: a global perspective. American Association of Petroleum Geologists Memoir, 65, 1-28.

Jackson, M.P.A., Cornelius, R.R., Craig, C.R., Gansser, A., Stöcklin J., Talbot, C.J. 1990. Salt diapirs of the Great Kavir, Central Iran. Geological Society of America, Memoir, 177, 139 pp.

Jackson, M.P.A., Harrison, J.C. 2006. An allochthonous salt canopy on Axel Heiberg Island, Sverdrup Basin. Arctic Canada Geology, 34, 1045-1048

Jackson, M.P.A., Talbot, C.J., 1986. External shapes, strain rates, and dynamics of salt structures. Geological Society of America Bulletin, 97, 305-323.

Jackson M.P.A., Talbot, C.J., 1989. Anatomy of mushroom-shaped diapirs. Journal of structural geology, 11, 211-230.

Jackson, M.P.A., Talbot, C.J. 1991. Glossary of salt tectonics. Bureau of Economic Geology, University of Texas at Austin, Geological Circular, 91-4.

Jackson M.P.A., Vendeville B. 1994. Regional extension as a geologic trigger for diapirism. Geologic Society of American Bullettin, 106, 57-73.

Jacques, J.M., Parsons, M.E., Price, A.D., Schwartz, D.M., 2003. Improving geologic understanding with gravity and magnetic data: Examples from Gabon, Nigeria and the Gulf of Mexico. First Break, 21 (11), 57-62.

Kessels, W., Flentgeh, I., Kolditz, H. 1985. DC Geoelectric sounding to determine water content in the salt mine Asse (FRG). Geophysical Prospecting, 33, 436-446.

Key, K., Constable, W., Steven C., Weiss, C. J. 2005. Mapping 3D salt using the 2D marine magnetotelluric method: Case study from Gemini Prospect, Gulf of Mexico. Geophysics, 71, B17-B27.

Klitgord, K. D., and H. Schouten, 1986. Plate kinematics of the central Atlantic. In: Vogt, P. R., Tucholke, B. E. (eds) The Geology of North America, vol. M, The Western North Atlantic Region. Geological Society of America, Boulder, Colorado, 351-378.

Kirschvink. J.L., 1980. The least-squares line and plane and the analysis of paleomagnetic data. Geophysical Journal of the Royal Astronomical Society, 62, 699-718.

Koyi, H., Jenyon, M.K., Petersen, K. 1993. The efects of basement faulting on diapirism. Journal of Petroleum Geology, 16(3), 285-312

Krijgsman, W., Garcés, M., Langereis, C.G., Daams, R., van Dam, J., van der Meulen, A.J., Agustí, J., Cabrera, L., 1996. A new chronology for the middle to late Miocene continental record in Spain. Earth and Planetary Science Letters, 142, 367-380.

Krzywiec, P. 2004. Triassic evolution of the Klodawa salt structure: basement-controlled salt tectonics within the Mid-Polish Trough (Central Poland). Geol Quarterly, 48:123-134

Kulenkampff, J., Just, A., Aschmann, L., Jacobs, F. 2005. Laboratory investigations for the evaluation of in situ geophysical measurements in a salt mine. In: Harvey, P.K., Brewer, T.S., Pezard, P.A., Petrov, V.A. (Eds). Petrophysical Properties of Crystalline Rocks. Geological Society, London, Special Publications, 240, 75-94.

Larrasoaña, J.C., Murealga, X., Garcés, M., 2006. Magnetobiochronology of Lower Miocene (Ramblian) continental sediments from the Tudela Formation (western Ebro basin, Spain). Earth and Planetary Science Letters, 243, 409-423.

Lanaja J.M. 1987. Contribución de la exploración petrolífera al conocimiento de la Geología de España. IGME, Madrid

Ledo, J.J., Queralt, P., Pous, J. 1998. Effects of galvanic distortion on magnetotelluric data over three-dimensional regional structure. Geophysical Journal International, 132, 295-301.

Lefort, J.P., Aifa, T., Jelenska, M., Kadzialko-Hofmokl, M., Max, M.D., 2001. Paleomagnetic and AMS evidence for the Variscan ductile clockwise toration of the ile de Groix blueschists (South Britany, France): consequence on the Late Hercynian structural pattern of westernmost Europe. Tectonophysics, 337 (3-4), 223-235.

Letouzey, J., Colletta, B., Vially, R., Chermette, J.C. 1995. Evolution of salt related structures in compressional setting. In: Jackson, M.P.A., Roberts, D.G., Snelson, S. (eds) Salt tectonics: a global prespective. American Association of Petroleum Geologists Memoir, 65, 41-60.

Lowrie, W., 1990. Identification of ferromagnetic minerah in a rock by coerciviry and unblocking temperature properties. Geophysical Research Letters, 17: 159-162.

Malinowski, M., Grad, M., Guterch, A., Takács, E., Śliwiński, Z., Antonowicz, L., Iwanowska, E., Keller G.R., Hegedűs E. 2007. Effective sub-Zechstein salt imaging using low-frequency seismics – Results of the GRUNDY 2003 experiment across the Variscan front in the Polish Basin. Tectonophysics, 439, 89-106.

Malod, J. A., Mauffret, A. 1990. Iberian plate motions during the Mesozoic. Tectonophysics, 184, 261 - 278.

Martí, A., Queralt, P., Roca, E., 2004. Geoelectric dimensionality in complex geological areas: Application to the Spanish Betic Chain. Geophysical Journal international, 157, 961-974.

Martí, A., Queralt, P., Roca, E., Ledo, J., Galindo-Zaldívar, J. 2009. Geodynamic implications for the formation of the Betic-Rif orogen from magnetotelluric studies. Journal of Geophysical Research, 114, B01103.

Martín-Chivelet, J., Berástegui, X., Rosales, I., Et Al., 2002. Cretaceous. In: Gibbons, W., Moreno, T (eds) The Geology of Spain. Geological Society, London, 255-292.

Martínez del Olmo, W. 1999. Diapirismo de sales triásicas: consecuencias estructurales y sedimentarias en el Prebético Oriental, (Cordillera Bética, SE de España). Libro Homenaje a José Ramírez del Pozo. AGGP, Madrid, 175-187.

Martínez-Poyatos D, Gutiérrez Marco J.C., Pardo Alonso M.V., Rábano I, Sarmiento G.N. 2004. La secuencia paleozoica postcámbrica. In: Vera JA (Ed) Geologia de España. SGE-IGME, Madrid, 81-83.

Mas, J.R., Alonso, A., Meléndez, N. 1982. El Cretácico basal "Weald" de la Cordillera Ibérica suroccidental (NW. de la provincia de Valencia y E. de la de Cuenca). Journal of Iberian geology, 8, 309-336.

Matsuo K. Negi, T. 1999. Oil exploration in the difficult Minami-Noshiro area. Part 2. Magnetotelluric survey. Lead Edge, 18, 1411-1413.

Mattei, M., Petrocelli, V., Lacava D., Schiattarella, M., 2004. Geodynamic implications of Pleistocene ultrarapid vertical-axis rotations in the Southern Apennines, Italy. Geology, 32 (9), 789-792.

McNeice, G. W., Jones, A. G. 2001. Multisite, multifrequency tensor decomposition of magnetotelluric data. Geophysics, 66, 158-173.

Melendez, A. 1979. El Cretácico del Macizo de Caroch (provincias de Valencia y Albacete) Distribución de las facies del Cretácico inferior en el SE. de la provincia de Albacete. Sus relaciones. Cuadernos de Geología Ibérica, 5, 435-452.

Minegishi, M., Tanaka, H., Nakagami K. Amano, H. 1999. Oil exploration in the difficult Minami-Noshiro area. Part 1: 3D-Seismic. Lead Edge, 18, 1408-1410.

Moissenet, E. 1985. Les dépressions tarditectoniques des Chaînes Ibériques méridionales: Distension, diapirisme et dépots neogènes associés. Comptes Rendus de l'Académie des Sciences, Paris, 300, 523-528.

Moissenet, E. 1989. Les fossés néogènes de la Chaîne. Ibérique: leur évolution dans le temps. Bulletin de la Société géologique de France, 8 (5). 919-926

Montenat, C., Ott d'Estevou, P., Pierson d'Autrey, L. 1996. Miocene basins of the eastern Prebetic Zone: some tectonosedimentary aspects. In: Friend, P.F. Dabrío, C .J., (Eds.) Tertiary basins of Spain, the stratigraphic record of crustal kinematics. Cambridge University Press, Cambridge, World and regional geology, 6: 346-352.

Moseley, F. 1968 Canical folding and fracture patterns in the Pre-betic of Southeast Spain Geological Journal, 6 : 97-104

Muñoz, G., Mateus, A., Pous, J., Heise, W., Santos, F.M., Almeida, E. 2008. Unraveling middle-crust conductive layers in Paleozoic Orogens through 3D modeling of magnetotelluric data: The Ossa-Morena Zone case study (SW Iberian Variscides). Journal of Geophysical Research, 113, B06106, 1-23.

Nagihara, S., Hall, S.A. 2001. Three-dimensional gravity inversion using simulated annealing: Constraints on the diapiric roots of allochtonous salt structures. Geophysics, 66, 1438-1449.

Nagy, Z., 1996. Advances in the combined interpretation of seismics with magnetotellurics. Geophysical Prospect, 44, 1041-1083.

Nagy, E.A., 2000. Extensional deformation and paleomagnetism at the western margin of the Gulf extension province, Puertecitos Volcanic Province, northeastern Baja California, Mexico. Geololgical Society of America Bulletin, 112 (6), 857-870.

Nalpas, T., Brun, J.P. 1993. Salt flow and diapirism related to extension at crustal scale. Tectonophysics, 228: 349-362.

Nettleton, L.L., 1971. Elementary gravity and magnetic for geologists and seismologists. Society of Exploration Geophysicists Monograph Series, 1, 1-121.

Netzeband, G., Hübscher, C., Gajewski, D., 2006. The structural evolution of the Messinian evaporites in the Levantine Basin. Marine Geolology, 230, 249-273.

Newman, G.A., Hoversten, G.M., Alumbaugh, L. 2002. Three-dimensional magnetotelluric modeling and inversion: application to sub-salt imaging. In: Zhdanov, M. S., Wannamaker P.E. (Eds) Three-dimensional electromagnetic: Proceedings of the second international Symposium Methods. Geochemistry and Geophysics, 35,

127-152.

Nilsen, K.T., Vendeville, B.C., Johansen, J.T. 1995. Influence of regional tectonics on halokinesis in the Nordkapp Basin, Barents Sea. In: M.P.A. Jackson, D.G. Roberts, S. Snelson (Eds), Salt Tectonics: A Global Perspective. American Association of Petroleum Geologist Memoir, 65, 413-436.

Noel, M., Batt, C. 1990. A method for correcting geographically separated remanence directions for the purpose of archaeomagnetic dating. Geophysical Journal International, 102, 753-756.

Ortí, F. 1973 El Keuper del Levante español, Litoestratigrafía, Petrología y Paleogeografía de la cuenca. Tesis Doctoral. Universidad de Barcelona. 174 págs.

Ortí, F. 1974. El Keuper del Levante español. Estudios Geologicos, 30, 7-46.

Ortí, F., Salvany, J.M. 1990. Formaciones evaporitícas de la Cuenca del Ebro y cadenas periféricas y de la zona de Levante. Nuevas aportaciones y guía de superficie. ENRESA-Universitat de Barcelona, Estudi 6

Ortí, F., Pérez-López, A. 1994. El Triásico Superior del Levante. Guía de campo. IV Congreso sobre el Pérmico y Triásico de España. Cuenca.

Osete, M.L., Rey, D., Villalaín J.J., Juárez. M.T., 1997. The late Carboniferous to Late Triassic segment of the apparent polar wander path of Iberia. Geologie in Mijnbow, 76, 105-119.

Osete, M.L., Palencia, A., 2006. Polos paleomagnéticos de Iberia en los últimos 300 millones de años. Física de la Tierra, 18, 157-181.

Ott d'Estevou, P., Montenat, Ch., Ladure, F., Pierson d'Autrey, L. 1988. Évolution tectono-sédimentaire du domaine prébétique oriental (Espagne) au Miocène. Comptes Rendus de l'Académie des Sciences, Paris, 307, 789-796.

Pearson, W.C. 2006. Identification of magnetic anomalies from basement, intrasedimentary faults and salt domes and basement structural interpretation enhance prospectiveness for upper Jurassic and lower Cretaceous gas exploration in the Sabine Uplift Area of Texas and Louisiana: Example from Black Lake Gasfield Area, Natchitoches Parish, Louisiana. SEG Expanded Abstracts, 25.

Peñalver, E., Gaudant, P. 2010 Limnic food web and salinity of the Upper Miocene

Bicorb palaeolake (eastern Spain). Palaeogeography, Palaeoclimatology, Palaeoecology, 297, 3-4,683-696.

Peper, T., Cloetingh, S., 1992. Lithosphere dynamics and tectono-stratigraphic evolution of the Mesozoic Betic rifted margin (southeastern Spain). Tectonophysics, 203, 345-361.

Pérez-López, A.D., 1991. El Triásico de facies Germánica del Sector central de la Cordillera Bética. Tesis Doctoral. Universidad de Granada, 400 pp.

Pérez-López, A., Pérez-Valera, F. 2007. Palaeogeography, facies and nomenclature of the Triassic units in the different domains of the Betic Cordillera (S Spain). Palaeogeography, Paleoclimatology, Palaeoecology, 254, 606-626.

Pérez-López, A., Solé de Porta, N., Márquez Sanz, L., Márquez Aliaga, A. 1992. Caracterización y datación de una unidad carbonática de edad Noriense (Fm. Zamoranos) en el Trías de la Zona Subbética. Rev Soc Geol España 5:113-127.

Pérez-López, A., Solé de Porta. N., Ortí, F. 1996. Facies carbonato-evaporíticas del Trías Superior y tránsito al lías en el Levante español nuevas precisiones estratigráficas. Cuadernos de Geología Ibérica, 20:245-269.

Pérez-Rivarés, F.J., Garcés, M., Arenas C., Pardo, G. 2004. Magnetostratigraphy of the Miocene continental deposits of the Montes de Castejón (central Ebro basin, Spain): geochronological and paleoenvironmental implications. Geological Acta, 2 , 221-234.

Platt, J.P. 2007. From orogenic hinterlands to Mediterranean-style backarc basins: a comparative analysis Journal of the Geological Society, 164, 297-311

Platt, J.P., Vissers, R.L.M. 1989. Extensional collapse of thickened continental lithosphere: A working hypothesis for the Alboran Sea and Gibraltar arc. Geology, 17, 540-543

Platt, J.P., Whitehouse, M.J., Kelley, S.P., Carter, A., Hollick, L. 2003. The ultimate arc: differential displacement, oroclinal bending, and vertical axis rotation in the External Betic-Rif arc. Tectonics, 22, 1017

Pinto, V. Casas, A. Rivero, L., Torné, M. 2005. 3D gravity modeling of the Triassic salt diapirs of the Cubeta Alavesa (northern Spain). Tectonophysics, 405, 65-75.

Podladchikov, Y., Talbot, C., Poliakov, A.N.B. 1993. Numerical-models of complex diapirs. Tectonophysics, 228, 189-198.

Pous J, Ayala C, Ledo J, Marcuello A., Sabat F., 1995a. 3D modeling of magnetotelluric and gravity data of Mallorca island (Western Mediterranean). Geophysical Research Letters, 22 (6), 735-738.

Pous J, Ledo J Marcuello A, Daigniéres M., 1995b. Electrical resistivity model of the crust and upper mantle from a magnetotelluric survey through the central Pyrenees. Geophysical Journal International, 121, 750-762.

Pueyo, E.L., Millan, H., Pocoví, A., 2002. Rotation velocity of a thrust: A paleomagnetic study in the external Sierras (southern Pyrenees). Sedimentary Geology, 146, 191-208.

Rios, L.M., Beltrán, F.J., Zapatero, M.A., Goy, J.L., Zazo, C, Martínez, C. 1980. Cartografía y Memoria de la Hoja 769 (Navarres): Mapa Geológico de España, Instituto Geológico y Minero de España, Madrid, escala 1:50.000.

Roca, E. 1996. La evolución geodinámica de la Cuenca Catalano-Balear y áreas adyacentes desde el Mesozoico hasta la actualidad. Acta Geológica Hispánica 29, 3-25.

Roca, E., Anadón, P., Utrilla, R., Vázquez, A. 1996. Rise, closure and reactivation of the Bicorb-Quesa diapir, eastern Prebetics, Spain. Journal of the Geological Society of London, 153, 311-321.

Roca, E., Sans, M., Koyi, H. 2006. Polyphase deformation of diapiric areas in models and in the eastern Prebetics (Spain). American Association of Petroleum Geologists Bulletin, 90, 115-136.

Rodi, W., Mackie, R.L. 2001. Nonlinear conjugate gradients algorithm for 2-D magnetotelluric inversion. Geophysics, 66, 174-187.

Rondeel, H.E., Weijermars, R. Van Dorssen, H.G. 1984. Reactivation of early reverse faults associated with oblique strike slip faulting: a mechanism for crustal thickening. Geologie en Mijnbouw, 63, 387-398.

Ron, H., Garfunkel, Z., Nur, A., Freund, R., 1984. Block rotation by strike-slip faulting - Structural and paleomagnetic evidence. Journal of Geophysical Research, B7, 6256-6270.

Roperch, P., Sempere, T., Macedo, O., Arriagada, C., Fornari, M., Tapia, C., García, M. and Laj C. 2006. Counterclockwise rotation of late Eocene – Oligocene fore-arc deposits in southern Peru and its significance for oroclinal bending in the central Andes, Tectonics, 25, TC3010.

Rowan, M.G., Ratlift, R.A., 2012. Cross-section restoration of salt-related deformation: best practices and potential pitfalls. Journal of Structural Geology (in press).

Rowan, M.G., Vendeville, B.C. 2006. Foldbelts with early salt withdrawal and diapirism: Physical model and examples from northern Gulf of Mexico and the Flinders Ranges, Australia. Marine and Petroleum Geology, 23 (9-10), 871-891.

Rowan, M.G., Lawton, T.F., Giles, K.A., Ratliffe, R.A. 2003. Near-salt deformation in La Popa basin, Mexico, & the northern Gulf of Mexico: A general model for passive diapirism. American Association of Petroleum Geologists Bulletin, 87, 733-756.

Rubinat, M., Ledo, J., Roca, E., Rosell, O., Queralt, P. 2010. Magnetotelluric characterization of a salt diapir: a case study on Bicorb-Quesa Diapir (Prebetic Zone, SE Spain). Journal of the Geological Society of London, 167, 145-153.

Rubinat, M., Roca E., Escalas M., Queralt P., Ferrer O., Ledo J.J., 2012. The influence of basement structure on the evolution of the Bicorb-Quesa Diapir (eastern Betics, Iberian Peninsula): contractive thin-skinned deformation above a pre- existing extensional basement fault. International Journal of Earth Sciences (in press).

Ruiz-Sánchez, F.J., Santisteban, C. 2004. Tres nuevas localidades con fauna de micromamíferos fósiles de edad Aragoniense inferior-medio en el sector sureste de la cuenca de Quesa-Bicorp (prov. de Valencia, España). Geogaceta, 35,123-125. Salas R, Casas A (1993) Mesozoic extensional tectonics, stratigraphy and Alpine cycle of the Eastern Iberian basin. Tectonophysics 228(1-2):33-55

Salas, R., Casas, A. 1993. Mesozoic extensional tectonics, stratigraphy and Alpine cycle of the Eastern Iberian basin. Tectonophysics, 228(1-2):33-55

Salas, R., Guimerà, J., Mas, R., Martín-Closas, C., Meléndez, A., Alonso, A. 2001. Evolution of the Mesozoic Central Iberian Rift System and its Cainozoic Inversion (Iberian Chain). In: Ziegler PA, Cavazza W, Robertson AFH, Crasquin-Soleau S (Eds) Peri Tethyan Rift/Wrench Basins and Passive margins. Mémoires du Muséum national d'histoire naturelle, 186, 145-185.

Sans, M. 2003. From thrust tectonics to diapirism. The role of evaporites in the kinematic evolution of the eastern South Pyrenean front: Geologica Acta , 1, 239 -259.

Sans, M., Koyi, H.A. 2001. Modeling the role of erosion in diapir development in contractional settings. In: Koyi H.A., Mancktelow N.S. (Eds) Tectonic modeling: A volume in honor of Hans Ramberg, Vol 193. Geological Society of American Memoir, 111-122

Santisteban, C., Ruiz-Sánchez, F.J., Bello. D. 1989. Los depósitos lacustres del Terciario de Bicorp (Valencia). Acta Geologica Hispanica, 24, 299-307.

Santisteban, C., Ruiz-Sánchez, F.J., Lacombra, J.I. 1994. Estratigrafía, edad y evolución de los depósitos terciarios de la cuenca de antepaís de Quesa-Bicorp (Valencia). Comunicaciones al II Congreso del Grupo Español del Terciario, Jaca: 209-212

Schultz-Ela, D. 2003. Origin of “drag” folds bordering salt diapirs. American Association of Petroleum Geologists Bulletin, 87, 757-780.

Simpson, F., Bahr K. 2005. Practical Magnetotellurics. Press syndicate of the University of Cambridge.

Smith, P., Whitehead, M. 1989. Seismics, gravity and magnetics, a complementary study of the Pasqualin structure, Timor Sea, Australia. Exploration Geophysics, 20, 25-29.

Sopeña, A., De Vicente, G. 2004. Cordilleras Ibérica y Costero-Catalana. Rasgos generales. In: Vera JA (ed) Geología de España. SGE-IGME, Madrid, 467-470.

Sopeña, A., Sánchez-Moya, Y. 2004. Las cuencas continentales del fin de la Orogenia Varisca. In: Vera JA (ed) Geología de España. SGE-IGME, Madrid, 479-481.

Stewart, S.A. 2006. Implications of passive salt diapir kinematics for reservoir segmentation by radial and concentric faults. Marine and Petroleum Geology, 23 (8), 843-853.

Stewart, S.A, Clark, J.A. 1999. Impact of salt on the structure of the Central North Sea hydrocarbon fairways. In: Fleet, A.J., Boldy S.A.R. (Eds), Petroleum Geology of N.W. Europe, Fifth Conference, Geological Society, London, 179-200

Suarez Alba, J. 2007. La Mancha Triassic and lower Lias stratigraphy, a well log

interpretation. Journal of Iberian Geology 33(1), 55-78.

Talbot, C.J., Aftabi, P., 2004. Geology and models of salt extrusion at Qum Kuh, central Iran. Journal of the Geological Society, 161 (2), 321-334.

Talbot, C.J. and Jackson, M.P.A. 1987. Internal kinematics of salt diapirs. American Association of Petroleum Geologists Bulletin, 71, 1068-1093.

Telford, W.M., Geldart, L.P., Sheriff, R.E. and Keys, D.A. 1976. Applied geophysics. Cambridge University Press, Cambridge.

Ter Borgh, M.M., Oldenhuis, R., Biermann, C., Smit, J.H.W., Sokoutis, D., 2011, The effects of basement ramps on deformation of the Prebetics (Spain): A combined field and analogue modeling study. Tectonophysics 502:62-74

Tikhonov, A. N. 1950. On determining electrical characteristics of the deep layers of the earth's crust. Doklady, 73, 295-297.

Torres-Roldán, R. L., 1979. The tectonic subdivision of the Betic zone (Betic Cordilleras, Southern Spain): its significance and one possible geotectonic scenario for the westernmost Alpine belt. American Journal of Science 279, 19-51.

Tournerie, B., Chouteau, M. 2005. Three-dimensional magnetotelluric survey to image structure and stratigraphy of a sedimentary basin in Hungary. Physics of the Earth and Planetary Interiors, 150, 197-212.

Utrilla. R., Vazquez. A., Anadón, P. 1998. Paleohydrology of the Upper Miocene Bicorb Lake (eastern Spain) as inferred from stable isotopic data from inorganic carbonates. Sedimentary Geology, 121, 91-206

Van der Straaten, H.C. 1993. Neogene strike-slip faulting in southeastern Spain: the deformation of the pull-apart basin of Abarán. Geologie en Mijnbouw, 71: 205-225.

Vegas, R., Banda, E. 1982. Tectonic franework and Alpine evolution of the Iberian Peninsula. Earth Evolution Science, 4, 320-343.

Vendeville, B.C., Jackson, M.P.A. 1992. The rise of diapirs during thin-skinned extension: Marine and Petroleum Geology, 9(4):331-353

Vendeville, B., Nilsen, K.T. 1995. Episodic growth of salt diapirs driven by horizontal shortening, in Travis C J, Vendeville BC, Harrison H, Peel FJ, Hudec MR,

Perkins BJ (Eds) Salt, sediment and hydrocarbons: Gulf Coast Section SEPM Foundation 16th Annual Research Conference, 285-295.

Vendeville, B.C., Hongxing, G., Jackson, M.P.A. 1995. Scale models of salt tectonics during basement-involved extension. Petroleum Geoscience, 1, 179-183

Vera, J.A. 1983. Las zonas externas de las cordilleras Béticas. In: Comba, J.A. (Ed) Geologia de España 2, Libro Jubilar J. M. Rios. IGME, Madrid, 218-251.

Vera, J.A., García-Hernández, M., López-Garrido, A.C., Comas, M.C., Ruiz-Ortiz, P.A., Martín-Algarra, A. 1982. El Cretácico de la Cordillera Bética. In: El Cretácico de España, Universidad Complutense de Madrid, 515-632.

Vera, J.A., 2004. Geología de España. Sociedad Geológica de España-Instituto Geológico y Minero Español, Madrid.

Vozoff, K. 1991. The magnetotelluric method. In: Nabighian, M.N., (Ed) Electromagnetic Methods in Applied Geophysics. Society of Exploration Geophysicists, Tulsa, 641-711.

Vissers, R.L.M., Platt, J.P., van der Wai, D. 1995. Late orogenic extension of the Betic Cordillera and the Alboran Domain: a lithospheric view. Tectonics 14, 786-803.

Watson, G.S., Enkin, R.J., 1993. The fold test in paleomagnetism as a parameter-estimation problem. Geophysical Research Letters, 20, 2135-2137.

Weaver, J.T., Agarwall, A.K., Lilley, F.E.M. 2000. Characterization of the magnetotelluirc tensor in terms of its invariants. Geophysical Journal International, 14, 321-336.

Weinberger, R., Agnon, A., Ron, H., Garfunkel, Z., 1995. Rotation about an inclined axis: Three dimensional matrices for reconstructing paleomagnetic and structural data. Journal of Structural Geology, 17 (6), 777-782.

Weinberger, R., Agnon, A., Ron H., 1997. Paleomagnetic reconstruction of a diapir emplacement: A case study from Sedom diapir, the Dead Sea Rift. Journal of Geophysical Research 102(B3), 5173-5192.

Withjack, M., Callaway, S. 2000. Active normal faulting beneath a salt layer: An experimental study of deformation patterns in the cover sequence: American Associetion of Petroleum Geologist Bulletin, 85, 627-65.

Worrall, D.M., Snelson, S., 1989. Evolution of the northern Gulf of Mexico, with

emphasis on Cenozoic growth faulting and the role of salt. In: Bally A.W., Palmer A.R. (Eds). The Geology of North America: an overview. Boulder, Colorado, Geologycal Society of America, A., 97-138.

Yaramanci, U. 2000. Surface Nuclear Magnetic Resonance (SNMR) - A new method for exploration of ground water and aquifer properties. Annanli di Geofisica, 43, 1159-1175.

Zaleski, S., Julien, P., 1992. Numerical simulation of Rayleigh-Taylor instability of single and multiple salt diapirs. Tectonophysics, 206, 55-69.

Zhang, G., Hynes, A., Irving, E., 1996. Block rotations along strike-slip Finlay-Ingenika fault, north-central British Columbia: Implications from paleomagnetic and tectonic studies. Tectonics, 15 (2), 272-287.

Ziegler, P.A. 1989 Evolution of the North Atlantic -an over-view. In: Extensional Tectonics ans Stratigraphy of the North Atlantic Margins (Ed). By A.J. Tankard and HR Balkwell) AAPG Memoir, 46, 111-129

Zijderveld, J.D.A. 1967. AC demagnetization of rocks: analysis of results, in: D.W. Collison, S.K. Runcorn, K.M. Creer (Eds), Methods in Paleomagnetism, Elsevier, New York, 254-286.